BLACK HOLES ON SUPERCOMPUTERS: NUMERICAL RELATIVITY APPLICATIONS TO ASTROPHYSICS AND HIGH-ENERGY PHYSICS*

Ulrich Sperhake

DAMTP, Centre for Mathematical Sciences, University of Cambridge
Wilberforce Road, Cambridge, CB3 0WA, United Kingdom

(Received October 14, 2013)

We review the state-of-the-art of the numerical modeling of black-hole spacetimes in the framework of General Relativity in four and more spacetime dimensions. The latest developments of the applications of these techniques to study black holes in the context of astrophysics, gravitational wave physics and high-energy physics are summarized.

DOI:10.5506/APhysPolB.44.2463
PACS numbers: 04.25.D–, 04.25.dg, 04.30.Db, 04.50.Gh

1. Introduction

When Einstein published his theory of General Relativity, he was rather pessimistic about the chances of finding physically relevant solutions to his field equations. Quite remarkably, his pessimism was proven unfounded soon afterwards when Schwarzschild found his famous solution describing a static, spherically symmetric vacuum spacetime in four dimensions

$$ds^2 = -\left(1-\frac{2M}{r}\right)dt^2 + \left(1-\frac{2M}{r}\right)^{-1}dr^2 + r^2d\theta^2 + r^2\cos^2\theta\, d\phi^2 \,. \quad (1)$$

The relative simplicity of the Schwazrschild solution, as well as other analytic solutions as, for example, the Friedmann–Lemaître–Robertson–Walker metric, is a consequence of the high degree of symmetry which substantially reduces the complexity of the Einstein equations. It is noteworthy, in this context, that the axisymmetric Kerr solution [1] describing a rotating black hole (BH) was not found until about half a century after the publication

* Presented at the LIII Cracow School of Theoretical Physics "Conformal Symmetry and Perspectives in Quantum and Mathematical Gravity", Zakopane, Poland, June 28–July 7, 2013.

of general relativity. By now, many analytic solutions have been found describing a wide class of BH spacetimes with different numbers of dimensions and/or different types of asymptotic structure. All these solutions, however, have in common a rather high degree of symmetry.

Ever since Einstein's discovery of his theory, BH solutions have been an invaluable tool for understanding many properties of general relativity; see, for instance, Hawking and Ellis [2]. Until the 1960s, however, there was rather little confidence in their relevance as real physical objects. This picture started changing through astrophysical observations of X-ray sources, such as Cygnus X-1, which eventually were explained through accretion of matter from a main sequence star to a compact stellar object in binary systems [3]. Mass estimates for the compact objects in many such systems resulted in values well above upper limits for neutron stars leaving a BH as the plausible explanation. Roughly at the same time, observations of quasi-stellar objects at cosmological distances came to be interpreted as accretion onto supermassive BHs; see *e.g.* [4]. Observations of stellar dynamics near the center of galaxies and of iron Kα emission line profiles have by now provided further strong evidence that BHs of masses in the range of $10^6 \ldots 10^{10}\ M_\odot$ reside at the center of many galaxies. By now, BHs are believed to play a key role in many astrophysical processes. Moreover, binary systems containing BHs are expected to be one of the strongest sources of gravitational waves (GWs) [5] expected to be detected with laser interferometric devices such as the ground based LIGO, Virgo, GEO600, KAGRA or future space based missions of LISA type [6–10]. Most recently, BHs started becoming important objects of study in different areas of high-energy physics. Through the *gauge–gravity duality* [11, 12] BH spacetimes may provide unprecedented opportunities to study field theories in the strong-coupling regime and attempts to explain the *hierarchy problem* in physics in terms of Tera-Electron-Volt (TeV) gravity models with extra spatial dimensions [13, 14] has even resulted in experimental efforts to test the possibility of generating microscopic BHs at the Large Hadron Collider at CERN.

In view of the remarkable role that BHs play in many areas at the forefront of contemporary physics, their theoretical modeling is a matter of vital importance. While analytic solutions still play an invaluable role in these studies, the BH systems involved all too often do not admit the spacetime symmetries required for the derivation of analytic solutions. Their modeling therefore must resort to other techniques which can be roughly classified into three approaches. *(i)* Black-hole perturbation theory (see *e.g.* [15] for a review) employs an expansion of the spacetime metric around an already known solution and models the deviations from this background in the framework of the Einstein equations in linearized form or at some finite order in the perturbations. *(ii)* The post-Newtonian formalism (see *e.g.* [16]) represents an expansion of general relativity around Newtonian physics in terms of the involved objects' velocities divided by the speed of light v/c or, equivalently, the ratio mass-to-distance M/r which measures the strength of the gravitational interaction. *(iii)* Numerical relativity where the Einstein equations in their fully non-linear form are solved using numerical methods on supercomputers; see *e.g.* [17] for an introduction to high-performance computing. Purpose of these notes is to provide an overview of the formalism, the methodology and the diagnostic tools that have been used with great success for about one decade now in the numerical relativity modeling of BH spacetimes.

These notes are organized as follows. We discuss formulations of the Einstein equations in Sec. 2 and in Sec. 3 how these can be reduced to an effectively four-dimensional system in the case of higher-dimensional spacetimes with appropriate symmetries. Additional tools required to successfully evolve numerically generated spacetimes are summarized in Sec. 4 and the diagnostic tools for their analysis in Sec. 5. We review some of the most important applications of numerical relativity to physical systems in Sec. 6 and conclude in Sec. 7.

Notation: We use the *spacelike* convention for the metric, *i.e.* a signature "$- + + + \ldots$", define the Riemann curvature tensor as $R^{\alpha}{}_{\beta\gamma\delta} = \partial_\gamma \Gamma^{\alpha}_{\delta\beta} - \partial_\delta \Gamma^{\alpha}_{\gamma\beta} + \Gamma^{\alpha}_{\gamma\rho}\Gamma^{\rho}_{\delta\beta} - \Gamma^{\alpha}_{\delta\rho}\Gamma^{\rho}_{\gamma\beta}$ and the Ricci tensor through $R_{\alpha\beta} = R^{\mu}{}_{\alpha\mu\beta}$. Greek indices cover the D-dimensional spacetime coordinates, *e.g.* $\alpha = 0, \ldots, D-1$. Upper case Latin indices denote the $D-1$ spatial coordinates, *e.g.* $I = 1, \ldots, D-1$. When we reduce higher-dimensional spacetimes to an effective four-dimensional description, we will use late, lower case Latin indices $i, j, \ldots = 1, \ldots, 3$ for the reduced spatial domain and early, lower case Latin indices $a, b, \ldots = 4, \ldots, D-1$ for extra spatial dimensions.

2. Formulations of the Einstein equations

Put simply, the goal of numerical relativity is to generate solutions to the Einstein equations in D spacetime dimensions given by

$$R_{\alpha\beta} - \frac{1}{2} R g_{\alpha\beta} + \Lambda g_{\alpha\beta} = \frac{8\pi G}{c^4} T_{\alpha\beta}\,. \tag{2}$$

Here, $R_{\alpha\beta}$ and R are the Ricci tensor and scalar, $g_{\alpha\beta}$ denotes the spacetime metric, Λ is the cosmological constant, $T_{\alpha\beta}$ the energy momentum tensor and the gravitational constant and speed of light are given in SI units by $G = 6.67384 \times 10^{-11}$ m^3/(kg s^2), $c = 299, 792, 458$ m/s. We shall frequently choose units such that $G = c = 1$. Restoring SI values for the results is straightforward in all these cases from dimensional analysis.

In the numerical modeling, dynamic physical systems are typically viewed as an *initial value problem*, *i.e.* the simulation starts with a given snapshot of the system and its evolution in time is governed by the physical laws in the form of evolution equations. In this context, the tensorial form (2) of the Einstein equations is not directly useful for a numerical implementation. Up to the sign of the metric components, time and space are, of course, on equal footing in general relativity and the tensor form of the equations beautifully incorporates this particular feature. It is not obvious at all from Eq. (2), therefore, whether the Einstein equations actually represent an initial value problem or, put into an alternative mathematical language, whether they represent a set of *hyperbolic*, *parabolic* or *elliptic* differential equations or some mixture thereof. In order to answer this question, it is necessary to formulate the Einstein equations in a form which expresses more clearly a split between space and time.

2.1. The ADM equations

The canonical spacetime split of the Einstein equations has originally been developed by Arnowitt, Deser and Misner (ADM) [18] and later reformulated by York [19]. Let us consider a spacetime or, in more mathematical terms, a manifold $\mathcal{M}$ endowed with a Lorentzian metric $g_{\alpha\beta}$. We further assume that there exists a *foliation* of the spacetime, that is, a scalar function $t : \mathcal{M} \to \mathbb{R}$ with the following properties. *(i)* The one form $\mathbf{d}t$ is timelike everywhere; *(ii)* The hypersurfaces defined by $t = \text{const.}$ are non-intersecting; *(iii)* $\cup_{t\in\mathbb{R}} \Sigma_t = \mathcal{M}$. Note that the function t also defines a vectorfield ∂_t with the property $\langle \mathbf{d}t, \partial_t \rangle = 1$.

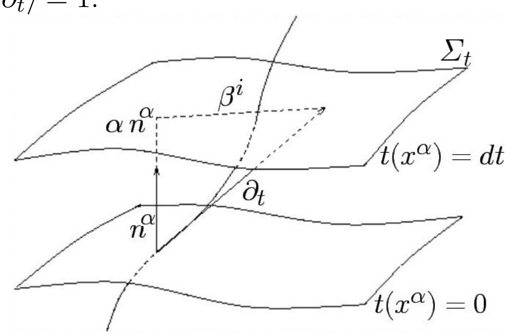

Fig. 1. Graphical illustration of the foliation. Only two of the spatial dimensions are displayed in the figure.

Definition: The *lapse* function α is defined such that the timelike unit vector field n^μ is related to the one form $\mathbf{d}t$ by $n_\mu = -\alpha(\mathbf{d}t)_\mu$. We further define the *shift vector* $\beta^\mu = (\partial_t)^\mu - \alpha n^\mu$. The lapse function and shift vector are graphically illustrated in Fig. 1.

Remark: Let x^I, $I = 1, \ldots, D-1$ be a set of coordinates labeling points inside a given hypersurface Σ_t. The spacetime coordinate system defined by (t, x^I) is often referred to as *adapted* to the spacetime split. A vector V^α is tangent to Σ_t iff $\langle \mathbf{d}t, V \rangle = (\mathbf{d}t)_\mu V^\mu = 0$. In adapted coordinates, this implies that the time component $V^t = 0$. For tensors of higher rank, the same holds for every component in which the tensor is tangent to Σ_t. In adapted coordinates one therefore often switches from spacetime indices $\alpha, \beta, \ldots$ to spatial indices $I, J, \ldots$ ignoring the vanishing time components of vectors and tensors if they are tangent to Σ_t.

Definition: We define the *projection operator* $\perp^\alpha{}_\mu \equiv \delta^\alpha{}_\mu + n^\alpha n_\mu$. The projection of an arbitrary tensor T is obtained by projecting each index

$$(\perp T)^{\alpha\beta\ldots}{}_{\gamma\delta\ldots} = \perp^\alpha{}_\mu \perp^\beta{}_\nu \ldots \perp^\rho{}_\gamma \perp^\sigma{}_\delta \ldots T^{\mu\nu\ldots}{}_{\rho\sigma\ldots} \,. \tag{3}$$

Remarks: For a vector tangent to Σ_t, we have $n_\mu V^\mu = 0$ and $\perp^\alpha{}_\mu V^\mu = V^\alpha$. The projection of the metric is often referred to as the *first fundamental form* or *spatial metric* (or *3-metric* in the case $D = 4$). It is given by

$$\gamma_{\alpha\beta} = \perp^\mu{}_\alpha \perp^\nu{}_\beta g_{\mu\nu} = g_{\alpha\beta} + n_\alpha n_\beta = \perp_{\alpha\beta} \,. \tag{4}$$

Even though the spatial metric γ and the projector $\perp$ turn out to represent the same tensor, we keep using both symbols depending on whether the emphasis is on projection or spatial geometry. For a vector tangent to Σ_t, we have $g_{\mu\nu} V^\mu V^\nu = \gamma_{\mu\nu} V^\mu V^\nu$. In adapted coordinates we further have $\gamma_{\mu\nu} V^\mu V^\nu = \gamma_{IJ} V^I V^J$. A tensor tangent to Σ_t in all components has vanishing products with the unit timelike field n in all components, so that the raising and lowering of indices with the spacetime metric $g_{\alpha\beta}$ is equivalent to raising and lowering indices with the spatial metric γ_{IJ}, *e.g.* $T^{IJ}{}_K = \gamma^{JM} T^I{}_{MK}$, where the inverse spatial metric is defined by the condition $\gamma^{IM} \gamma_{MJ} = \delta^I{}_J$.

In a coordinate basis $(\partial_t, \partial_I = \partial/\partial x^I)$ adapted to the spacetime split, one straightforwardly shows that the components of the spacetime metric are given by

$$g_{\alpha\beta} = \left(\begin{array}{c|c} -\alpha^2 + \beta_M \beta^M & \beta_J \\ \hline \beta_I & \gamma_{IJ} \end{array} \right) \quad \Leftrightarrow \quad g^{\alpha\beta} = \left(\begin{array}{c|c} -\alpha^{-2} & \alpha^{-2}\beta^J \\ \hline \alpha^{-2}\beta^I & \gamma^{IJ} - \alpha^{-2}\beta^I\beta^J \end{array} \right), \tag{5}$$

e.g. $g_{tJ} = g(\partial_t, \partial_J) = g(\beta, \partial_J) + \alpha g(n, \partial_J) = \beta_J + 0$. Alternatively, we can write the line element

$$ds^2 = -\alpha^2 dt^2 + \gamma_{IJ} \left(dx^I + \beta^I dt \right) \left(dx^J + \beta^J dt \right) \,. \tag{6}$$

Definition: We define the *spatial covariant derivative* of a tensor field as the projection in all indices of its spacetime covariant derivative $DT \equiv \perp(\nabla T)$ or

$$D_\rho T^{\alpha_1\ldots\alpha_p}{}_{\beta_1\ldots\beta_q} = \perp^\sigma{}_\rho \perp^{\alpha_1}{}_{\mu_1} \ldots \perp^{\alpha_p}{}_{\mu_p} \perp^{\nu_1}{}_{\beta_1} \ldots \perp^{\nu_q}{}_{\beta_q} \nabla_\sigma T^{\mu_1\ldots\mu_p}{}_{\nu_1\ldots\nu_q} \,. \quad (7)$$

One can show (see *e.g.* [20]) that D defined in this way is the covariant derivative operator associated with the Levi-Civita connection of the spatial metric $\gamma_{\alpha\beta}$ and is unique in being *(i)* torsion free on Σ_t provided ∇ is torsion free on $\mathcal{M}$ and *(ii)* metric compatible $D_I\gamma_{JK} = (\perp\nabla\gamma)_{IJK} = 0$.

Definition: In order to formulate the Einstein equations in the form of a spacetime split, we need to define one further variable, the *extrinsic curvature* or *second fundamental form* $K_{\alpha\beta} \equiv -\perp\nabla_\beta n_\alpha$.

Remarks: Note that $\nabla_\beta n_\alpha$ is not symmetric in its indices but the projection and, thus, $K_{\alpha\beta}$ is. One can show that the Lie derivative of the spatial metric along the unit timelike field is related to the extrinsic curvature through

$$\mathcal{L}_n\gamma_{\alpha\beta} = n^\mu\nabla_\mu\gamma_{\alpha\beta} + \gamma_{\mu\beta}\nabla_\alpha n^\mu + \gamma_{\alpha\mu}\nabla_\beta n^\mu = -2K_{\alpha\beta} \quad \Leftrightarrow \quad K_{\alpha\beta} = -\tfrac{1}{2}\mathcal{L}_n\gamma_{\alpha\beta} \,. \quad (8)$$

From its definition and Eq. (8), we derive two intuitive interpretations of the extrinsic curvature. *(i)* It measures the change in the direction of the unit normal field n^μ between different points in the hypersurface Σ_t; *(ii)* It represents a measure for the change in time of the spatial metric. As illustrated in Fig. 2, the extrinsic curvature thus describes how the $D-1$ dimensional hypersurfaces Σ_t are embedded in the D-dimensional spacetime.

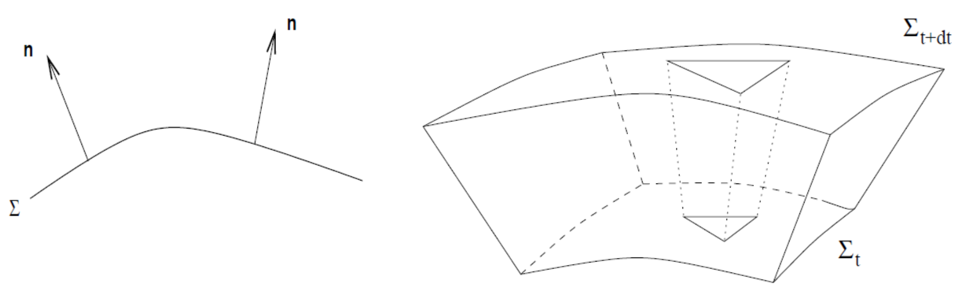

Fig. 2. The extrinsic curvature represents a measure for the change in direction of the unit timelike normal field n at different points in Σ_t (left panel) and the change in the spatial metric (right panel).

We have now assembled all the tools to calculate the projections of the Riemann tensor onto spatial and time directions. A tedious but straightforward calculation shows the following results

$$\perp^{\mu}{}_{\alpha}\perp^{\nu}{}_{\beta}\perp^{\gamma}{}_{\rho}\perp^{\sigma}{}_{\delta}\ R^{\rho}{}_{\sigma\mu\nu} = \mathcal{R}^{\gamma}{}_{\delta\alpha\beta} + K^{\gamma}{}_{\alpha}K_{\delta\beta} - K^{\gamma}{}_{\beta}K_{\delta\alpha}\,, \tag{9}$$
$$\perp^{\mu}{}_{\alpha}\perp^{\nu}{}_{\beta}\ R_{\mu\nu} + \perp_{\mu\alpha}\perp^{\nu}{}_{\beta}n^{\rho}n^{\sigma}\ R^{\mu}{}_{\rho\nu\sigma} = \mathcal{R}_{\alpha\beta} + KK_{\alpha\beta} - K^{\mu}{}_{\beta}K_{\alpha\mu}\,, \tag{10}$$
$$R + 2\ R_{\mu\nu}n^{\mu}n^{\nu} = \mathcal{R} + K^2 - K^{\mu\nu}K_{\mu\nu}\,, \tag{11}$$
$$\perp^{\gamma}{}_{\rho}n^{\sigma}\perp^{\mu}{}_{\alpha}\perp^{\nu}{}_{\beta}\ R^{\rho}{}_{\sigma\mu\nu} = D_{\beta}K^{\gamma}{}_{\alpha} - D_{\alpha}K^{\gamma}{}_{\beta}\,, \tag{12}$$
$$n^{\sigma}\perp^{\nu}{}_{\beta}\ R_{\sigma\nu} = D_{\beta}K - D_{\mu}K^{\mu}{}_{\beta}\,, \tag{13}$$
$$\perp_{\alpha\mu}\perp^{\nu}{}_{\beta}n^{\sigma}n^{\rho}\ R^{\mu}{}_{\rho\nu\sigma} = \frac{1}{\alpha}\mathcal{L}_m K_{\alpha\beta} + K_{\alpha\mu}K^{\mu}{}_{\beta} + \frac{1}{\alpha}D_{\alpha}D_{\beta}\alpha\,, \tag{14}$$
$$\perp^{\mu}{}_{\alpha}\perp^{\nu}{}_{\beta}R_{\mu\nu} = -\frac{\mathcal{L}_m K_{\alpha\beta}}{\alpha} - 2K_{\alpha\mu}K^{\mu}{}_{\beta} - \frac{D_{\alpha}D_{\beta}\,\alpha}{\alpha} + \mathcal{R}_{\alpha\beta} + KK_{\alpha\beta}\,, \tag{15}$$
$$R = -\frac{2}{\alpha}\mathcal{L}_m K - \frac{2}{\alpha}\gamma^{\mu\nu}D_{\mu}D_{\nu}\alpha + \mathcal{R} + K^2 + K^{\mu\nu}K_{\mu\nu}\,, \tag{16}$$

where $m^{\mu} = \alpha n^{\mu} = (\partial_t)^{\mu} + \beta^{\mu}$ and $\mathcal{R}^{\gamma}{}_{\delta\alpha\beta}$, $\mathcal{R}_{\alpha\beta}$ and $\mathcal{R}$ denote the Riemann tensor, Ricci tensor and Ricci scalar associated with the spatial metric $\gamma_{\alpha\beta}$. Equations (9), (10), (11) and (12) are known as the Gauss, the contracted Gauss, the scalar Gauss and the Codazzi equations, respectively.

We next use these expressions to rewrite the D-dimensional Einstein equations (2) in terms of the ADM variables α, β^I, γ_{IJ} and K_{IJ}. It turns out useful, for this purpose, to apply a similar split to the energy-momentum tensor $T_{\alpha\beta}$.

Definition: The energy density, momentum density and stress tensor are defined as

$$\begin{aligned} \rho \ &\equiv\ T_{\mu\nu}n^{\mu}n^{\nu}\,, \quad j_{\alpha} \equiv -T_{\mu\nu}n^{\mu}\perp^{\nu}{}_{\alpha}\,, \quad S_{\alpha\beta} \equiv \perp^{\mu}{}_{\alpha}\perp^{\nu}{}_{\beta}T_{\mu\nu}\,, \quad S \equiv \gamma^{\mu\nu}S_{\mu\nu} \\ \Leftrightarrow\ & T_{\alpha\beta} = S_{\alpha\beta} + n_{\alpha}j_{\beta} + n_{\beta}j_{\alpha} + \rho n_{\alpha}n_{\beta}\,, \quad T = S - \rho\,. \end{aligned} \tag{17}$$

The spacetime projections of the Einstein equations (2) are then given by

$$\mathcal{L}_m\gamma_{IJ} = -2\alpha K_{IJ}\,, \tag{18}$$
$$\begin{aligned}\mathcal{L}_m K_{IJ} &= -D_I D_J\alpha + \alpha\big\{\mathcal{R}_{IJ} + KK_{IJ} - 2K_{IM}K^{M}{}_{J} \\ &\quad +4\pi[(S-\rho)\gamma_{IJ} - 2S_{IJ}]\big\}\,,\end{aligned} \tag{19}$$
$$\mathcal{H} \equiv \mathcal{R} + K^2 - K^{MN}K_{MN} - 2\Lambda - 16\pi\rho = 0\,, \tag{20}$$
$$\mathcal{M}_I \equiv -D_I K + D_M K^{M}{}_{I} - 8\pi j_I = 0\,. \tag{21}$$

Here, the Lie derivatives are given by

$$\mathcal{L}_m K_{IJ} = \partial_t K_{IJ} - \beta^M\partial_M K_{IJ} - K_{MJ}\partial_I\beta^M - K_{IM}\partial_J\beta^M\,, \tag{22}$$
$$\mathcal{L}_m\gamma_{IJ} = \partial_t\gamma_{IJ} - \beta^M\partial_M\gamma_{IJ} - \gamma_{MJ}\partial_I\beta^M - \gamma_{IM}\partial_J\beta^M\,. \tag{23}$$

Equation (18) is merely a consequence of the definition of the extrinsic curvature. Equation (19) represents a set of $D(D-1)/2$ evolution equations for K_{IJ}. These two equations determine the time evolution of the physical system. The *Hamiltonian* and *momentum constraints* (20), (21), on the other hand, do not contain time derivatives but represent conditions which must be satisfied by the data on each hypersurface Σ_t. By virtue of the contracted Bianchi identities, the constraints (20), (21) are preserved under evolution in time, so that, in practice, it is necessary to solve the constraints on the initial hypersurface $\Sigma_{t=0}$ only. We note, however, that the preservation of the constraints is only valid at the continuum level. Numerical discretization will naturally involve some violations of the constraints and, as we shall discuss further below, avoiding rapid growth of such constraint violating modes represents one of the important ingredients in obtaining numerically stable evolutions.

In summary, the spacetime split of the Einstein equations results in a mixed set of evolution equations and constraints. Note also that the Einstein equations (18)–(21) do not make any predictions for the lapse function and shift vector. These are indeed freely specifiable functions and represent the gauge freedom of general relativity. We shall return to them in Sec. 4.2 below.

2.2. Well-posedness

The initial value formulation (18)–(21) of the Einstein equations provides us with a system of partial differential equations that can be coded up on a computer and used to calculate the evolution in time of some initial snapshot of a physical system. These equations, often referred to as the ADM equations, have indeed been used in numerical relativity applications, but they have not resulted in long-term stable evolutions of generic spacetimes. It is now understood that these difficulties of the ADM equations are related to the issue of *well posedness* of partial differential equations. A comprehensive discussion of the question of well-posedness is beyond the scope of these lecture notes. We refer interested Readers to the Living Review articles by Reula [21] and Sarbach and Tiglio [22] as well as Hilditch's review [23], and merely present a simplified discussion that suffices in motivating modifications to the ADM system.

Let us consider for this purpose an initial value problem in one spatial dimension for a single field variable $\phi(t,x)$.

Definition: The initial value problem is *well posed* if there exists a norm $||.||$ which maps functions $f(x)$ to $\mathbb{R}$, and there exists a function $F(t)$ which is independent of the choice of initial data $\phi(0,x)$, such that

$$||\delta\phi(t,.)|| \leq F(t)||\delta\phi(0,.)|| \,. \tag{24}$$

Here, $\delta\phi$ denotes the change in the time evolution of ϕ resulting from a small initial perturbation $\delta\phi(0, x)$.

Remarks: This condition limits how slightly different initial configurations deviate from each other during the time evolution given by the initial value problem. Note, however, that the growth in deviations $\delta\phi$ can still be quite rapid, *e.g.* exponential.

An important criterion to determine the well posedness of a system of differential equations is given by the *hyperbolicity* properties of the system. Note that this concept of hyperbolicity is a different one from that of hyperbolic, parabolic or elliptic systems mentioned above. Hyperbolicity is often defined in terms of the *principal part* of the system of differential equations which is the part containing the highest derivatives (dropping the lower derivative or those terms containing only non-differentiated factors). For simplicity, we consider a quasilinear, first-order system in one spatial variable for a set of variables $\boldsymbol{U}(t, x)$

$$\partial_t \boldsymbol{U} = P(t, x, \boldsymbol{U}, \partial_x)\boldsymbol{U} \, . \tag{25}$$

Definition: The system (25) is called *strongly hyperbolic* if P is a smooth differential operator and its associated principal symbol (the coefficient matrix in front of the ∂ operators) is symmetrizeable [24]. For the special case of constant-coefficient systems, this definition simplifies to the requirement that the principal symbol has only real eigenvalue and a complete set of linearly independent eigenvectors. If the principal symbol has real eigenvalues and no conditions are required for the eigenvectors, the system is called *weakly hyperbolic*.

Remark: For more general systems of equations, strong and weak hyperbolicity can be defined in a more general fashion; see *e.g.* [21, 22, 24, 25].

Most importantly for our purposes, it can be shown that strong hyperbolicity implies well-posedness [26, 27]. The ADM equations, on the other hand, have been shown to be weakly but not strongly hyperbolic for the case of fixed gauge conditions [24]; similarly, a first-order reduction of the ADM equations has been shown to be weakly hyperbolic [28]. Even though these studies do not yet cover the entire set of ADM formulations under general gauge conditions, the ADM equations are not considered a good choice for obtaining long-term stable numerical simulations of generic BH spacetimes.

A well-posed modification of the ADM equations which has been used with great success in numerical relativity is the Baumgarte–Shapiro–Shibata–Nakamura (BSSN) system [29, 30] which is the subject of the next section.

2.3. The BSSN formulation

The BSSN formulation applies a split of the extrinsic curvature into trace and tracefree part, a conformal rescaling of the spatial metric and the traceless part of the extrinsic curvature and promotes the contracted Christoffel symbols to the status of independently evolved variables. Specifically, the BSSN variables are defined by

$$\begin{aligned}
\chi &= \gamma^{-1/(D-1)}\,, \qquad K = \gamma^{MN}K_{MN}\,, \\
\tilde{\gamma}_{IJ} &= \chi\gamma_{IJ} \quad \Leftrightarrow \quad \tilde{\gamma}^{IJ} = \frac{1}{\chi}\gamma^{IJ}\,, \\
\tilde{A}_{IJ} &= \chi\left(K_{IJ} - \frac{1}{D-1}\gamma_{IJ}K\right) \Leftrightarrow K_{IJ} = \frac{1}{\chi}\left(\tilde{A}_{IJ} + \frac{1}{D-1}\tilde{\gamma}_{IJ}K\right)\,, \\
\tilde{\Gamma}^I &= \tilde{\gamma}^{MN}\tilde{\Gamma}^I_{MN}\,,
\end{aligned} \tag{26}$$

where $\gamma \equiv \det\gamma_{IJ}$ and $\tilde{\Gamma}^I_{MN}$ is the Christoffel symbol defined in the usual manner from the conformal spatial metric $\tilde{\gamma}_{IJ}$. These definitions imply two algebraic and one differential auxiliary constraints (in addition to the Hamiltonian and momentum constraint) given by

$$\tilde{\gamma} = 1\,, \qquad \tilde{\gamma}^{MN}\tilde{A}_{MN} = 0\,, \qquad \mathcal{G}^I \equiv \tilde{\Gamma}^I - \tilde{\gamma}^{MN}\tilde{\Gamma}^I_{MN} = 0\,. \tag{27}$$

Inserting these definitions into the ADM equations and using the Hamiltonian in the evolution equation for K and the momentum constraint in that for $\tilde{\Gamma}^i$ results in the BSSN equations

$$\partial_t\chi = \beta^M\partial_M\chi + \frac{2}{D-1}\chi\left(\alpha K - \partial_M\beta^M\right)\,, \tag{28}$$

$$\partial_t\tilde{\gamma}_{IJ} = \beta^M\partial_M\tilde{\gamma}_{IJ} + 2\tilde{\gamma}_{M(I}\partial_{J)}\beta^M - \frac{2}{D-1}\tilde{\gamma}_{IJ}\partial_M\beta^M - 2\alpha\tilde{A}_{IJ}\,, \tag{29}$$

$$\begin{aligned}
\partial_t K &= \beta^M\partial_M K - \chi\tilde{\gamma}^{MN}D_M D_N\alpha + \alpha\tilde{A}^{MN}\tilde{A}_{MN} + \frac{1}{D-1}\alpha K^2 \\
&\quad + \frac{8\pi}{D-2}\alpha\left[S + (D-3)\rho\right] - \frac{2}{D-2}\alpha\Lambda\,,
\end{aligned} \tag{30}$$

$$\begin{aligned}
\partial_t\tilde{A}_{IJ} &= \beta^M\partial_M\tilde{A}_{IJ} + 2\tilde{A}_{M(I}\partial_{J)}\beta^M - \frac{2}{D-1}\tilde{A}_{IJ}\partial_M\beta^M + \alpha K\tilde{A}_{IJ} \\
&\quad - 2\alpha\tilde{A}_{IM}\tilde{A}^M{}_J + \chi\left(\alpha\mathcal{R}_{IJ} - D_I D_J\alpha - 8\pi\alpha S_{IJ}\right)^{\mathrm{TF}}\,,
\end{aligned} \tag{31}$$

$$\begin{aligned}
\partial_t\tilde{\Gamma}^I &= \beta^M\partial_M\tilde{\Gamma}^I + \frac{2}{D-1}\tilde{\Gamma}^I\partial_M\beta^M - \tilde{\Gamma}^M\partial_M\beta^I + \tilde{\gamma}^{MN}\partial_M\partial_N\beta^I \\
&\quad + \frac{D-3}{D-1}\tilde{\gamma}^{IM}\partial_M\partial_N\beta^N - \tilde{A}^{IM}\left[(D-1)\alpha\frac{\partial_M\chi}{\chi} + 2\partial_M\alpha\right] \\
&\quad + 2\alpha\tilde{\Gamma}^I_{MN}\tilde{A}^{MN} - 2\frac{D-2}{D-1}\alpha\tilde{\gamma}^{IM}\partial_M K - 16\pi\alpha j^I - \sigma\partial_M\beta^M\mathcal{G}^I\,,
\end{aligned} \tag{32}$$

where the superscript TF denotes the tracefree part. The addition of the last term in (32) has been suggested by Yo *et al.* [31] to damp violations of the auxiliary constraint $\mathcal{G}^I$. In practice, the constant σ is typically set a value of order unity. We furthermore need the following expressions for the covariant derivative of the lapse function and the spatial Ricci tensor in terms of the fundamental variables

$$D_I D_J \alpha = \tilde{D}_I \tilde{D}_J \alpha + \frac{1}{\chi}\partial_{(I}\chi\,\partial_{J)}\alpha - \frac{1}{2\chi}\tilde{\gamma}_{IJ}\tilde{\gamma}^{MN}\partial_M\chi\,\partial_N\alpha\,, \tag{33}$$

$$\mathcal{R}_{IJ} = \mathcal{R}^{\chi}_{IJ} + \tilde{R}_{IJ}\,, \tag{34}$$

$$\mathcal{R}^{\chi}_{IJ} = \frac{1}{2\chi}\tilde{\gamma}_{IJ}\left[\tilde{\gamma}^{MN}\tilde{D}_M\tilde{D}_N\chi - \frac{D-1}{2\chi}\tilde{\gamma}^{MN}\partial_M\chi\,\partial_N\chi\right] + \frac{D-3}{2\chi}\left(\tilde{D}_I\tilde{D}_J\chi - \frac{1}{2\chi}\partial_I\chi\,\partial_J\chi\right), \tag{35}$$

$$\tilde{R}_{IJ} = -\frac{1}{2}\tilde{\gamma}^{MN}\partial_M\partial_N\tilde{\gamma}_{IJ} + \tilde{\gamma}_{M(I}\partial_{J)}\tilde{\Gamma}^M + \tilde{\gamma}^{MN}\left[2\tilde{\Gamma}^K_{M(I}\tilde{\Gamma}_{J)KN} + \tilde{\Gamma}^K_{IM}\tilde{\Gamma}_{KJN}\right] + \tilde{\Gamma}^M\tilde{\Gamma}_{(IJ)M}\,. \tag{36}$$

Some comments are in order at this stage. *(i)* Some implementations of the BSSN system use the variables $W \equiv \sqrt{\chi}$ or $\phi \equiv -(\ln\chi)/4$ in place of χ. *(ii)* In the evolution equation (32) for $\tilde{\Gamma}^t$, some numerical codes drop the constraint damping term $\sigma\partial_M\beta^M\mathcal{G}^I$ and instead replace $\tilde{\Gamma}^I$ in terms of its definition through the Christoffel symbols wherever $\tilde{\Gamma}^I$ appears in undifferentiated form; *cf.* Alcubierre and Brügmann [32]. *(iii)* The two algebraic constraints in Eq. (27) can be enforced straightforwardly after completion of every timestep. From experience, it appears that enforcing $\tilde{\gamma}^{MN}\tilde{A}_{MN} = 0$ is necessary for numerical stability, whereas imposing the condition $\tilde{\gamma} = 1$ is optional but not necessary. We conclude this summary of the BSSN system with the Hamiltonian and momentum constraints which are given by

$$\mathcal{H} = \mathcal{R} + \frac{D-2}{D-1}K^2 - \tilde{A}^{MN}\tilde{A}_{MN} - 16\pi\rho - 2\Lambda = 0\,, \tag{37}$$

$$\mathcal{M}_I = \tilde{\gamma}^{MN}\tilde{D}_M\tilde{A}_{NI} - \frac{D-2}{D-1}\partial_I K - \frac{D-1}{2\chi}\tilde{A}^M{}_I\partial_M\chi - 8\pi j_I\,. \tag{38}$$

2.4. The Generalized Harmonic Gauge formulation

An alternative well-posed formulation that has been used with great success in numerical relativity applications, most notably in Pretorius' breakthrough [33], is the Generalized Harmonic Gauge (GHG) formulation. This system is reviewed in great detail in Ringström's notes [34] in this issue and we here restrict ourselves to a brief summary.

It has been realized a long time ago that the Einstein equations take on a mathematically appealing form if one imposes the *harmonic gauge* condition $\Box x^\alpha = -g^{\mu\nu}\Gamma^\alpha_{\mu\nu} = 0$. Taking the derivative of this condition eliminates a specific combination of second derivatives from the Ricci tensor such that its principal part is that of the scalar wave operator

$$R_{\alpha\beta} = -\tfrac{1}{2}g^{\mu\nu}\partial_\mu\partial_\nu g_{\alpha\beta} + \dots\,, \tag{39}$$

where the dots denote terms involving at most the first derivative of the metric. In consequence of this simplification of the principal part, the Einstein equations in harmonic gauge are manifestly hyperbolic and harmonic coordinates have played a key part in establishing local uniqueness of the solution to the Cauchy problem in general relativity [35–37].

It has been realized by Friedrich [38] and Garfinkle [39] that the appealing form of the Ricci tensor can be maintained for arbitrary coordinates defined through

$$H^\alpha \equiv \Box x^\alpha = -g^{\mu\nu}\Gamma^\alpha_{\mu\nu}\,, \tag{40}$$

by promoting the H^α to the status of independently evolved variables; see also [40, 41]. With this definition, it turns out convenient to consider the generalized class of equations

$$R_{\alpha\beta} - \nabla_{(\alpha}\mathcal{C}_{\beta)} = 8\pi\left(T_{\alpha\beta} - \frac{1}{D-2}Tg_{\alpha\beta}\right) + \frac{2}{D-2}\Lambda g_{\alpha\beta}\,, \tag{41}$$

where $\mathcal{C}^\alpha \equiv H^\alpha - \Box x^\alpha$. The addition of the term $\nabla_{(\alpha}\mathcal{C}_{\beta)}$ replaces the contribution of $\nabla_{(\alpha}\Box x_{\beta)}$ to the Ricci tensor in terms of $\nabla_{(\alpha}H_{\beta)}$ and thus changes the principal part to that of the scalar wave operator. A solution to the Einstein equations is now obtained by solving Eq. (41) subject to the constraint $\mathcal{C}_\alpha = 0$.

Starting point for a Cauchy evolution are initial data $g_{\alpha\beta}$ and $\partial_t g_{\alpha\beta}$ which satisfy the constraints $\mathcal{C}^\alpha = 0 = \partial_t\mathcal{C}^\alpha$. A convenient manner to construct such initial data is to compute initial H^α directly from Eq. (40) so that $\mathcal{C}^\alpha = 0$ by construction. It can then be shown [41] that the ADM constraints (20), (21) imply $\partial_t\mathcal{C}^\mu$. By virtue of the contracted Bianchi identities, the evolution of the constraint system obeys the equation

$$\Box\mathcal{C}_\alpha = -\mathcal{C}^\mu\nabla_{(\mu}\mathcal{C}_{\nu)} - \mathcal{C}^\mu\left[8\pi\left(T_{\mu\alpha} - \frac{1}{D-2}Tg_{\mu\alpha}\right) + \frac{2}{D-2}\Lambda g_{\mu\alpha}\right]\,, \tag{42}$$

and the constraint $\mathcal{C}^\alpha = 0$ is preserved under time evolution in the continuum limit.

A key addition to the GHG formalism has been devised by Gundlach *et al.* [42] in the form of damping terms which prevent growth of numerical violations of the constraints $\mathcal{C}^\alpha = 0$ due to discretization or roundoff errors.

Including these damping terms and using the definition (40) to substitute higher derivatives in the Ricci tensor, the generalized Einstein equations (41) can be written as

$$g^{\mu\nu}\partial_\mu\partial_\nu g_{\alpha\beta} = -2\partial_\nu g_{\mu(\alpha}\partial_{\beta)}g^{\mu\nu} - 2\partial_{(\alpha}H_{\beta)} + 2H_\mu \Gamma^\mu_{\alpha\beta} - 2\Gamma^\mu_{\nu\alpha}\Gamma^\nu_{\mu\beta} - 16\pi T_{\alpha\beta} + \frac{16\pi T - 4\Lambda}{D-2}g_{\alpha\beta} - 2\kappa\left[2n_{(\alpha}\mathcal{C}_{\beta)} - \lambda g_{\alpha\beta}n^\mu \mathcal{C}_\mu\right] , \tag{43}$$

where κ, λ are user-specified parameters. An alternative first-order-system of the GHG formulation has been presented in Lindblom *et al.* [41].

2.5. Beyond BSSN: Improvements for future applications

Most BH evolutions in generic $D = 4$ dimensional spacetimes have been performed with the GHG and the BSSN formulation. It is interesting to note in this context the complementary nature of the two formulations' respective strengths and weaknesses. In particular, the constraint subsystem of the BSSN equations contains a zero-speed mode [43–45] which may lead to large Hamiltonian constraint violations. The GHG system does not contain such modes and furthermore admits a simple way of controlling constraint violations in the form of damping terms [42]. Finally, the wave-equation-type principal part of the GHG system allows for the straightforward construction of constraint preserving boundary conditions [46–48]. On the other hand, the BSSN formulation is remarkably robust and allows for the simulation of BH binaries over a wide range of the parameter space with little if any modifications of the gauge conditions; *cf.* Sec. 4.2. Combination of these advantages in a single system has motivated the exploration of improvements to the BSSN system and in recent years resulted in the identification of a conformal version of the $Z4$ system, originally developed by Bona *et al.* [49–51], as a highly promising candidate [52–55].

The key idea behind the $Z4$ system is to replace the Einstein equations with a generalized class of equations given by

$$G_{\alpha\beta} = 8\pi T_{\alpha\beta} - \nabla_\alpha Z_\beta - \nabla_\beta Z_\alpha + g_{\alpha\beta}\nabla_\mu Z^\mu + \kappa_1\left[n_\alpha Z_\beta + n_\beta Z_\alpha + \kappa_2 g_{\alpha\beta} n_M Z^M\right] , \tag{44}$$

where Z_α is a vector field of constraints which is decomposed into space and time components according to $\Theta \equiv -n^\mu Z_\mu$ and $Z_i = \perp^\mu{}_i Z_\mu$. Clearly, a solution to the Einstein equations is recovered provided the constraint $Z_\mu = 0$ is satisfied. The conformal version of the $Z4$ system is obtained in the same manner as the BSSN system and leads to time evolution equations for a set of variables nearly identical to the BSSN variables but augmented by the constraint variable Θ. The resulting evolution equations given in the literature vary in minor details, but clearly represent relatively minor modifications for existing BSSN codes [52, 53, 55]. Investigations have shown that the conformal $Z4$ system is indeed suitable for implementation of constraint preserving boundary systems [56] and that constraint violations in simulations of gauge waves and BH and neutron-star spacetimes are smaller than those obtained for the BSSN system, in particular when constraint damping is actively enforced [52, 55]. This behavior also manifests itself in more accurate results for the gravitational radiation in binary inspirals [55]. In summary, the conformal $Z4$ formulation is a very promising candidate for future numerical studies of BH spacetimes, including, in particular, the asymptotically anti-de Sitter (AdS) case where a rigorous control of the outer boundaries is of utmost importance; *cf.* Sec. 4.4 below.

Another modification of the BSSN equations is based on the use of densitized versions of the trace of the extrinsic curvature and the lapse function as well as the traceless part of the extrinsic curvature with mixed indices [57, 58]. Some improvements in simulations of colliding BHs in higher dimensional spacetimes have been found by careful exploration of the densitization parameter space by Witek [59].

2.6. Alternative approaches to formulate the Einstein equations

The formulations discussed in the previous subsections are based on a space-time split of the Einstein equations. A natural alternative to such a split is given by the characteristic approach pioneered by Bondi and Sachs [60, 61]. Here, at least one coordinate is null and thus adapted to the characteristics of the vacuum Einstein equations. For generic four-dimensional spacetimes with no symmetry assumptions, the characteristic formalism results in a natural hierarchy of 2 evolution equations, 4 hypersurface equations relating variables on hypersurfaces of constant retarded (or advanced) time, as well as 3 supplementary and 1 trivial equations. A comprehensive overview of characteristic methods in numerical relativity is given in Winicour's Living Review article [62]. Although characteristic codes have been developed with great success in spacetimes with additional symmetry assumptions, evolutions of generic BH spacetimes face the problem of formation of caustics, resulting in a breakdown of the coordinate system; see [63] for a recent investigation. One possibility to avoid the problem of caustic formation is the *Cauchy-characteristic matching*, the combination of a space-time based numerical scheme in the interior strong-field region with a characteristic scheme in the outer parts. In the form of Cauchy-characteristic extraction, *i.e.* ignoring the injection of information from the characteristic evolution into the inner Cauchy evolution, this approach has been used to extract gravitational waves with high accuracy from numerical simulations of compact objects [64, 65].

For simulations of spacetimes with high degrees of symmetry, it often turns out convenient to directly impose the symmetries on the shape of the line element rather than use one of the general formalisms discussed so far. As an example, we consider the classic study by May and White [66, 67] of the dynamics of spherically symmetric perfect fluid stars. A spherically symmetric spacetime can be described in terms of the simple line element

$$ds^2 = -a^2(x,t)dt^2 + b^2(x,t)dx^2 - R^2(x,t)d\Omega_2^2\,, \tag{45}$$

where $d\Omega_2^2$ is the line element of the 2-sphere. May and White employ Lagrangian coordinates co-moving with the fluid shells which is imposed through the form of the energy-momentum tensor $T^0{}_0 = -\rho(1+\epsilon)$, $T^1{}_1 = T^2{}_2 = T^3{}_3 = P$. Here, the rest-mass density ρ, internal energy ϵ, and pressure P are functions of the radial and time coordinates. Plugging the line element (45) into the Einstein equations (2) with $D=4$, $\Lambda=0$ and the equations of conservation of energy momentum $\nabla_\mu T^\mu{}_\alpha = 0$ results in a set of equations for the spatial and time derivatives of the metric and matter functions amenable for a numerical treatment; *cf.* Sec. II in [66] for details.

3. Higher dimensional numerical relativity

Many BH studies, in particular those connected with high-energy physics, involve higher-dimensional spacetimes [68, 69]. For this reason, we have kept the number of spacetime dimensions D as a free parameter in the above discussion of the Einstein equations. In practice, however, numerical relativity simulations of generic D-dimensional spacetimes are restricted by the computational resources available. Traditional BH simulations in $D=4$ dimensions are performed on clusters using $\mathcal{O}(100)$ cores and need $\mathcal{O}(100)$ Gb of memory for storage of the field variables on the computational domain. Each of the three spatial dimensions is resolved with $\mathcal{O}(100)$ grid points, such that each extra dimension increases the number of grid points and, hence, the memory requirement by a factor of around 100. The number of floating point operations needed for each evolution step in time increases even faster because in addition to the increase in grid points, the number of terms in the Einstein equations also increases with D. In spite of the rapid advance of computer technology, numerical relativity simulations of fully generic spacetimes are in all likelihood unrealistic for any number $D>5$. Bearing also in mind that the community already has available robust codes for $D=4$, it appears tempting to reduce the description of higher-dimensional spacetimes with appropriate degrees of symmetry to an effectively four-dimensional problem; see [70–72] for recent reviews.

It turns out that many particularly interesting BH studies fall into this category. In this section, we will discuss two approaches that have been developed to reformulate the equations governing D-dimensional vacuum spacetimes with SO$(D-3)$ isometry as an effectively four-dimensional problem.

For cases of even higher symmetry, the approach of directly enforcing these symmetries on the line element as discussed in Sec. 2.6 has also been used with great success, but it appears unlikely that this approach can be pushed beyond spacetimes that vary in more than one or two spatial directions.

3.1. Dimensional reduction by isometry

The idea of dimensional reduction has originally been developed by Geroch [73] for four-dimensional spacetimes possessing one Killing field as for example in the case of axisymmetry; for numerical applications, see for example [74–76]. This formalism has been generalized to the case of arbitrary spacetime dimensions and number of Killing vectors by Cho and collaborators in [77, 78]. A comprehensive summary of this approach including examples and the complete form of the Einstein equations is given by Zilhão [79]. The starting point is the general D-dimensional spacetime metric written in coordinates adapted to the symmetry

$$\begin{aligned} ds^2 = G_{\mu\nu}dx^\mu dx^\nu \;&=\; \left(g_{\bar\mu\bar\nu} + e^2\kappa^2 g_{ab}B^a{}_{\bar\mu}B^b{}_{\bar\nu}\right)dx^{\bar\mu}dx^{\bar\nu} \\ &\quad +2e\kappa B^a{}_{\bar\mu}g_{ab}dx^{\bar\mu}dx^b + g_{ab}dx^a dx^b\,. \end{aligned} \tag{46}$$

Here, barred Greek indices $\bar\mu$, ... run from 0 to 3, early Latin indices a, ... from 4 to $D-1$ and κ and e represent a scale parameter and a coupling constant that will soon drop out and play no role in the eventual spacetime reduction. We note that the 3+1 split of the metric in Eq. (5) is merely a special case of this general metric decomposition and that the metric (46) is fully general in the same sense as the spacetime metric in the ADM split.

The special case of a SO$(D-3)$ isometry corresponds to the rotational symmetry on an S^{D-4} sphere and admits $(n+1)n/2$ Killing fields $\xi_{(\boldsymbol{i})}$, where $n \equiv D-4$ stands for the number of extra dimensions. For $n=2$, for instance, there exist three Killing fields given in spherical coordinates by $\xi_{(\mathbf{1})} = \partial_\phi$, $\xi_{(\mathbf{2})} = \sin\phi\,\partial_\theta + \cot\theta\,\cos\phi\,\partial_\phi$, $\xi_{(\mathbf{3})} = \cos\phi\,\partial_\theta - \cot\theta\,\sin\phi\,\partial_\phi$.

Killing's equation $\mathcal{L}_{\xi_{(\boldsymbol{i})}}g_{AB} = 0$ implies that

$$\mathcal{L}_{\xi_{(\boldsymbol{i})}}g_{ab} = 0\,, \qquad \mathcal{L}_{\xi_{(\boldsymbol{i})}}B^a{}_{\bar\mu} = 0\,, \qquad \mathcal{L}_{\xi_{(\boldsymbol{i})}}g_{\bar\mu\bar\nu} = 0\,. \tag{47}$$

From these conditions, we can draw the following conclusions. *(i)* $g_{ab} = e^{2\psi(x^\mu)}h_{ab}$, where h_{ab} is the metric on the S^n sphere with unit radius and ψ is a free field; *(ii)* $g_{\bar\mu\bar\nu} = g_{\bar\mu\bar\nu}(x^{\bar\mu})$ in adapted coordinates; *(iii)* $[\xi_{(\boldsymbol{i})}, B_{\bar\mu}] = 0$.

For $n \geq 2$, there furthermore exist no non-trivial vector fields on S^{D-4} that commute with all Killing fields, so that $B^a{}_{\bar{\mu}} = 0$. The case of $D = 5$ is special in that there exists only one Killing field $\xi_{(\mathbf{1})}$ for $\mathrm{SO}(D-3)$ isometry and this last conclusion cannot be made. Instead, we consider for $D = 5 \Leftrightarrow n = 1$ the more restricted class of $\mathrm{SO}(D-2)$ isometries, *i.e.* axially symmetric spacetimes, for which $B^a{}_{\bar{\mu}} = 0$.

A tedious but straightforward calculation [79] shows that the components of the D-dimensional Ricci tensor can then be written as

$$\begin{aligned}
R_{ab} &= \Big\{(D-5) - e^{2\psi}\left[(D-4)\partial^{\bar{\mu}}\psi\partial_{\bar{\mu}}\psi + \nabla^{\bar{\mu}}\partial_{\bar{\mu}}\psi\right]\Big\}\, h_{ab}\,,\\
R_{\bar{\mu}a} &= 0\,,\\
R_{\bar{\mu}\bar{\nu}} &= \mathcal{R}_{\bar{\mu}\bar{\nu}} - (D-4)(\nabla_{\bar{\nu}}\partial_{\bar{\mu}}\psi - \partial_{\bar{\mu}}\psi\,\partial_{\bar{\nu}}\psi)\,,\\
R &= \mathcal{R} + (D-4)\Big[(D-5)e^{-2\psi} - 2\nabla^{\bar{\mu}}\partial_{\bar{\mu}}\psi - (D-3)\partial^{\bar{\mu}}\psi\,\partial_{\bar{\mu}}\psi\Big]\,,
\end{aligned} \tag{48}$$

where $\mathcal{R}_{\bar{\mu}\bar{\nu}}$ and $\mathcal{R}$ respectively denote the 3+1 dimensional Ricci tensor and scalar associated with the 3+1 metric $\bar{g}_{\bar{\mu}\bar{\nu}} \equiv g_{\bar{\mu}\bar{\nu}}$. The D-dimensional vacuum Einstein equations with vanishing cosmological constant $\Lambda = 0$ then become

$$\mathcal{R}_{\bar{\mu}\bar{\nu}} = (D-4)(\nabla_{\bar{\nu}}\partial_{\bar{\mu}}\psi + \partial_{\bar{\mu}}\psi\,\partial_{\bar{\nu}}\psi)\,, \tag{49}$$

$$e^{2\psi}\left[(D-4)\partial^{\bar{\mu}}\psi\,\partial_{\bar{\mu}}\psi + \nabla^{\bar{\mu}}\partial_{\bar{\mu}}\psi\right] = (D-5)\,. \tag{50}$$

One important comment is in order at this stage. If we describe the three spatial dimensions in terms of the Cartesian coordinates $(x,\, y,\, z)$, one of these is a quasi-radial coordinate. Without loss of generality, we choose z and the computational domain is given by $x,\, y \in \mathbb{R}$, $z \geq 0$. In consequence of the radial nature of the z direction, $e^{2\psi} = 0$ at $z = 0$. Numerical problems arising from this coordinate singularity can be avoided by working instead with a rescaled version of the variable $e^{2\psi}$. More specifically, we also include the BSSN conformal factor χ in the redefinition and define

$$\zeta \equiv \frac{\chi}{z^2} e^{2\psi}\,. \tag{51}$$

The BSSN version of the D-dimensional vacuum Einstein equations (49) is then given by Eqs. (28)–(32) where the indices I, J, M, ... now run from 1 to 3, *i.e.* are replaced by i, j, m, ..., and we have quasi-matter terms

$$
\begin{aligned}
\frac{4\pi(\rho+S)}{D-4} &= (D-5)\frac{\chi}{\zeta}\frac{\tilde{\gamma}^{zz}\zeta-1}{z^2}-\frac{2D-7}{4\zeta}\tilde{\gamma}^{mn}\partial_m\eta\;\partial_n\chi-\chi\frac{\tilde{\Gamma}^z}{z}-\frac{KK_\zeta}{\zeta}\\
&\quad-\frac{K^2}{3}+\frac{D-6}{4}\frac{\chi}{\zeta^2}\tilde{\gamma}^{mn}\partial_m\zeta\;\partial_n\zeta+\frac{\tilde{\gamma}^{mn}}{2\zeta}\left(\chi\tilde{D}_m\partial_n\zeta-\zeta\tilde{D}_m\partial_n\chi\right)\\
&\quad+(D-4)\frac{\tilde{\gamma}^{zm}}{z}\left(\frac{\chi}{\zeta}\partial_m\zeta-\partial_m\chi\right)+\frac{D-1}{4}\tilde{\gamma}^{mn}\frac{\partial_m\chi\;\partial_n\chi}{\chi}\\
&\quad-\frac{1}{2}\frac{\tilde{\gamma}^{zm}}{z}\partial_m\chi-(D-5)\left(\frac{K_\zeta}{\zeta}+\frac{K}{3}\right)^2, \qquad (52)\\
\frac{8\pi\chi S_{ij}^{\mathrm{TF}}}{D-4} &= -\left(\frac{K_\zeta}{\zeta}+\frac{K}{3}\right)\tilde{A}_{ij}+\frac{1}{2}\left[\frac{2\chi}{z\zeta}\left(\delta^z{}_{(j}\partial_{i)}\zeta-\zeta\tilde{\Gamma}^z_{ij}\right)+\frac{1}{2\chi}\partial_i\chi\;\partial_j\chi\right.\\
&\quad-\tilde{D}_i\partial_j\chi+\frac{\chi}{\zeta}\tilde{D}_i\partial_j\zeta+\frac{1}{2\chi}\tilde{\gamma}_{ij}\tilde{\gamma}^{mn}\partial_n\chi\left(\partial_m\chi-\frac{\chi}{\zeta}\partial_m\zeta\right)\\
&\quad\left.-\tilde{\gamma}_{ij}\frac{\tilde{\gamma}^{zm}}{z}\partial_m\chi-\frac{\chi}{2\zeta^2}\partial_i\zeta\;\partial_j\zeta\right]^{\mathrm{TF}}, \qquad (53)\\
\frac{16\pi j_i}{D-4} &= \frac{2}{z}\left(\delta^z{}_i\frac{K_\zeta}{\zeta}-\tilde{\gamma}^{zm}\tilde{A}_{mi}\right)+\frac{2}{\zeta}\partial_iK_\zeta-\frac{K_\zeta}{\zeta}\left(\frac{1}{\chi}\partial_i\chi+\frac{1}{\zeta}\partial_i\zeta\right)\\
&\quad+\frac{2}{3}\partial_iK-\tilde{\gamma}^{nm}\tilde{A}_{mi}\left(\frac{1}{\zeta}\partial_n\zeta-\frac{1}{\chi}\partial_n\chi\right). \qquad (54)
\end{aligned}
$$

The evolution of the field ζ is determined by Eq. (50) which in terms of the BSSN variables becomes

$$
\begin{aligned}
\partial_t\zeta &= \beta^m\partial_m\zeta-2\alpha K_\zeta-\frac{2}{3}\zeta\partial_m\beta^m+2\zeta\frac{\beta^z}{z}, \qquad (55)\\
\partial_tK_\zeta &= \beta^m\partial_mK_\zeta-\frac{2}{3}K_\zeta\partial_m\beta^m+2\frac{\beta^z}{z}K_\zeta-\frac{1}{3}\zeta(\partial_t-\mathcal{L}_\beta)K-\chi\zeta\frac{\tilde{\gamma}^{zm}}{z}\partial_m\alpha\\
&\quad-\frac{1}{2}\tilde{\gamma}^{mn}\partial_m\alpha\;(\chi\partial_n\zeta-\zeta\partial_n\chi)+\alpha\left[(5-D)\chi\frac{\zeta\tilde{\gamma}^{zz}-1}{z^2}+\chi\zeta\frac{\tilde{\Gamma}^z}{z}\right.\\
&\quad+(4-D)\chi\frac{\tilde{\gamma}^{zm}}{z}\partial_m\zeta+\frac{2D-7}{2}\zeta\frac{\tilde{\gamma}^{zm}}{z}\partial_m\chi+\frac{6-D}{4}\frac{\chi}{\zeta}\tilde{\gamma}^{mn}\partial_m\zeta\;\partial_n\zeta\\
&\quad+\frac{2D-7}{4}\tilde{\gamma}^{mn}\partial_m\zeta\;\partial_n\chi+\frac{1-D}{4}\frac{\zeta}{\chi}\tilde{\gamma}^{mn}\partial_m\chi\;\partial_n\chi+(D-6)\frac{K_\zeta^2}{\zeta}\\
&\quad\left.+\frac{2D-5}{3}KK_\zeta+\frac{D-1}{9}\zeta K^2+\frac{1}{2}\tilde{\gamma}^{mn}\left(\zeta\tilde{D}_m\partial_n\chi-\chi\tilde{D}_m\partial_n\zeta\right)\right]. \qquad (56)
\end{aligned}
$$

It has been demonstrated by Zilhão *et al.* [80] how all terms containing factors of z in the denominator[1] can be regularized using the symmetry properties of tensors and their derivatives across $z = 0$ and assuming that the spacetime does not contain a conical singularity.

3.2. The Cartoon method

The *Cartoon method* has originally been developed by Alcubierre *et al.* [81] in order to evolve axisymmetric four-dimensional spacetimes using an effectively two-dimensional Cartesian grid. For this purpose, the grid merely includes a small number of ghostzones in the third spatial dimension which are needed to evaluate derivatives through finite differencing expressions. Integration in time, however, is performed exclusively on the two-dimensional plane, whereas the ghostzones are filled in after each timestep by appropriate interpolation of the fields in the plane and subsequent rotation of the solution using the axial spacetime symmetry. A generalized version of this method has been applied to $D = 5$ dimensional spacetimes by Yoshino and Shibata [82]. For arbitrary spacetime dimensions, however, even the relatively small number of ghostzones required in every extra dimension leads to a substantial increase in the computational resources; for fourth-order finite differencing, for example, five ghostzones are required in each extra dimension resulting in an increase of the computational domain by an overall factor 5^{D-4}. An elegant scheme to avoid this difficulty while preserving all advantages of the Cartoon method has been developed by Shibata and Yoshino [83] and is sometimes referred to as the *modified Cartoon method.*

Let us consider, for illustrating this method, a D-dimensional spacetime with $\mathrm{SO}(D-3)$ symmetry and Cartesian coordinates $x^\mu = (t, x, y, z, w^a)$, where $a = 4, \ldots, D-1$. Without loss of generality, the coordinates are chosen such that the $\mathrm{SO}(D-3)$ symmetry implies rotational symmetry in the planes spanned by each choice of two coordinates from (z, w^a). The goal is to obtain a formulation of the D-dimensional Einstein equations (28)–(36) with $\mathrm{SO}(D-3)$ symmetry that can be evolved exclusively on the xyz hyperplane. The tool employed for this purpose is to use the spacetime symmetries in order to trade derivatives off the hyperplane, *i.e.* in the w^a directions, for derivatives inside the hyperplane. Furthermore, the symmetry implies relations between the D-dimensional components of the BSSN variables.

These relations are obtained by applying a coordinate transformation from Cartesian to polar coordinates in any of the two-dimensional planes spanned by z and w, where $w \equiv w^a$ for any particular choice

[1] Note that in their work the radial variable is y instead of z.

of $a \in [4, \ldots, D-1]$

$$\begin{aligned} \rho &= \sqrt{z^2+w^2}\,, \qquad & z = \rho\cos\varphi\,, \\ \varphi &= \arctan\frac{w}{z}\,, \qquad & w = \rho\sin\varphi\,. \end{aligned} \tag{57}$$

Spherical symmetry in $n = D-4$ dimensions implies the existence of $n(n+1)/2$ Killing vectors, one for each plane with rotational symmetry. For each Killing vector ξ, the Lie derivative of the spacetime metric vanishes $\mathcal{L}_\xi g_{\mu\nu}$. For the zw plane, in particular, the Killing vector field is $\xi = \partial_\varphi$ and the Killing condition is given by the simple relation

$$\partial_\varphi g_{\mu\nu} = 0\,. \tag{58}$$

All ADM and BSSN variables are constructed from the spacetime metric and a straightforward calculation demonstrates that, therefore, the Lie derivatives along ∂_φ of all these variables vanish. For $D \geq 6$, we can always choose the coordinates such that for $\mu \neq \varphi$, $g_{\mu\varphi} = 0$ which implies the vanishing of the BSSN variables $\beta^\varphi = \tilde{\gamma}^{\mu\varphi} = \tilde{\Gamma}^\varphi = 0$. The case of SO$(D-3)$ isometry in $D = 5$ dimensions is special in the same sense as already discussed in Sec. 3.1 and the vanishing of the $\mu\varphi$ components does not in general hold. As before, we therefore consider in $D = 5$ the more restricted class of SO$(D-2)$ isometry. Finally, the Cartesian coordinates w^a can always be chosen such that the diagonal metric components are equal

$$\gamma_{w^1w^1} = \gamma_{w^2w^2} = \ldots \equiv \gamma_{ww}\,. \tag{59}$$

We note that these properties are independent of the particular choice of plane from the coordinates $(z,\, w^a)$. We can now exploit these properties in order to trade derivatives in the desired manner. We shall illustrate this for the second w derivative of the ww component of a symmetric tensor-density of weight $\mathcal{W}$ which transforms under change of coordinates according to

$$T_{\bar{\alpha}\bar{\beta}} = D^{\mathcal{W}} \frac{\partial x^\mu}{\partial x^{\bar{\alpha}}} \frac{\partial x^\nu}{\partial x^{\bar{\beta}}} T_{\mu\nu}\,, \qquad D \equiv \det\left(\frac{\partial x^\mu}{\partial x^{\bar{\alpha}}}\right)\,. \tag{60}$$

Specifically, we consider the coordinate transformation (57), where $D = \rho$. This transformation implies

$$\partial_w T_{ww} = \frac{\partial\rho}{\partial w}\partial_\rho T_{ww} + \frac{\partial\varphi}{\partial w}\partial_\varphi T_{ww}\,, \tag{61}$$

where

$$T_{ww} = D^{-\mathcal{W}} \left(\frac{\partial\rho}{\partial w}\frac{\partial\rho}{\partial w}T_{\rho\rho} + 2\frac{\partial\rho}{\partial w}\frac{\partial\varphi}{\partial w}T_{\rho\varphi} + \frac{\partial\varphi}{\partial w}\frac{\partial\varphi}{\partial w}\right)\,. \tag{62}$$

Inserting (62) into (61) and setting $T_{\rho\varphi} = 0$ yields a lengthy expression involving derivatives of $T_{\rho\rho}$ and $T_{\varphi\varphi}$ with respect to ρ and φ. The latter vanish due to symmetry and we substitute for the ρ derivatives using

$$\begin{aligned}
\partial_\rho T_{\rho\rho} &= \left(\frac{\partial z}{\partial\rho}\partial_z + \frac{\partial w}{\partial\rho}\partial_w\right)\left[D^{\mathcal{W}}\left(\frac{\partial z}{\partial\rho}\frac{\partial z}{\partial\rho}T_{zz} + 2\frac{\partial z}{\partial\rho}\frac{\partial w}{\partial\rho}T_{zw} + \frac{\partial w}{\partial\rho}\frac{\partial w}{\partial\rho}T_{ww}\right)\right], \\
\partial_\rho T_{\varphi\varphi} &= \left(\frac{\partial z}{\partial\rho}\partial_z + \frac{\partial w}{\partial\rho}\partial_w\right)\left[D^{\mathcal{W}}\left(\frac{\partial z}{\partial\varphi}\frac{\partial z}{\partial\varphi}T_{zz} + 2\frac{\partial z}{\partial\varphi}\frac{\partial w}{\partial\varphi}T_{zw} + \frac{\partial w}{\partial\varphi}\frac{\partial w}{\partial\varphi}T_{ww}\right)\right].
\end{aligned} \tag{63}$$

This gives a lengthy expression relating the z and w derivatives of T_{ww}. Finally, we recall that we need the relation of these derivatives in the xyz hyperplane and therefore set $w = 0$. In order to obtain an expression for the second w derivative of T_{ww}, we first differentiate the expression with respect to w and then set $w = 0$. The final result is given by

$$\partial_w T_{ww} = 0\,, \qquad \partial_w\partial_w T_{ww} = \frac{\partial_z T_{ww}}{z} + 2\frac{T_{zz} - T_{ww}}{z^2}\,. \tag{64}$$

Note that the density weight dropped out of this calculation, so that Eq. (64) is valid for the BSSN variables $\tilde{A}_{\mu\nu}$ and $\tilde{\gamma}_{\mu\nu}$.

Applying a similar procedure to all components of scalar, vector and symmetric tensor densities gives all expressions necessary to trade derivatives off the xyz hyperplane for those inside it. We summarize the expressions using the following notation: a late Latin index, $i = 1, \ldots, 3$ stands for either x, y or z, whereas an early Latin index, $a = 4, \ldots, D-1$ represents any of the w^a directions. For scalar, vector and tensor fields Ψ, V and T we obtain

$$\begin{aligned}
0 &= \partial_a\Psi = \partial_i\partial_a\Psi = V^a = \partial_i V^a = \partial_a\partial_b V^c = \partial_a V^i = \partial_a T_{bc} = \partial_i\partial_a T_{bc} \\
&= T_{ia} = \partial_a\partial_b T_{ic} = \partial_a T_{ij} = \partial_i\partial_a T_{jk}\,, \\
\partial_a\partial_b\Psi &= \delta_{ab}\frac{\partial_z\Psi}{z}\,, \\
\partial_a V^b &= \delta^b{}_a\frac{V^z}{z}\,, \\
\partial_i\partial_a V^b &= \delta^b{}_a\left(\frac{\partial_i V^z}{z} - \delta_{iz}\frac{V^z}{z^2}\right), \\
\partial_a\partial_b V^i &= \delta_{ab}\left(\frac{\partial_z V^i}{z} - \delta^i_z\frac{V^z}{z^2}\right), \\
T_{ab} &= \delta_{ab}T_{ww}\,, \\
\partial_a\partial_b T_{cd} &= (\delta_{ac}\delta_{bd} + \delta_{ad}\delta_{bc})\frac{T_{zz} - T_{ww}}{z^2} + \delta_{ab}\delta_{cd}\frac{\partial_z T_{ww}}{z}\,,
\end{aligned}$$

$$
\begin{aligned}
\partial_a T_{ib} &= \delta_{ab} \frac{T_{iz} - \delta_{iz} T_{ww}}{z}, \\
\partial_i \partial_a T_{jb} &= \delta_{ab} \left(\frac{\partial_i T_{jz} - \delta_{jz} \partial_i T_{ww}}{z} - \delta_{iz} \frac{T_{jz} - \delta_{jz} T_{ww}}{z^2} \right), \\
\partial_a \partial_b T_{ij} &= \delta_{ab} \left(\frac{\partial_z T_{ij}}{z} - \frac{\delta_{iz} T_{jz} + \delta_{jz} T_{iz} - 2\delta_{iz}\delta_{jz} T_{ww}}{z^2} \right).
\end{aligned} \tag{65}
$$

By trading or eliminating derivatives using these relations, a numerical code can be generated to evolve D-dimensional spacetimes with $\mathrm{SO}(D-3)$ symmetry on a strictly three-dimensional computational grid. We finally note that z is a quasi-radial variable so that $z \geq 0$.

4. Additional ingredients for numerical relativity

In the previous two sections, we have seen how the Einstein equations can be recast as an initial value problem and how we can reformulate the higher-dimensional evolution equations as an effectively four-dimensional problem assuming rotational symmetries in the extra dimensions. We thus have at hand a choice of formulations to evolve a spacetime using supercomputers. The complete modeling of BH spacetimes, however, requires a set of further ingredients. Specifically, we need to address the following issues:

- We have described how the fields evolve according to Einstein's theory. But we need to provide initial data that *(i)* satisfy the Hamiltonian and momentum constraints and *(ii)* represent a realistic initial snapshot of the physical system under consideration.

- The Einstein equations do not predict the lapse function α and the shift vector β^I. These represent the coordinate freedom and need to be chosen in a way that ensures a long-term stability of the numerical evolutions.

- We need to discretize the evolution equations such that a computer can handle them; computers deal with numbers and discretization prescribes the particular way to convert the continuum equations into a recipe for evolving large but finite sets of numbers.

- Once we have a complete numerical evolution, we need to extract physical results. Quite often, quantities we are familiar with from the Newtonian physics are not well defined in general relativity and even quantities that are, typically require a good deal of care to be extracted in a gauge invariant manner from the sets of numbers provided by the computer.

The purpose of this section is to review the main techniques used to address these items.

4.1. Initial data

As we have seen in Sec. 2, initial data to be used in time evolutions of the Einstein equations need to satisfy the Hamiltonian and momentum constraints (20), (21). A comprehensive overview of this approach to generate initial data is given by Cook's Living Review [84]; for recent lecture notes see also [85]. Here, we merely summarize some key concepts.

One obvious way to obtain such constraint satisfying initial data is to directly use analytical solutions to the Einstein equations as, for example, the Schwarzschild solution in $D = 4$ in isotropic coordinates

$$ds^2 = -\left(\frac{M-2r}{M+2r}\right)^2 dt^2 + \left(1+\frac{M}{2r}\right)^4 \left[dr^2 + r^2\left(d\theta^2 + \sin^2\theta\, d\phi^2\right)\right] . \quad (66)$$

Naturally, the numerical evolution of an analytically known spacetime solution does not generate new physical insight. It still serves as an important way to test numerical codes and, more importantly, analytically known solutions often form the starting point to construct generalized classes of initial data whose time evolution is not known without numerical study. Classic examples of such generalized analytic initial data are the Misner [86] and Brill–Lindquist [87] solutions describing n non-spinning BHs at the moment of time symmetry. In Cartesian coordinates, the Brill–Lindquist data generalized to arbitrary D is given by

$$K_{IJ} = 0\,, \quad \gamma_{IJ} = \psi^{\frac{4}{D-3}}\delta_{IJ}\,, \quad \psi = 1+\sum_A \frac{\mu_A^{D-3}}{4\left[\sum_{k=1}^{D-1}\left(x^k - x_0^k\right)^2\right]^{\frac{D-3}{2}}}\,, \quad (67)$$

where the summations over A and k run over the number of BHs, and the spatial coordinates, respectively, and μ_A are parameters related to the mass of the Ath BH through the surface area S_{D-2} of the $(D-2)$ hypersphere by $\mu_a^{D-3} = 16\pi M/[(D-2)S_{D-2}]$.

A systematic way to generate solutions to the constraints describing BHs is based on the York–Lichnerowicz split [88–90] originally developed for $D = 4$ spacetime dimensions. This split employs a conformal spatial metric defined by $\gamma_{ij} = \psi^4\bar{\gamma}_{ij}$; note that in contrast to the BSSN variable $\tilde{\gamma}_{ij}$, in general $\det\bar{\gamma}_{ij} \neq 1$. By applying a *conformal traceless split* to the extrinsic curvature according to

$$K_{ij} = A_{ij} + \tfrac{1}{3}\gamma_{ij}K\,, \qquad A^{ij} = \psi^{-10}\bar{A}_{ij} \quad \Leftrightarrow \quad A_{ij} = \psi^{-2}\bar{A}_{ij}\,, \quad (68)$$

and further decomposing $\bar{A}_{ij}$ into a longitudinal and a transverse traceless part, the momentum constraints simplify significantly; see [84] for details as well as a discussion of the alternative *physical transverse-traceless split* and *conformal thin-sandwich decomposition* [91]. The conformal thin-sandwich approach, in particular, provides a method to generate initial data for the lapse and shift which minimize the initial rate of change of the spatial metric, *i.e.* data in a quasi-equilibrium configuration [92, 93].

Under the further assumption of vanishing trace of the extrinsic curvature $K=0$, a flat conformal metric $\bar{\gamma}_{ij}=f_{ij}$, where f_{ij} describes a flat Euclidean space, and asymptotic flatness $\lim_{r\to\infty}\psi=1$, the momentum constraint admits an analytic solution known as the Bowen–York data [94]

$$\bar{A}_{ij}=\frac{3}{2r^2}\left[P_i n_j+P_j n_i-(f_{ij}-n_i n_j)P^k n_k\right]+\frac{3}{r^3}\left(\epsilon_{kil}S^l n^k n_j+\epsilon_{kjl}S^l n^k n_i\right)\,, \tag{69}$$

where $r=\sqrt{x^2+y^2+z^2}$, the unit radial vector is $n^i=x^i/r$ and P^i, S^i are user-specified parameters. By calculating the momentum associated with the asymptotic translational and rotational Killing vectors $\xi^i_{(k)}$ [95], one can show that P^i and S^i represent the total linear and angular momentum of the initial hypersurface. The linearity of the momentum constraint further allows us to superpose solutions $\bar{A}^{(A)}_{ij}$ of the type (69) and the total momenta are merely obtained by summing the individual $P^i_{(A)}$, $S^i_{(A)}$. For the generalization of Misner data, it is necessary to construct inversion-symmetric solutions of the type (69) using the method of images [84, 94]. Such a procedure is not required for generalizing Brill–Lindquist data where a superposition of solutions $\bar{A}^{(a)}_{ij}$ of the type (69) can be used directly to calculate the extrinsic curvature from Eq. (68) and insert the resulting expressions into the vacuum Hamiltonian constraint given with the above listed simplifications by

$$\bar{\nabla}^2\psi+\tfrac{1}{8}K^{mn}K_{mn}\psi^{-7}=0\,. \tag{70}$$

Here, $\bar{\nabla}^2$ is the Laplace operator associated with the flat metric f_{ij}. This elliptic equation is commonly solved by decomposing ψ into a Brill–Lindquist piece $\psi_{\rm BL}=\sum_{A=1}^N m_A/|\vec{r}-\vec{r}_A|$ plus a regular piece $u=\psi-\psi_{\rm BL}$, where $\vec{r}_A$ denotes the location of the Ath BH and m_A its bare-mass parameter. Brandt and Brügmann [96] have proven existence and uniqueness of C^2 regular solutions u to Eq. (70) and the resulting *puncture* data are the starting point of the majority of numerical BH evolutions using the BSSN moving puncture technique.

In spite of its popularity, there remain a few caveats with puncture data that have inspired explorations of alternative initial data. In particular, it has been shown by Garat and Price [97] that there exist no conformally flat spatial slices of the Kerr spacetime. Constructing puncture data of a single BH with the non-zero Bowen–York parameter S^i will, therefore, inevitably result in a hypersurface containing a BH plus some additional content which typically manifests itself in numerical evolutions as spurious gravitational waves, colloquially referred to as the "junk radiation". For rotation parameters close to the limit of extremal Kerr BHs, the amount of spurious radiation rapidly increases leading to an upper limit of the dimensionless spin parameter $\chi \approx 0.93$ for conformally flat Bowen–York-type data [98–101]; BH initial data of the Bowen–York type with a spin parameter above this value rapidly relax to rotating BHs with spin $\chi \approx 0.93$, probably through absorption of some fraction of the spurious radiation. Lovelace *et al.* [101, 102] overcome this limit by instead constructing initial data with an extended version of the conformal thin-sandwich method applied to superposed Kerr–Schild BHs [103].

In practice, puncture data are the method-of-choice for most evolutions performed with the BSSN-moving-puncture technique whereas GHG evolution schemes commonly start from conformal-thin-sandwich data using either conformally flat or Kerr–Schild background data. Alternatively to both these approaches, Pretorius has also employed initial data containing scalar fields which rapidly collapse to one or more BHs; see *e.g.* [33].

4.2. Gauge conditions

We have seen in Sec. 2 that the Einstein equations do not make any predictions about the gauge functions; the ADM equations leave lapse α and shift β^i unspecified and the GHG equations make no predictions about the source functions H^α. Instead, these functions can be freely specified by the user and represent the coordinate diffeomorphism or gauge invariance of the theory of general relativity. Whereas the physical properties of a spacetime remain unchanged under gauge transformations, the performance of numerical evolution schemes depends sensitively on the coordinate choice. It is well-known, for example, that evolutions of the Schwarzschild spacetime employing geodesic slicing $\alpha = 1$ and vanishing shift $\beta^i = 0$ inevitably reach the BH singularity after a coordinate time interval $t = \pi M$ [104]; computers respond to singular functions with non-assigned numbers (NaNs) which rapidly swamp the entire computational domain and render further evolution in time practically useless. This problem can be avoided by controlling the lapse function such that the evolution in proper time slows down in the vicinity of singular points in the spacetime. Such slicing conditions are called *singularity avoiding* and have been studied systematically in the form of the Bona–Massó family of slicing conditions [105]; see also [39, 106]. A potential problem arising from the use of singularity avoiding slicing is the different progress in proper time in different regions of the computational domain resulting in a phenomenon often referred to as *grid stretching* or *slice stretching* which can be compensated with suitable non-zero choices for the shift vector [107].

The particular coordinate conditions used with great success in the BSSN based moving puncture approach [108, 109] are variants of the so-called "1+log" slicing and "Γ-driver" shift condition [107]

$$\begin{aligned} \partial_t\alpha &= \beta^M\partial_M\alpha - 2\alpha K\,, && (71)\\ \partial_t\beta^i &= \beta^M\partial_M\beta^I + \tfrac{3}{4}B^I\,, && (72)\\ \partial_t B^I &= \beta^M\partial_M B^I + \partial_t\tilde{\Gamma}^I - \beta^M\partial_M\tilde{\Gamma}^I - \eta B^I\,. && (73)\end{aligned}$$

Here, η is specified either as a constant, a function depending on the coordinates x^i and BH parameters [110], a function of the BSSN variables [111, 112], or evolved as an independent variable [113]. Van Meter *et al.* have furthermore suggested a first-order-in-time evolution equation for β^i resulting from integration of Eqs. (72), (73)

$$\partial_t\beta^I = \beta^M\partial_M\beta^I + \tfrac{3}{4}\tilde{\Gamma}^I - \eta\beta^I\,. \tag{74}$$

Some numerical relativity codes omit the advection derivatives of the form $\beta^M\partial_M$ from Eqs. (71)–(74).

BH simulations with the GHG formulation employ a wider range of coordinate conditions. For example, Pretorius' breakthrough evolutions [33] set $H_i = 0$ and

$$\Box H_t = -\xi_1\frac{\alpha-1}{\alpha^\eta} + \xi_2 n^\mu\partial_\mu H_t\,, \tag{75}$$

with parameters $\xi_1 = 19/m$, $\xi_2 = 2.5/m$, $\eta = 5$, where m denotes the mass of a single BH. One of the different choices used in the Caltech–Cornell–CITA SpEC code specifies H_α such that the dynamics are minimized at early stages of the evolution, gradually changes these to harmonic gauge $H_\alpha = 0$ during the binary inspiral and uses a damped harmonic gauge near merger

$$H_\alpha = \mu_0\left[\ln\left(\frac{\sqrt{\gamma}}{\alpha}\right)\right]^2\left[\ln\left(\frac{\sqrt{\gamma}}{\alpha}\right)n_\alpha - \alpha^{-1}g_{\alpha m}\beta^m\right]\,, \tag{76}$$

where μ_0 is a free parameter; see [114, 115] for details. We note in this context that the GHG source functions H^α are related to the ADM lapse and shift functions through [40]

$$\begin{aligned} n^\mu H_\mu &= -K - n^\mu\partial_\mu\ln\alpha\,, && (77)\\ \gamma^{\mu i}H_\mu &= -\gamma^{mn}\Gamma^i_{mn} + \gamma^{im}\partial_m\ln\alpha + \frac{1}{\alpha}n^\mu\partial_\mu\beta^i\,. && (78)\end{aligned}$$

4.3. Discretization of the equations

In the previous sections, we have derived formulations of the Einstein equations in the form of an initial value problem. Given an initial snapshot of the physical system under consideration, the evolution equations, as for example in the form of the BSSN equations (28)–(32), then predict the evolution of the system in time. These evolution equations take on the form of a set of non-linear partial differential equations which relate a number of grid variables and their time and spatial derivatives. Computers, on the other hand, exclusively operate with (large sets of) numbers and for a numerical simulation we need to translate the differential equations into expressions relating arrays of numbers. This procedure is typically referred to as *discretization* and the most common approach to achieve this goal, *finite differencing*, will be the subject of this section.

Alternative methods of discretization are *finite element*, *finite volume* and *spectral* methods. While the former two are popular over a wide range of computational applications, they have not been applied to time evolutions of BH spacetimes yet. Spectral methods provide a particularly efficient and accurate approach for numerical modeling provided the functions do not develop discontinuities. Even though BH spacetimes contain singularities, the use of singularity excision provides a tool to remove these from the computational domain. The Caltech–Cornell–CITA group has used this approach with great success to evolve inspiralling and merging BH binaries with very high accuracy; see *e.g.* [116–119]. Spectral methods have also been used successfully for the modeling of spacetimes with high degrees of symmetry [120–122] and play an important role in the construction of initial data [123–125]. The main advantage of finite differencing methods is their comparative simplicity. Furthermore, it is not yet clear to what extent spectral methods are able to match the strong robustness of finite difference techniques that have facilitated rather straightforward evolutions of BHs in various extreme cases such as collisions near the speed of light [126–128] or binaries with mass ratios up to 1:100 [129–131]. An in-depth discussion of spectral methods is beyond the scope of these notes but the interested Reader is referred to the review by Grandclément and Novak [132].

4.3.1. Finite differencing

We discuss finite differencing for the case of one time and one spatial dimension labeled by t and x, respectively; the extension to more spatial dimensions will be evident. Let us consider for this purpose a physical domain covering some range in the t and x direction, $t_{\rm ini} \leq t \leq t_{\rm fin}$ and $x_{\rm min} \leq x \leq x_{\rm max}$. The first step in discretizing the problem is to replace this domain by a finite set of points

$$x_i = x_0 + k\,\Delta x\,, \qquad t_n = t_0 + n\,\Delta t\,, \tag{79}$$

where $t_0 = t_{\rm ini}$, $x_0 = x_{\rm min}$, $k = 0, \ldots, K-1$ and $n = 0, \ldots, N-1$ are integer indices and Δt and Δx are the spacing in time and space assumed to be constants in the remainder of this discussion. This is illustrated in Fig. 3 which shows some grid points at two values of time t_n and t_{n+1}. A physical variable $f(t,x)$ is represented in this picture by an array of numbers $f^n_k \equiv \hat{f}(t_n, x_k)$ representing approximations to an exact *continuum solution* $f(t_n, x_k)$. In practice, one often uses one single array of numbers containing all function values at a fixed value of time $f_k|_{t=t_n}$. A set of initial data then corresponds to a set of values $f_k|_{t=t_0}$ and our task is to derive an algorithm for calculating the values $f_k|_{t=t_1}$ from the $f_k|_{t=t_0}$, then calculate the $f_k|_{t=t_2}$ from $f_k|_{t=t_1}$ and so on.

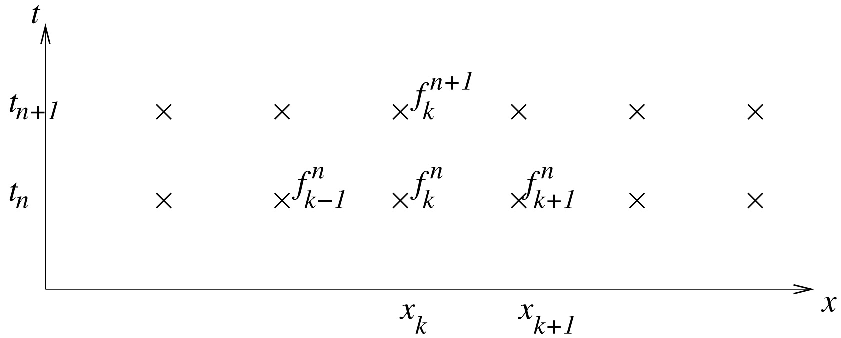

Fig. 3. A 1+1 dimensional domain with coordinates t and x is represented by a finite set of points $(t_n,\, x_k)$ labeled by indices n and k. A grid variable f is represented by its values f^n_k at the points $(t_n,\, x_k)$ in the spacetime.

This is achieved by replacing derivatives $\partial_x f$ and $\partial_t f$ appearing in the differential equations with approximations involving values of f at several neighboring grid points through Taylor expansion. As an example, we consider derivative $\partial_x f$ at a grid point $(t_n,\, x_k)$. By Taylor expanding f around this point, we obtain

$$\begin{aligned} f_{k-1} &= f_k - f'_k \Delta x + \tfrac{1}{2} f''_k \Delta x^2 + \mathcal{O}\left(\Delta x^3\right)\,, \\ f_k &= f_k\,, \\ f_{k+1} &= f_k + f'_k \Delta x + \tfrac{1}{2} f''_k \Delta x^2 + \mathcal{O}\left(\Delta x^3\right)\,, \end{aligned} \tag{80}$$

where primes denote spatial derivatives and we have suppressed the index n. We next write the derivative $f'_k = (\partial_x f)_k$ as a linear combination

$$f'_k = A f_{k-1} + B f_k + C f_{k+1}\,, \tag{81}$$

insert the expressions (80) and compare the coefficients on both sides of the resulting equation. We thus obtain three equations for A, B and C

$$0 = A + B + C\,, \qquad 1 = (-A + C)\Delta x\,, \qquad 0 = \tfrac{1}{2}A\Delta x^2 + \tfrac{1}{2}C\Delta x^2\,. \quad (82)$$

The solution is quickly found to be $A = -1/(2\Delta x)$, $B = 0$ and $C = 1/(2\Delta x)$ so that

$$f'_k = \frac{f_{k+1} - f_{k-1}}{2\Delta x} + \mathcal{O}\left(\Delta x^2\right)\,. \quad (83)$$

The term $\mathcal{O}(\Delta x^2)$ demonstrates that this approximation is accurate to second order in the grid resolution Δx. By including more neighbors and higher-order terms in the Taylor expansion, it is straightforward to obtain the higher-order approximations for f'_k. The same procedure can be applied to time derivatives and a first-order approximation is given by

$$\dot{f}^n = \frac{f^{n+1} - f^n}{\Delta t} + \mathcal{O}(\Delta t)\,, \quad (84)$$

where we now suppress the spatial index k and $\dot{f} \equiv \partial_t f$.

One of the simplest partial differential equations is the *advection equation* $\partial_t f + \partial_x f = 0$, where we can use Eqs. (83) and (84) to replace $\partial_x f$ and $\partial_t f$ and, after solving for f_k^{n+1}, obtain an *explicit* expression for the function value on the new time slice t_{n+1} exclusively in terms of function values at t_n

$$f_k^{n+1} = f_k^n + \frac{\Delta t}{\Delta x}\frac{f_{k+1}^n - f_{k-1}^n}{2}\,. \quad (85)$$

While this provides a simple algorithm to successively update grid points at time t_{n+1} in terms of already known function values at t_n, it unfortunately turns out to be numerically unstable. For this simple example, the unstable behavior of the *forward in time centered in space* scheme (85) can be demonstrated analytically by performing a Fourier decomposition and using von Neumann's stability analysis [133]. A simple cure for this problem consists in replacing the centered *stencil* (83) by a first-order version

$$f'_k = \frac{f_k - f_{k-1}}{\Delta x} + \mathcal{O}(\Delta x) \quad (86)$$

and replace $\partial_x f$ in the advection equation using this expression. Numerical stability is a complex topic worthy of a review in its own right and we have included this relatively simple example of a numerically unstable algorithm here as a warning sign that apparently useful algorithms may turn out to be unsuitable in practice. For a more extended discussion of stability analysis, we refer the Reader to the classic book *Numerical Recipes* [134] and references therein.

The finite differencing expressions discussed here are of relatively low order and require at most one neighbor in each spatial direction in order to update a grid variable in time. In practice, most BH evolution codes use 4th, 6th or 8th order accurate stencils for spatial discretization and a 4th order Runge–Kutta scheme for integration in time.

4.3.2. Mesh refinement

Black-hole spacetimes often involve length scales that differ by orders of magnitude. The BH horizon extends over lengths of the order of $\mathcal{O}(1)\ M$, where M is the mass of the BH. Inspiralling BH binaries, on the other hand, emit gravitational waves with wavelengths of $\mathcal{O}(10^2)\ M$. Furthermore, gravitational waves are rigorously defined only at infinity. In practice, wave extraction is performed at finite radii but these need to be large enough to ensure that systematic errors are small. In order to accommodate accurate wave extraction, computational domains used for the modeling of asymptotically flat BH spacetimes typically have a size of $\mathcal{O}(10^3)\ M$. With present computational infrastructure it is not possible to evolve such large domains with a uniform high resolution that is sufficient to accurately model the steep profiles arising near the BH horizon. The solution to this difficulty is the use of mesh refinement, *i.e.* a grid resolution that depends on the location in space and may also vary in time.

The use of mesh refinement in BH modeling is simplified by the remarkably rigid nature of BHs which rarely exhibit complicated structure beyond some mild deformation of a sphere. The requirements of increased resolution are therefore simpler to implement than, say, in the modeling of airplanes or helicopters. In BH spacetimes, the grid resolution must be highest near the BH horizon and it decreases gradually at larger and larger distances from the BH. In terms of the internal bookkeeping, this allows for a particularly efficient manner to arrange regions of refinement which is often referred to as *moving boxes*. A set of nested boxes with outwardly decreasing resolution is centered on each BH of the spacetime and follows the BH motion. These sets of boxes are immersed in one or more common boxes which are large enough to accommodate those centered around the BHs. As the BHs approach each other, boxes originally centered on the BHs merge into one and become part of the common-box hierarchy. A snapshot of such moving boxes is displayed in Fig. 4.

Mesh refinement in numerical relativity has been pioneered by Choptuik in his seminal study on critical phenomena in the collapse of scalar fields [135]. The first application of mesh refinement to the evolution of BH binaries was performed by Brügmann [136]. There exists a variety of mesh refinement packages available for use in numerical relativity as for example Paramesh [137], or Samrai [138]. The most common package in use

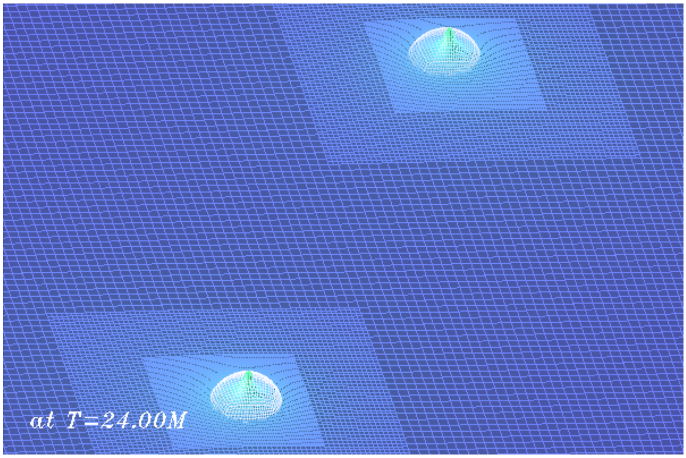

Fig. 4. Illustration of mesh refinement for a BH binary with one spatial dimension suppressed. Around each BH (marked by the spherical apparent horizon), two nested boxes are visible. These are immersed within one large, common grid or *refinement level*.

in contemporary numerical relativity codes is Schnetter's Carpet [139, 140] which is integrated into the Cactus Computational Toolkit [141]; see also the Einstein Toolkit webpage [142] and the lecture notes [143]. Carpet uses Berger–Oliger [144] mesh refinement which we will illustrate here for the case of two refinement levels in one spatial dimension. The generalization to more spatial dimensions and more levels covering a wider range of resolutions will be evident.

Let us consider for this purpose the two one-dimensional boxes illustrated in the top panel of Fig. 5 at time t: a coarse grid or refinement level represented by circles (black) and a fine grid represented by crosses (red). In practice, the resolutions are often chosen such that the grid spacing of the two levels differs by a factor of two and use the same Courant factor $\Delta t/\Delta x$. Furthermore, we assume that there is no staggering of grids such that every second point of the fine grid coincides with a point of the coarse grid. For simplicity, we discuss here the case of a simple evolution stencil such as those discussed in Sec. 4.3.1 where the update in time at location x_k requires information from one neighboring point in either direction. For the case of higher-order stencils or more complex time integration schemes employing *predictor-corrector* steps, the communication steps between the two refinement levels remain unchanged but apply to a larger number of points on the edge of the fine grid.

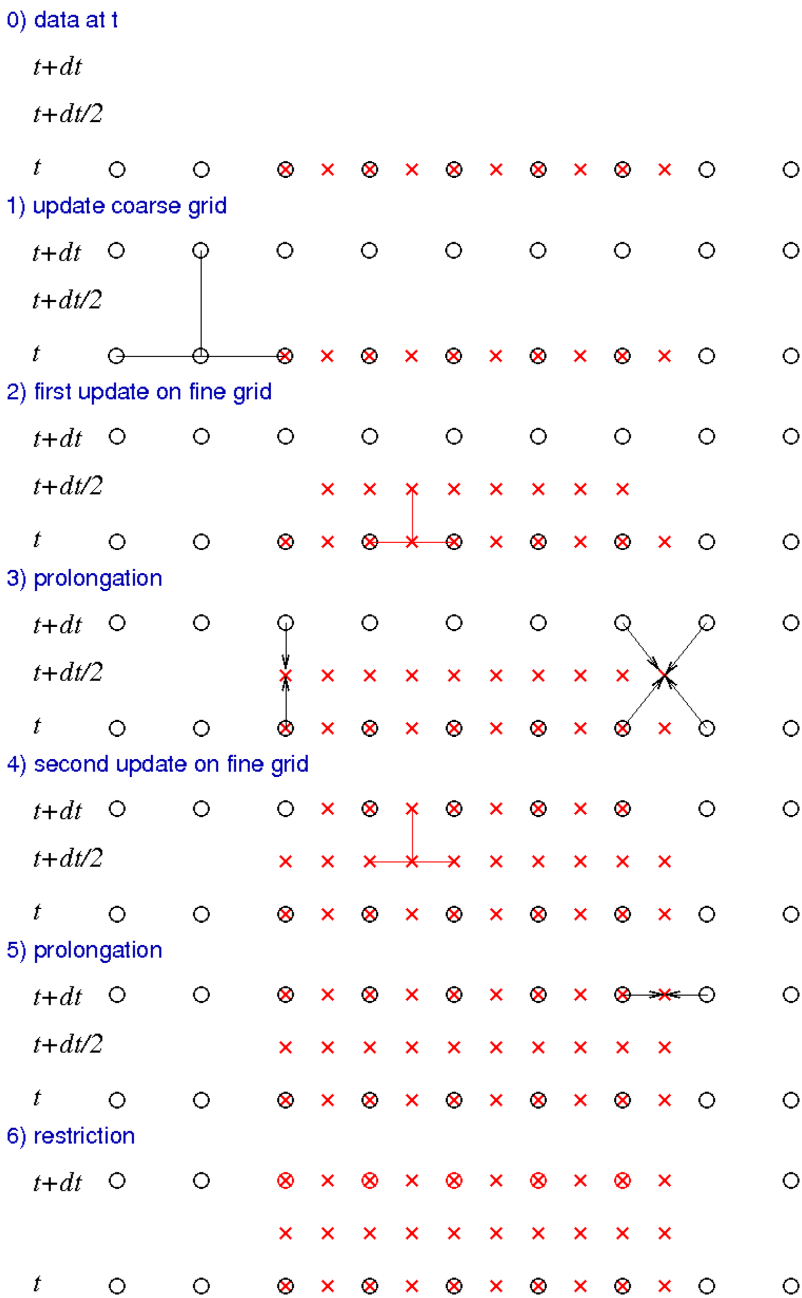

Fig. 5. Evolution of a grid variable from t to $t + dt$ using Berger–Oliger mesh refinement. See the text for details.

The goal of evolving data from time t to $t+dt$ is achieved in the following six steps:

1. Update of variables from t to dt on the coarser grid; *cf.* panel 0 to panel 1 (counted from top down) in Fig. 5. Note that the existence of the finer grid is not felt at this stage.

2. Update of variables from t to $t + dt/2$ on the finer grid; *cf.* panel 2 in Fig. 5. On the edge of the fine grid, this update cannot be performed because the neighbors required for the evolution stencil are not available.

3. Points on the outer boundary of the fine grid are filled through interpolation from data on the coarse grid. This process is called *prolongation*; *cf.* panel 3 in Fig. 5.

4. Update of variables from $t + dt/2$ to dt on the fine grid; *cf.* panel 4. Again, the outer edge of the fine grid cannot be updated due to lack of neighboring points.

5. Prolongation onto fine grid at time $t + dt$; *cf.* panel 5 in Fig. 5.

6. Over the range of overlap, data is interpolated from the fine to the coarse grid; *cf.* panel 6. This process is called *restriction*.

In this procedure, the prolongation and restriction operation constitute the communication between the two refinement levels which otherwise are evolved as if they were separate uniform domains. In the case of > 2 refinement levels, the same scheme is applied; evolution always starts on the coarsest grid and then takes place on consecutively finer grids until these have caught up in time with the next coarser refinement level. It is possible for the interior refinement components to change in size or move with respect to the coarser levels. Whenever new grid points arise in this process, they are initialized through interpolation from the next coarser refinement level analogous to the prolongation operation. Naturally, the outermost refinement level is not allowed to move or expand in this scheme. The order of interpolation typically depends on the order of finite differencing applied to the normal evolution of variables. Common choices are to use 5th order polynomials for interpolation in space and 2nd order polynomials in time; see Table 3 in [145] for an overview of choices by different numerical relativity groups. The main reason for using lower-order polynomials in time is the need to store data on an increasingly larger number of time levels for the higher-order interpolation which significantly increases the demand in computer memory.

Mesh refinement thus provides an efficient way to evolve grid points with a position dependent resolution. The only exception are points of the outer boundary of the outermost refinement level and, possibly, points near the BH singularity. These points require special handling which we discuss in the next subsection on boundary conditions.

4.4. Boundary conditions

In numerical relativity, we typically encounter two types of physical boundaries, *(i)* inner boundaries due to the treatment of spacetime singularities in BH solutions and *(ii)* the outer boundary either at infinite distance from the strong field sources or, in the form of an approximation to this scenario, at the outer edge of the computational domain at large but finite distances.

Singularity excision: BH spacetimes generically contain singularities, either physical singularities with a divergent Ricci scalar or coordinate singularities where the spacetime curvature is well behaved but some tensor components approach zero or infinite values. In the case of the Schwarzschild solution (1), for example, $r = 0$ corresponds to a physical singularity, whereas the singular behavior of the metric components g_{tt} and g_{rr} at $r = 2M$ merely reflects the unsuitable nature of the coordinates as $r \to 2M$ and can be cured, for example, by transforming to the Kruskal–Szekeres coordinates; *cf.* for example Chapter 7 in [146]. Both types of singularities give rise to trouble in the numerical modeling of spacetimes because computers only handle finite numbers. Some control is available in the form of gauge conditions as discussed in Sec. 4.2; the evolution of proper time is slowed down when the evolution gets close to a singularity. In general, however, BH singularities require some special numerical treatment.

Such a treatment is most commonly achieved in the form of *singularity* or *black hole excision* originally suggested by Unruh as quoted in Thornburg [147]. According to Penrose's *Cosmic Censorship Conjecture*, a spacetime singularity should be cloaked inside an event horizon and the spacetime region outside the event horizon is causally disconnected from the dynamics inside. The excision technique is based on the corresponding assumption that the numerical treatment of the spacetime inside the horizon has no causal effect on the exterior. In particular, excising a finite region around the singularity but within the horizon should leave the exterior spacetime unaffected. This is illustrated in Fig. 6 where the excision region is represented by small white circles which are excluded from the numerical evolution. Regular grid points, represented in the figure by black circles, on the other hand, are evolved normally. As we have seen in the previous section, the numerical evolution in time of functions at a particular grid point typically requires information from neighboring grid points. The updating of variables at regular points, therefore, requires data on the excision boundary represented in Fig. 6 by gray circles. Inside the BH horizon, represented by the large circle in the figure, however, information can only propagate inwards, so that the variables on the excision boundary can be obtained through extrapolation from gridpoints further outside; see for example [148]. Alternatively, one-sided derivative stencils such as the advection stencil in Eq. (86) can be employed. Singularity excision has been used with great success in many numerical BH evolutions [32, 33, 149–153].

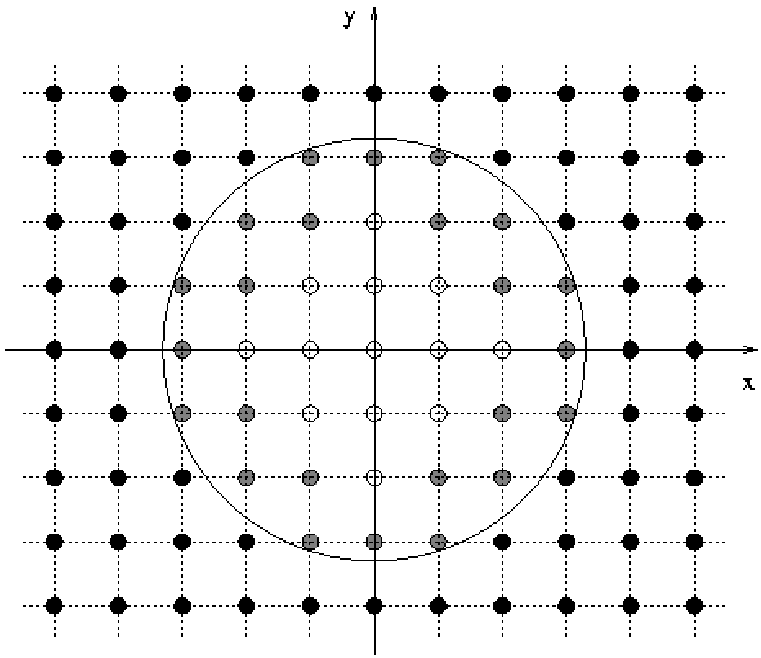

Fig. 6. Illustration of singularity excision. The small circles represent vertices of a numerical grid on a two dimensional cross section of the computational domain containing the spacetime singularity, in this case at the origin. A finite region around the singularity but with in the event horizon (large circle) is excluded from the numerical evolution (white circles). Gray circles represent the excision boundary where function values can be obtained through extrapolation. The regular evolution of exterior grid points (black circles) is performed using standard techniques using information also on the excision boundary.

Quite remarkably, the moving puncture method for evolving BHs does not employ any such specific numerical treatment near BH singularities, but instead applies the same evolution procedure for points arbitrarily close to singularities as for points far away and appears "to get away with it". In view of the remarkable success of the moving puncture method, various authors have explored the behavior of the puncture singularity in the case of a single Schwarzschild BH [154–159]. Initially, the puncture represents spatial infinity on the *other* side of the wormhole geometry compactified into a single point. Under numerical evolution using moving puncture gauge conditions, however, the region immediately around this singularity rapidly evolves into a so-called trumpet geometry which is partially covered by the numerical grid to an extent that depends on the numerical resolution; *cf.* Fig. 1 in Brown [158]. In practice, the singularity falls through the inevitably finite resolution of the computational grid which thus facilitates a *natural excision* of the spacetime singularity without the need of any special numerical treatment.

Outer boundary: In asymptotically flat spacetimes, the physical boundary condition is given by the fact that there exist no incoming modes, *i.e.* that information only propagates in the outward direction. In practice, such *outgoing radiation* or *Sommerfeld* boundary conditions are applied at large but finite distances from the strong-field region. For this purpose, we assume that a given grid variable f asymptotes to a constant background value f_0 in the limit of large r and contains a leading order deviation $u(t-r)/r^n$ from this value, where n is a constant, typically positive, integer number. For $r \to \infty$, we therefore have

$$f(t,r) = f_0 + \frac{u(t-r)}{r^n}\,, \tag{87}$$

where the dependence on retarded time represents the outgoing nature of the radiative deviations. In consequence, $\partial_t u + \partial_r u = 0$ which translates into the following condition for the grid variable f

$$\partial_t f + n\frac{f-f_0}{r} + \frac{x^I}{r}\partial_I f = 0\,, \tag{88}$$

where x^I denote Cartesian coordinates and $\partial_I = \partial/\partial x^I$. Because information only propagates outwards, the spatial derivative $\partial_I f$ is evaluated using a one-sided stencil, evaluated using the methods described in Sec. 4.3.1. A second-order accurate stencil in the x direction, for example, is given by $\partial_x f = (3f_k - 4f_{k-1} + f_{k-2})/(2\Delta x)$. This method is straightforwardly generalized to asymptotically expanding cosmological spacetimes of the de Sitter type containing BHs; *cf.* Eq. (9) in Zilhão *et al.* [160].

In asymptotically AdS spacetimes, the outer boundary represents a more challenging problem. This is largely a consequence of the singular behavior of the AdS metric even in the absence of a BH or any matter sources. The AdS metric is the maximally symmetric solution to the Einstein equations (2) with $T_{\alpha\beta} = 0$ and $\Lambda < 0$. This solution can be represented by the hyperboloid $X_0^2+X_D^2-\sum_{i=1}^{D-1} X_i^2 = L^2$ embedded in a flat $D+1$ dimensional spacetime with metric

$$ds^2 = -dX_0^2 - dX_D^2 + \sum_{i=1}^{D-1} dX_i^2 \,. \tag{89}$$

The anti-de Sitter spacetime AdS_D in global coordinates is then obtained by transforming to coordinates $\tau,\ \rho,\ \omega_i$

$$X_0 = L\frac{\cos\tau}{\cos\rho}\,, \qquad X_D = L\frac{\sin\tau}{\cos\rho}\,, \qquad X_i = L\tan\rho\,\omega_i \quad \text{for} \quad i = 1\ldots D-1\,, \tag{90}$$

with hyperspherical coordinates $\sum_{i=1}^{D-1}\omega_i^2 = 1$. In $D = 5$, for example, $\omega_1 = \sin\chi\,\sin\theta\,\cos\phi$, $\omega_2 = \sin\chi\,\sin\theta$, $\omega_3 = \sin\chi\,\cos\theta$, $\omega_4 = \cos\chi$ and $d\Omega_{D-2}^2 = d\chi^2 + \sin^2\chi\,(d\theta^2 + \sin^2\theta\,d\phi^2)$. The AdS_D metric is then given by

$$ds^2 = \frac{L^2}{\cos^2\rho}\left(-d\tau^2 + d\rho^2 + \sin^2\rho\,d\Omega_{D-2}^2\right)\,, \tag{91}$$

where $0 \le \rho < \pi/2$, $\ -\pi < \tau \le \pi$ and $\Lambda = -(D-1)(D-2)/(2L^2)$. By unwrapping the cylindrical time direction, the range of the time coordinate is often extended to $\tau \in \mathbb{R}$.

An alternative representation of the AdS spacetime is given by Poincaré coordinates $(t,\ z,\ x^i)$, $i = 1\ldots D-1$

$$\begin{aligned} X_0 &= \frac{1}{2z}\left[z^2 + L^2 + \sum_{i=1}^{D-2}\left(x^i\right)^2 - t^2\right]\,, \qquad X_a = \frac{Lx^a}{z}\,,\\ X_{D-1} &= \frac{1}{2z}\left[z^2 - L^2 + \sum_{i=1}^{D-2}\left(x^i\right)^2 - t^2\right]\,, \qquad X_D = \frac{Lt}{z}\,, \end{aligned} \tag{92}$$

where $a = 1,\ldots,D-2$. This leads to the metric

$$ds^2 = \frac{L^2}{z^2}\left[-dt^2 + dz^2 + \sum_{i=1}^{D-2}\left(dx^i\right)^2\right]\,, \tag{93}$$

with $z > 0,\ t \in \mathbb{R}$. It can be shown that the Poincaré coordinates cover only a half of the hyperboloid and that the other half corresponds to $z < 0$ [161].

Clearly, both the global (91) and the Poincaré version (93) of the AdS metric become singular at their respective outer boundaries $\rho \to \pi/2$ or $z \to 0$. The induced metric at infinity is therefore only defined up to a conformal rescaling. This remaining freedom manifests itself in the boundary topology of the global and Poincaré metrics which, respectively, become in the limit $\rho \to \pi/2$ and $z \to 0$

$$ds^2_{\rm gl} \sim -d\tau^2 + d\Omega^2_{D-2}\,, \qquad ds^2_{\rm P} \sim -dt^2 + \sum_{i=1}^{D-2} \left(dx^i\right)^2\,. \tag{94}$$

In the context of the gauge–gravity duality, this implies that gravity in the global or Poincaré AdS are related to conformal field theories (CFT) on spacetimes of different topology: $\mathbb{R} \times S_{D-2}$ in the former and $\mathbb{R}^{D-1}$ in the latter case.

The boundary treatment inside a numerical modeling of asymptotically AdS spacetimes needs to take care of the singular nature of the metric. In practice, this is achieved through some form of regularization which makes use of the fact that the singular piece of an asymptotically AdS spacetime is known in analytic form, *e.g.* through Eqs. (91) or (93). Bantilan *et al.* [152] decompose the spacetime metric into an analytically known AdS part plus a deviation and numerically evolve the deviations which are regular at infinity. They notice, however, that particular care needs to be taken of the gauge conditions to ensure that the coordinates remain compatible with this decomposition throughout the simulation. An alternative approach consists in factoring out appropriate factors involving the bulk coordinate as, for example, the term $\cos\rho$ in the denominator on the right-hand side of Eq. (91). This method is employed, for example, in the studies of Chesler and Yaffe [122], Heller *et al.* [162], and Bizoń and Rostworowski [163].

We finally note that the boundary plays an active role in AdS spacetimes. The visualization of the AdS spacetime in the form of a Penrose diagram demonstrates that it is not globally hyperbolic, *i.e.* there exists no Cauchy surface on which initial data can be specified in such a way that the entire future of the spacetime is uniquely determined. This is in marked contrast to the Minkowski spacetime. Put in other words, the outer boundary of asymptotically flat spacetimes is represented in a Penrose diagram by a null surface such that information cannot propagate from infinity into the interior spacetime. In contrast, the outer boundary of asymptotically AdS spacetimes is timelike and, hence, the outer boundary actively influences the evolution of the interior. The specification of boundary conditions in numerical relativity applications to the gauge–gravity duality or AdS/CFT correspondence therefore reflects part of the description of the physical system under study. Chesler and Yaffe [120], for example, use this degree of freedom to perturb a strongly coupled $\mathcal{N} = 4$ supersymmetric Yang–Mills plasma away from equilibrium and evolve its subsequential isotropization.

5. Diagnostics

Once we have numerically generated a spacetime, there still remains the question of how to extract physical information from the large chunk of numbers the computer has written to the hard drive. This analysis of the data faces two main problems in numerical relativity applications, *(i)* the gauge or coordinate dependence of the results and *(ii)* the fact that many quantities we are familiar with from the Newtonian physics are hard or not even possible to define in a rigorous fashion in general relativity. In spite of these difficulties, a number of valuable diagnostic tools have been developed and purpose of this section is to review how these are extracted.

The physical information is often most conveniently calculated from the ADM variables and we assume for this discussion that a numerical solution is available in the form of the ADM variables γ_{IJ}, K_{IJ}, α and β^I. Even if the time evolution has been performed using other variables as, for example, the BSSN or GHG variables the conversion between these and their ADM counterparts according to Eq. (26) or (5) is straightforward.

Before reviewing the extraction of physical information from a numerical simulation, we note a potential subtlety arising from the convention used for Newton's constant in higher-dimensional spacetimes. We wrote the Einstein equations in the form (2) and chose units, where $G = 1$ and $c = 1$. In particular, we thus adopted the convention of not applying any geometrical factors to G in $D \neq 4$ dimensions. As we shall see below, with this convention the Schwarzschild radius of a static BH in D dimensions is given by

$$R_{\mathrm{S}}^{D-3} = \frac{16\pi GM}{(D-2)\varOmega_{D-2}}\,, \qquad \varOmega_{D-2} = \frac{2\pi^{(D-1)/2}}{\varGamma\left(\frac{D-1}{2}\right)}\,, \tag{95}$$

where $\varOmega_{D-2}$ denotes the area of the unit S^{D-2} hypersphere. As a consequence, Hawking's entropy formula $S = \mathcal{A}_{\mathrm{AH}}/(4G)$ remains unchanged in D dimensions but Newton's force law in the limit of weak fields and small velocities acquires geometrical factors and is given by [164]

$$\boldsymbol{F} = \frac{(D-3)8\pi G}{(D-2)\varOmega_{D-2}}\frac{Mm}{r^{D-2}}\hat{\boldsymbol{r}}\,. \tag{96}$$

Here, M and m are the masses of the two bodies and $\hat{\boldsymbol{r}}$ is the unit vector along the line of sight between the particles.

5.1. Global quantities and horizons

For spacetimes described by a metric that is asymptotically flat and time independent, the total mass-energy and linear momentum are given by the ADM mass and ADM momentum. These quantities arise from boundary terms in the Hamiltonian of general relativity and were derived by Arnowitt, Deser and Misner [18] in their canonical analysis of the theory. They are given in terms of the ADM variables by

$$M_{\rm ADM} = \frac{1}{16\pi G}\lim_{r\to\infty}\oint_{S_r}\delta^{MN}(\partial_N\gamma_{MK}-\partial_K\gamma_{MN})\hat{r}^K dS\,, \tag{97}$$

$$P_I = \frac{1}{8\pi G}\lim_{r\to\infty}\oint_{\Omega_r}(K_{MI}-\delta_{MI}K)\hat{r}^M dS\,. \tag{98}$$

Here, the spatial tensor components γ_{IJ} and K_{IJ} are assumed to be given in Cartesian coordinates. $\hat{r}^M$ is the outgoing unit vector normal to the area element dS of the $D-2$ dimensional hypersphere and $dS = r^{D-2}d\Omega_{D-2}$. Under a more restrictive set of assumptions about the fall-off behavior of the metric and extrinsic curvature components, one can also derive an expression for the global angular momentum

$$J_I = \frac{1}{8\pi}\lim_{r\to\infty}\oint(K_{JK}-K\gamma_{JK})\xi^J_{(\boldsymbol{I})}\hat{r}^K dS\,, \tag{99}$$

where $\xi_{(\boldsymbol{I})}$ are the Killing vectors associated with the asymptotic rotational symmetry given in $D=4$ by $\xi_{(\boldsymbol{x})} = -z\partial_y + y\partial_z$, $\xi_{(\boldsymbol{y})} = -x\partial_z + z\partial_x$ and $\xi_{(\boldsymbol{z})} = -y\partial_x + x\partial_y$. For a more-in-depth discussion of the ADM mass and momentum as well as the conditions required for the definition of the angular momentum, the Reader is referred to Sec. 7 of Gourgoulhon's notes [20].

As an example, we calculate the ADM mass of the D-dimensional Schwarzschild BH in Cartesian, isotropic coordinates (t, x^I) described by the spatial metric

$$\gamma_{IJ} = \psi^{\frac{4}{D-3}}\delta_{ij}\,, \qquad \psi = 1 + \frac{\mu}{4r^{D-3}}\,, \tag{100}$$

and vanishing extrinsic curvature $K_{IJ} = 0$. A straightforward calculation shows that

$$\partial_K\gamma_{IJ} = -\psi^{\frac{4}{D-3}-1}\frac{\mu}{r^{D-1}}x_K\delta_{IJ}\,, \tag{101}$$

and $\hat{r}^K = \frac{x^K}{r}$, so that

$$\delta^{MN}(\partial_N\gamma_{MK}-\partial_K\gamma_{MN})\frac{x^K}{r} = (D-2)\psi^{\frac{4}{D-3}-1}\frac{\mu x_K}{r^{D-1}}\frac{x^K}{r} = (D-2)\frac{\mu}{r^{D-2}}\,, \tag{102}$$

where we have used the fact that in the limit $r\to\infty$ we can raise and lower indices with the Euclidean metric δ_{ij} and $\psi\to 1$. From Eq. (97) we thus obtain

$$\begin{aligned} M_{\rm ADM} &= \frac{1}{16\pi G}\lim_{r\to\infty}\oint_{S_r}(D-2)\frac{\mu}{r^{D-2}}r^{D-2}d\Omega_{D-2} = \frac{D-2}{16\pi G}\mu\oint d\Omega_{D-2} \\ &= \frac{D-2}{16\pi G}\mu\Omega_{D-2} = \frac{D-2}{16\pi G}\mu\frac{2\pi^{\frac{D-1}{2}}}{\Gamma\left(\frac{D-1}{2}\right)}\,. \end{aligned} \tag{103}$$

The Schwarzschild radius in areal coordinates is given by $R_{\rm S}^{D-3} = \mu$ and we have recovered Eq. (95).

The Schwarzschild radius marks the location of the event horizon of a static BH defined as the boundary between points in the spacetime from which null geodesics can escape to infinity and points from which they cannot. The event horizon is, therefore, by definition a concept that depends on the entire spacetime. In the context of numerical simulations, this implies that an event horizon can only be computed if information about the entire spacetime is stored which results in large data sets even by contemporary standards. Nevertheless, event horizon finders have been developed by Diener [165] and Cohen *et al.* [166]. For many purposes, however, it is more convenient to determine the existence of a horizon using data from a spatial hypersurface Σ_t only. Such a tool is available in the form of an *apparent horizon*. Apparent horizons are one of the most important diagnostic tools in numerical relativity and are reviewed in detail in Thornburg's Living Review article [167]. According to the cosmic censorship conjecture, existence of an apparent horizon implies an event horizon whose cross section with Σ_t either lies outside the apparent horizon or coincides with it.

The key concept underlying the apparent horizon is that of a trapped surface defined as a surface where the expansion $\Theta := \nabla_\mu k^\mu$ of a congruence of outgoing null geodesics with tangent vector k^μ vanishes. A trapped surface is defined as a surface, where $\Theta = 0$ and an apparent horizon is defined as the outermost trapped surface on a spatial hypersurface Σ_t. Translated into the ADM variables, the condition $\Theta = 0$ can be shown to lead to an elliptic equation for the unit normal direction s^I to the $D-2$ dimensional horizon surface

$$\hat{D}_M s^M - K + K_{MN} s^M s^N = 0\,. \tag{104}$$

Here, $\hat{D}$ denotes the covariant derivative with respect to the $D-2$ dimensional metric induced on the horizon surface. Numerical algorithms to solve this equation have been developed by several authors [168–172].

By eliminating $R_{\rm S}$ from Eq. (95) and the formula $A_{\rm hor} = \Omega_{D-2} R_{\rm S}^{D-2}$ for the area of a $D-2$ sphere of radius $R_{\rm S}$, we obtain an expression that relates the horizon area to a mass commonly referred to as the *irreducible mass*

$$M_{\rm irr} = \frac{(D-2)\Omega_{D-2}}{16\pi G} \left(\frac{A_{\rm hor}}{\Omega_{D-2}} \right)^{\frac{D-3}{D-2}}\,. \tag{105}$$

The irreducible mass is identical to the ADM mass for a static BH, but can be defined in this way for non-static BHs as well. In $D = 4$ dimensions this becomes $16\pi G^2 M_{\rm irr}^2 = A_{\rm hor}$. Furthermore, a rotating BH in $D = 4$ is described by a single spin parameter S and the BH mass consisting of rest mass and rotational energy has been shown by Christodoulou [173] to be given by

$$M_{\rm Chr}^2 = M_{\rm irr}^2 + \frac{S^2}{4M_{\rm irr}^2}\,. \tag{106}$$

By adding the square of the linear momentum P^2 to the right-hand side of this equation, we obtain the total energy of a spacetime containing a single BH with spin S and linear momentum P. In $D = 4$, Christodoulou's formula (106) can be used to calculate the spin from the equatorial circumference $C_{\rm e}$ and the horizon area according to [174]

$$\frac{2\pi A_{\rm hor}}{C_{\rm e}^2} = 1 + \sqrt{1-j^2}\,, \tag{107}$$

where $j = S/M_{\rm Chr}^2$ is the dimensionless spin parameter of the BH. Even though this relation is strictly valid only for the case of single stationary BHs, it provides a useful approximation in binary spacetimes as long as the BHs are sufficiently far apart.

5.2. Gravitational wave extraction

Probably the most important physical quantity to be extracted from dynamic BH spacetimes is the gravitational radiation. It is commonly extracted from numerical simulations in the form of either the Newman–Penrose scalar or a master function obtained through BH perturbation theory. Simulations using a characteristic formulation also facilitate wave extraction in the form of the Bondi mass loss formula. Here, we will focus on the former two methods; wave extraction using the Bondi formalism is discussed in detail in [62].

Newman–Penrose scalar: The formalism to extract GWs in the form of the Newman–Penrose scalar is currently fully understood only in $D = 4$ dimensions. Extension of this method is likely to require an improved understanding of the Goldberg–Sachs theorem in $D > 4$ which is subject to ongoing research [175]. The extraction method is based on the Newman–Penrose formalism originally developed in [176]. In this formalism, the outgoing GW signal is encoded in the Newman–Penrose scalar Ψ_4; see *e.g.* [177] and references therein. This scalar is defined in terms of a complex null tetrad $\mathbf{n}$, $\mathbf{k}$, $\mathbf{m}$, $\bar{\mathbf{m}}$ defined such that all their inner products vanish except $-\mathbf{k}\cdot\mathbf{n} = 1 = \mathbf{m}\cdot\bar{\mathbf{m}}$. In practice, a null tetrad can be conveniently defined in terms of the unit timelike normal vector n^α and a triad u^i, v^i, w^i of spatial vectors constructed through the Gram–Schmidt orthonormalization starting with

$$u^i = [x,\, y,\, z]\,, \qquad v^i = \left[xz,\, yz,\, -x^2-y^2\right]\,, \qquad w^i = \epsilon^i{}_{mn} v^m w^n\,, \tag{108}$$

where ϵ^{imn} represents the three-dimensional Levi-Civita tensor and x, y, z are standard Cartesian coordinates. An orthonormal tetrad of the required type is then given by

$$\mathbf{k}^\alpha = \frac{1}{\sqrt{2}}\left(n^\alpha + u^\alpha\right)\,, \qquad \mathbf{n}^\alpha = \frac{1}{\sqrt{2}}\left(n^\alpha - u^\alpha\right)\,, \qquad \mathbf{m}^\alpha = \frac{1}{\sqrt{2}}\left(v^\alpha + iw^\alpha\right)\,, \tag{109}$$

where time components of the spatial triad vectors are set to zero. The Newman–Penrose scalar Ψ_4 is then defined as

$$\Psi_4 \equiv -C_{\alpha\beta\gamma\delta}\mathbf{n}^\alpha\bar{\mathbf{m}}^\beta\mathbf{n}^\gamma\bar{\mathbf{m}}^\delta\,. \tag{110}$$

In the literature, one may also find Ψ_4 defined without the minus sign, but all physical results derived from Ψ_4 are invariant under this ambiguity. We further note that in vacuum, the Weyl and Riemann tensor are identical. Most BH studies in numerical relativity consider vacuum spacetimes, so that we can replace $C_{\alpha\beta\gamma\delta}$ in Eq. (110) with $R_{\alpha\beta\gamma\delta}$. The calculation of Ψ_4 from the ADM variables can be achieved either by constructing the spacetime metric from the spatial metric, lapse and shift vector and calculation of the spacetime Riemann or Weyl tensor through its definition given at the end of Sec. 1. Alternatively, we can use the electric and magnetic part of the Weyl tensor given by [178]

$$E_{\alpha\beta} = \perp^\mu{}_\alpha \perp^\nu{}_\beta C_{\mu\rho\nu\sigma}n^\rho n^\sigma\,, \qquad B_{\alpha\beta} = \perp^\mu{}_\alpha \perp^\nu{}_\beta {}^*C_{\mu\rho\nu\sigma}\,, \tag{111}$$

where the * denotes the Hodge dual. By using the Gauss–Codazzi equations (9), (12), one can express the electric and magnetic parts in vacuum in terms of the ADM variables according to

$$E_{ij} = \mathcal{R}_{ij} - \gamma^{mn}(K_{ij}K_{mn} - K_{im}K_{jn})\,, \qquad B_{ij} = \gamma_{ik}\epsilon^{kmn}D_m K_{nj}\,. \tag{112}$$

The Weyl tensor is then given in terms of electric and magnetic parts by Eq. (3.10) in Ref. [178]. Inserting this relation together with (109) and (112) into the definition (110) gives us the final expression for Ψ_4 in terms of spatial variables

$$\begin{aligned}\Psi_4 \;=\; & -\frac{1}{2}\left[E_{mn}\left(v^m v^n - w^m w^n\right) - B_{mn}\left(v^m w^n + w^m v^n\right)\right] \\ & +\frac{i}{2}\left[E_{mn}(v^m w^n - w^m v^n) + B_{mn}(w^m w^n + v^m v^n)\right]\,.\end{aligned} \tag{113}$$

The GW signal is often presented in the form of multipolar components $\psi_{\ell m}$ defined by projection of Ψ_4 onto spherical harmonics of spin weight -2

$$\Psi_4(t,\theta,\phi) = \sum_{lm}\psi_{lm}(t)Y^{(-2)}_{lm}(\theta,\phi) \;\Leftrightarrow\; \psi_{lm}(t) = \int \Psi_4(t,\theta,\phi)\overline{Y^{(-2)}_{lm}}(\theta,\phi)d\Omega_2\,, \tag{114}$$

where the bar denotes the complex conjugate. The ψ_{lm} are often written in terms of amplitude and phase

$$\psi_{lm} = A_{lm} e^{i\phi_{lm}}\,. \tag{115}$$

The amount of energy, linear and angular momentum carried by the GWs can be calculated from Ψ_4 according to [179]

$$\frac{dE}{dt} = \lim_{r\to\infty}\left[\frac{r^2}{16\pi}\int_{\Omega_2}\left|\int_{-\infty}^{t}\Psi_4 d\tilde{t}\right|^2 d\Omega\right], \tag{116}$$

$$\frac{dP_i}{dt} = -\lim_{r\to\infty}\left[\frac{r^2}{16\pi}\int_{\Omega_2}\ell_i\left|\int_{-\infty}^{t}\Psi_4 d\tilde{t}\right|^2 d\Omega\right], \tag{117}$$

$$\frac{dJ_i}{dt} = -\lim_{r\to\infty}\left\{\frac{r^2}{16\pi}\mathrm{Re}\left[\int_{\Omega_2}\left(\hat{J}_i\int_{-\infty}^{t}\Psi_4 d\tilde{t}\right)\left(\int_{-\infty}^{t}\int_{-\infty}^{\hat{t}}\overline{\Psi}_4 d\tilde{t}d\hat{t}\right)d\Omega\right]\right\}, \tag{118}$$

where

$$\ell_i = [-\sin\theta\,\cos\phi,\ -\sin\theta\,\sin\phi,\ -\cos\theta]\,, \tag{119}$$

$$\hat{J}_x = -\sin\phi\,\partial_\theta - \cos\phi\left(\cot\theta\,\partial_\phi + \frac{i\,s}{\sin\theta}\right), \tag{120}$$

$$\hat{J}_y = \cos\phi\,\partial_\theta - \sin\phi\left(\cot\theta\,\partial_\phi + \frac{i\,s}{\sin\theta}\right), \tag{121}$$

$$\hat{J}_z = \partial_\phi \tag{122}$$

with the spin weight $s = -2$. In practice, one often starts the integration at the start of the numerical simulation (or shortly thereafter to avoid contamination from spurious GWs contained in the initial data) rather than at $-\infty$.

We finally note that the GW strain commonly used in GW data analysis is obtained from Ψ_4 by interacting twice in time

$$h \equiv h_+ - ih_\times = \int_{-\infty}^{t}\left(\int_{-\infty}^{\tilde{t}}\Psi_4 d\hat{t}\right)d\tilde{t}\,. \tag{123}$$

h is often decomposed into multipoles in analogy to Eq. (114). As before, the practical integration is often started at finite value rather than at $-\infty$. It has been noted that this process of integrating Ψ_4 twice in time is susceptible to large nonlinear drifts. These are due to fundamental difficulties that arise in the integration of finite-length, discretely sampled, noisy data streams which can be cured or at least mitigated by performing the integration in the Fourier instead of the time domain [180].

Perturbative wave extraction: The basis of this approach to extract GWs from numerical simulations in $D = 4$ is the Regge–Wheeler–Zerilli–Moncrief formalism developed for the study of perturbations of spherically symmetric BHs. The assumption for applying their formalism to numerically generated spacetimes is that at sufficiently large distances from the GW sources, the spacetime is well approximated by a spherically symmetric background (typically the Schwarzschild or Minkowski spacetime) plus non-spherical perturbations. These perturbations naturally divide into odd and even multipoles which obey the Regge–Wheeler [181] (odd) and the Zerilli [182] (even) equations respectively. Moncrief [182] developed a gauge invariant formulation for these perturbations in terms of a master function which obeys a wave-type equation with a background dependent scattering potential; for a review and applications of this formalism see, for example, [150, 183, 184].

An extension of this formalism to extract GWs in higher-dimensional spacetimes has been developed by Kodama and Ishibashi [185]. In our summary of this formalism, we follow the work of Witek *et al.* [186] where it has been applied to the extraction of GWs from head-on collisions. As in our discussion of formulations of the Einstein equations in higher dimensions in Sec. 3, it turns out useful to introduce coordinates that are adapted to the rotational symmetry on a S^{D-2} sphere. Here, we choose spherical coordinates for this purpose which we note by $(t,\, r,\, \vartheta,\, \theta,\, \phi^a)$, where $a = 4,\, \ldots,\, D-1$; we use the same convention for indices as in Sec. 3.

We then assume that in the far-field region, the spacetime is perturbatively close to a spherically symmetric BH background given in D dimensions by the Tangherlini [187] metric

$$ds^2_{(0)} = -A(r)^2 dt^2 + A(r)^{-1} dr^2 + r^2 \left[d\vartheta^2 + \sin^2\vartheta \, \left(d\theta^2 + \sin^2\theta \, d\Omega_{D-4} \right) \right] \,, \tag{124}$$

where

$$A(r) = 1 - \frac{R_{\rm S}^{D-3}}{r^{D-3}} \,, \tag{125}$$

and $R_{\rm S}$ is the Schwarzschild radius which we already encountered in Eq. (95). For a spacetime with $\mathrm{SO}(D-3)$ isometry, the perturbations away from the background (124) are given by

$$ds^2_{(1)} = h_{AB}dx^A dx^B + h_{A\vartheta}dx^A dx^\vartheta + h_{\vartheta\vartheta}d\vartheta^2 + h_{\theta\theta}d\Omega_{D-3}\,, \tag{126}$$

where we introduce early upper case Latin indices A, B, $\ldots = 0, 1$ and $x^A = (t, r)$. The class of axisymmetric spacetimes considered in [186] obeys SO$(D-2)$ isometry which can be shown to imply that $h_{A\theta} = h_{\vartheta\theta} = 0$ and that the remaining components of h in Eq. (126) only depend on the coordinates (t, r, ϑ). As a consequence, the expansion of the metric perturbations only contains scalar spherical harmonics, but not vector or tensor harmonics; *cf.* Sec. II C in [186]. The reformulation of the Kodama–Ishibashi formalism for spacetimes obeying the less restricted class of SO$(D-3)$ isometry is still under development.

Scalar harmonics are defined as solutions of the equation

$$\tilde{\Box}\mathcal{S} = -k^2\mathcal{S}\,, \qquad k = \ell(\ell + D - 3)\,, \qquad \ell = 0, 1, 2, \ldots\,, \tag{127}$$

where $\tilde{\Box}$ refers to the covariant derivative associated with the $(D-2)$ dimensional metric $\gamma_{\bar{i}\bar{j}}$ induced on the S^{D-2} sphere described by coordinates $x^{\bar{i}} \equiv (\vartheta, \theta, \phi^a)$. It turns out convenient to define

$$\mathcal{S}_{\bar{i}} \equiv -\frac{1}{k}\partial_{\bar{i}}\mathcal{S}\,, \qquad \mathcal{S}_{\bar{i}\bar{j}} \equiv \frac{1}{k^2}\tilde{D}_{\bar{i}}\partial_{\bar{j}}\mathcal{S} + \frac{1}{D-2}\gamma_{\bar{i}\bar{j}}\mathcal{S}\,. \tag{128}$$

The metric perturbations can then be written as

$$h_{AB} = f_{AB}\mathcal{S}\,, \qquad h_{A\bar{i}} = r f_A \mathcal{S}_{\bar{i}}\,, \qquad h_{\bar{i}\bar{j}} = 2r^2\left(H_{\rm L}\gamma_{\bar{i}\bar{j}}\mathcal{S} + H_{\rm T}\mathcal{S}_{\bar{i}\bar{j}}\right)\,, \tag{129}$$

where f_{AB}, f_A, $H_{\rm L}$ and $H_{\rm T}$ are functions of (t, r). These functions are obtained in a numerical simulation through projection of the metric components onto the spherical harmonics [186]. Note that the subscripts L and T do not denote indices but are merely labels standing for longitudinal and transversal. Furthermore, the harmonics as well as the expansion functions depend on the multipolar indices ℓ, m which we have suppressed in our notation for clarity. For example, when we write f_{AB}, we implicitly assume that this stands for $f^{\ell m}_{AB}$ for some fixed values of ℓ, m.

The gauge invariant functions of the Kodama–Ishibashi formalism are given in terms of the perturbation functions by

$$F = H_{\rm L} + \frac{1}{D-2}H_{\rm T} + \frac{1}{r}X_A\hat{D}^A r\,, \qquad F_{AB} = f_{AB} + \hat{D}_B X_A + \hat{D}_A X_B\,, \tag{130}$$

where

$$X_A \equiv \frac{r}{k}\left(f_A + \frac{r}{k}\hat{D}_A H_{\rm T}\right)\,, \tag{131}$$

and $\hat{D}_A$ denotes the covariant derivative associated with (t, r) sub-sector of the background metric. Finally, the master function Φ is conveniently written in terms of its time derivative which is given by

$$\partial_t \Phi = (D-2) r^{\frac{D-4}{2}} \frac{-F^r{}_t + 2r\partial_t F}{k^2 - D + 2 + \frac{(D-2)(D-1)}{2} \frac{R_S^{D-3}}{r^{D-3}}} \,. \tag{132}$$

From the master function, we can calculate the GW energy flux

$$\frac{dE_{\ell m}}{dt} = \frac{1}{32\pi} \frac{D-3}{D-2} k^2 \left(k^2 - D + 2\right) \left(\partial_t \Phi_{\ell m}\right)^2 \,, \tag{133}$$

and the total radiated energy is obtained from integration in time and summation over all multipoles

$$E = \sum_{\ell=2}^{\infty} \sum_{m=-\ell}^{\ell} \int_{-\infty}^{\infty} \frac{dE_{\ell m}}{dt} dt \,. \tag{134}$$

In axisymmetry, we can choose a frame such that the only non-zero multipoles are those with $m = 0$ and the sum extends only over ℓ.

5.3. Diagnostics in the AdS/CFT correspondence

The gauge–gravity duality, often also referred to as the AdS/CFT correspondence because of Maldacena's prototypical example [11], relates gravity in asymptotically AdS spacetimes to conformal field theories on the boundary of this spacetime. A key ingredient of the correspondence is the relation between fields interacting gravitationally in the bulk spacetime and expectation values of the field theory on the boundary. This so-called *dictionary* has been the subject of many studies in the literature (see, for example, [188–190]). Here, we restrict our attention to the extraction of the vacuum expectation values of the energy momentum tensor $\langle T_{IJ} \rangle$ of the field theory from the fall-off behavior of the AdS metric.

Through the AdS/CFT correspondence, the vacuum expectation values $\langle T_{ij} \rangle$ of the field theory are given by the quasi-local Brown–York [191] stress-energy tensor and thus are directly related to the bulk metric. Following de Haro *et al.* [188], it is convenient to consider the (asymptotically AdS) bulk metric in Fefferman–Graham [192] coordinates

$$ds^2 = g_{\mu\nu} dx^\mu dx^\nu = \frac{L^2}{r^2} \left[dr^2 + \gamma_{ij} dx^i dx^j \right] \,, \tag{135}$$

where

$$\gamma_{ij} = \gamma_{ij}\left(r, x^i\right) = \gamma_{(0)ij} + r^2 \gamma_{(2)ij} + \ldots + r^d \gamma_{(d)ij} h_{(d)ij} r^d \log r^2 + \mathcal{O}\left(r^{d+1}\right) . \tag{136}$$

Here $d \equiv D-1$, the $\gamma_{(a)ij}$ and $h_{(d)ij}$ are functions of the boundary coordinates x^i, the logarithmic term only appears for even d and powers of r are exclusively even up to order $d-1$. As shown in [188], the vacuum expectation value of the CFT momentum tensor for $d=4$ is then obtained from

$$\begin{aligned}\langle T_{ij}\rangle &= \frac{4L^3}{16\pi G}\left\{\gamma_{(4)ij} - \frac{1}{8}\gamma_{(0)ij}\left[\gamma_{(2)}^2 - \gamma_{(0)}^{km}\gamma_{(0)}^{ln}\gamma_{(2)kl}\gamma_{(2)mn}\right]\right.\\ &\left. -\frac{1}{2}\gamma_{(2)i}{}^{m}\gamma_{(2)jm} + \frac{1}{4}\gamma_{(2)ij}\gamma_{(2)}\right\}\,, \end{aligned} \tag{137}$$

and $\gamma_{(2)ij}$ is determined in terms of $\gamma_{(0)ij}$. The dynamic freedom of the CFT is thus encapsulated in the fourth-order term $\gamma_{(4)ij}$. Note that for $r \to 0$, the metric (135) asymptotes to the AdS metric in Poincaré coordinates (93).

The Brown–York stress tensor is also the starting point for an alternative method to extract the $\langle T_{IJ}\rangle$ that does not rely on Fefferman–Graham coordinates. It is given by

$$T^{\mu\nu} = \frac{2}{\sqrt{-\gamma}}\frac{\delta S_{\rm grav}}{\delta\gamma_{\mu\nu}}\,, \tag{138}$$

where we have foliated the D-dimensional spacetime into *timelike* hypersurfaces Σ_r in analogy to the foliation in terms of *spacelike* hypersurfaces Σ_t in Sec. 2.1. The spacetime metric is given by

$$ds^2 = \alpha^2 dr^2 + \gamma_{IJ}\left(dx^I + \beta^I dr\right)\left(dx^J + \beta^J dr\right)\,, \tag{139}$$

and n^μ now denotes the outward pointing normal vector to Σ_r. In analogy to the second fundamental form $K_{\alpha\beta}$ in Sec. 2.1, we define the extrinsic curvature on Σ_r by

$$\Theta^{\mu\nu} \equiv -\tfrac{1}{2}\left(\nabla^\mu n^\nu + \nabla^\nu n^\mu\right)\,. \tag{140}$$

Balasubramanian and Kraus provide in Ref. [189] a method to cure divergences that appear in the Brown–York tensor when the boundary is pushed to infinity by adding counter terms to the action $S_{\rm grav}$. Their work discusses asymptotically AdS spacetimes of different dimensions. For AdS_5, this procedure results in

$$T^{\mu\nu} = \frac{1}{8\pi G}\left[\Theta^{\mu\nu} - \Theta\gamma^{\mu\nu} - \frac{3}{L}\gamma^{\mu\nu} - \frac{L}{2}\mathcal{G}^{\mu\nu}\right]\,, \tag{141}$$

where $\mathcal{G}_{\mu\nu} = \mathcal{R}_{\mu\nu} - \mathcal{R}\gamma_{\mu\nu}/2$ is the Einstein tensor associated with the induced metric $\gamma_{\mu\nu}$. Applied to the AdS_5 metric in global coordinates, this expression gives a non-zero energy momentum tensor $T^{\mu\nu} \neq 0$ which translated into the vacuum expectation values $\langle T^{\mu\nu} \rangle$ can be interpreted as the Casimir energy of a quantum field theory on the spacetime with topology $\mathbb{R} \times S^3$ [189]. This Casimir energy is non-dynamical and in numerical applications to the AdS/CFT correspondence may simply be subtracted from $T^{\mu\nu}$; see *e.g.* [152].

The role of additional (*e.g.* scalar) fields in the AdS/CFT dictionary is discussed, for example, in [188, 190].

6. Results from numerical BH simulations

Numerical relativity has been a highly dynamic field of research in recent years and has generated a wealth of results about BH spacetimes. Recent overviews are given in [69, 193–198]. Here, we provide a selection of some of the most exciting results and important applications. We recommend the cited review articles for Readers interested in more detailed discussions. Applications of numerical relativity can be classified into the areas of gravitational wave physics, astrophysics, high-energy physics, the gauge–gravity duality and fundamental properties of BH spacetimes. We will discuss these fields in order.

6.1. Gravitational wave physics

The main motivation for numerical relativity has for a long time been the calculation of gravitational waveforms from compact objects with the purpose of constructing waveform catalogues for the analysis of GW observation and the extraction of physical information from these observations. Due to the weak interaction of GWs with any type of matter, including the detectors, digging physical signals from the noisy data stream represents a daunting task and heavily relies on the so-called *matched filtering* techniques [199]. Matched filtering is a method used to search for signals of known form in noisy data, and works by cross-correlating the actual "signal" (*i.e.*, the detector's output) with a set of theoretical templates. Roughly speaking, a waveform catalogue consists of a large number of waveforms, each one corresponding to a specific set of source parameters. By identifying the waveform that provides maximal overlap with the observed data, one obtains an estimate for the physical parameters of the GW source.

One of the strongest type of GW sources are stellar-mass BH binaries for the frequency window of ground based detectors and supermassive BH binaries for space missions of LISA type. BH binaries in (approximately) vacuum are comparatively "clean" sources in the sense that they are uniquely defined by a relatively small set of parameters: 2 parameters for the masses M_1 and M_2 of the BHs and 6 parameters for the spin vectors $\boldsymbol{S}_1$ and $\boldsymbol{S}_2$. Vacuum BH spacetimes have no preferred length scale which, for example, manifests itself in the presence of the mass M in the Schwarzschild metric (1) exclusively in terms of the form r/M. The modeling of BH spacetimes therefore needs to consider merely 7 parameters, the spins and mass ratio $q \equiv M_1/M_2$. The mass M can be fixed trivially by a simple rescaling of the spacetime metric. Put another way, a single numerical simulation determines a one parameter family of BH spacetimes with fixed q, $\boldsymbol{S}_1$ and $\boldsymbol{S}_2$. In principle, the eccentricity of the binary orbits can appear as an additional parameter, but is typically assumed to vanish because most binaries are expected to be circularized by GW emission by the time they enter the frequency band of GW detectors [200]. We note that GW observations need to consider additional, the so-called *extrinsic* parameters such as sky location or distance, but these do not play a role in the GW source modeling.

For illustration, we show in Fig. 7 the BH trajectories and wave strain h_{22} of the last $\sim$ 11 orbits in the inspiral and merger of a non-spinning BH binary with mass ratio $q = 1/4$; for more details of the simulation, see [201]. For most purposes in GW data analysis, waveforms of this type are too short; BH binaries often spend orders of magnitude more cycles in the detectors sensitivity band which need to be contained in the waveform model. Fortunately, the post-Newtonian (PN) theory [16] provides a method to complement numerical results with efficient predictions of the GW emission during the earlier stages of the inspiral; the PN approximation breaks down during the strong-field interaction of the binary in the late inspiral and merger. Complete, so-called *hybrid* waveforms, however, can be obtained by stitching together PN and numerical waveforms; see, for example, [116, 202]. In Fig. 8 we show an example of a hybrid waveform constructed for the binary system of Fig. 7; see [201] for details.

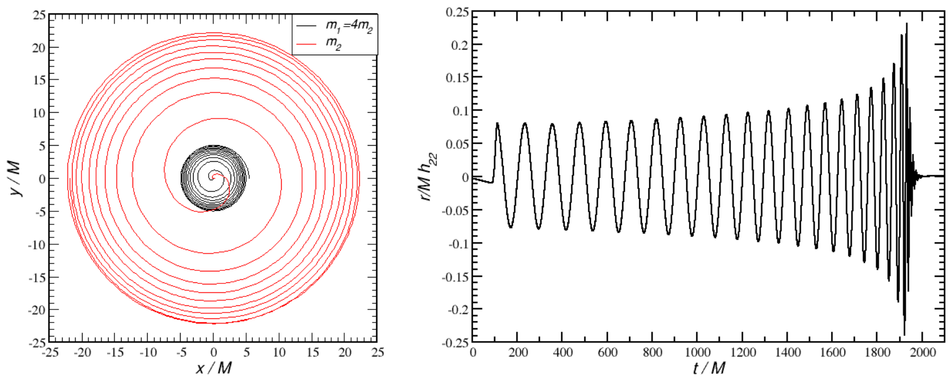

Fig. 7. Trajectories (left panel) and quadrupole wave strain (right panel) of the last 11 orbits of the inspiral of a non-spinning $q = 1/4$ BH binary.

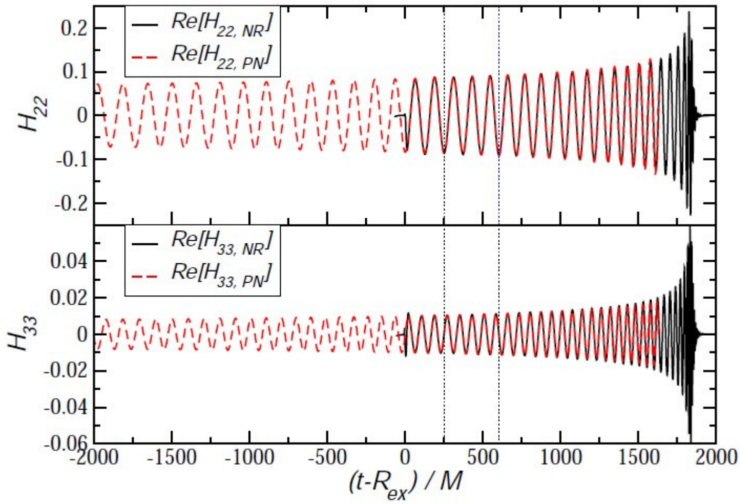

Fig. 8. A hybrid waveform for the $q = 1/4$ binary system of Fig. 7. The numerical (solid/black curves) and PN predictions (dashed/red curves) are shown for the strongest multipolar contributions h_{22} and h_{33}.

Even though, BH binaries are relatively clean systems determined by 7 parameters, the generation of a comprehensive template bank for a 7-dimensional parameter space requires a huge number of simulations if pursued by brute force; covering each parameter direction with a modest 10 simulations results in 10^7 simulations. The GW source modeling community has developed two approaches to tackle this problem in a more systematic way reducing substantially the number of required simulations.

So-called *phenomenological waveform models* use relatively simple functions based on a small number of model parameters to describe the phase and amplitude of the GW signal. One then uses numerical simulations to create a map between the physical BH parameters and the model parameters. This approach has so far been applied to non-spinning BH binaries and binary systems of rotating BHs with spins aligned with the orbital angular momentum [203–207]. Extension to spin-precessing binaries is presently under investigation and explored in particular with regard to the possibility of reducing the effective parameter space by using a single-spin approximation [208–210].

An alternative approach towards the generation of GW waveform models through inspiral, merger and ringdown is based on the effective-one-body (EOB) method [211, 212]. In this approach, the dynamics of the two-body problem in general relativity is mapped to the motion of a particle in an effective metric whose components are currently determined to 3PN order.

The EOB method improves upon this model by using additional pseudo-PN terms of higher order which are not derived from PN expressions, but calibrated via comparison with numerical relativity results [213–218]. Further improvements come from using a resummed version of the PN expanded results and from modeling nonadiabatic effects in the inspiral: see *e.g.* Sec. IV in [217]. The inspiral-plunge waveform resulting from this construction is then matched to a merger-ringdown signal composed of a superposition of quasinormal oscillation modes of a Kerr BH.

The community wide `NRAR` project [219] has pooled the efforts of 9 numerical relativity groups to start a more systematic exploration of the BH binary parameter space [145]. This project furthermore standardizes uncertainty measures for the numerical waveforms, generates automatic tools for the analysis of waveforms and performs comparisons of EOB model predictions with the newly generated waveforms. A catalogue of 171 waveforms has recently been published by the Caltech–Cornell–CITA Collaboration in [220].

The use of numerical relativity as well as hybrid waveforms in GW data analysis is currently explored in the framework of the community wide `Ninja` project [221]. Details of the hybridization process are given and waveforms are compared using tools that are directly employed in the analysis of the GW detector's data stream to determine the uncertainty in parameter estimation arising from uncertainties in the waveform models [222–224].

Finally, we note that the first numerical simulations of BH binaries in scalar–tensor theory of gravity have been performed in which the no-hair theorem is circumvented by introducing a scalar bubble [225] or evolving the binary in a scalar gradient [226].

6.2. Astrophysics

One of the most exciting results obtained through numerical relativity simulations concerns the gravitational *recoil* or *kick* generated through the anisotropic emission of GWs. The generation of recoil in the dynamics of compact objects in general relativity has been realized about half a century ago [227–229] but the precise magnitude of this effect has only been determined following the numerical relativity breakthroughs of the year 2005. In the context of astrophysical BHs, it is of particular interest whether kicks can be large enough to displace or even eject BHs from their host galaxies. Escape velocities from globular clusters and small galaxies are estimated to be in the range of a few tens to the order of 100 km/s but can be as large as $\sim 1\,000$ km/s for large elliptic host galaxies; see *e.g.* [230].

Kick velocities generated in the inspiral and merger of non-spinning binaries have been systematically studied by González *et al.* [231] (see also [232, 233]) and predict a maximum recoil of 175 km/s realized for a mass ratio $q \approx 1/3$; see Fig. 9. This value is significantly below the escape velocities from large galaxies, but may be sufficient to eject BHs from small hosts.

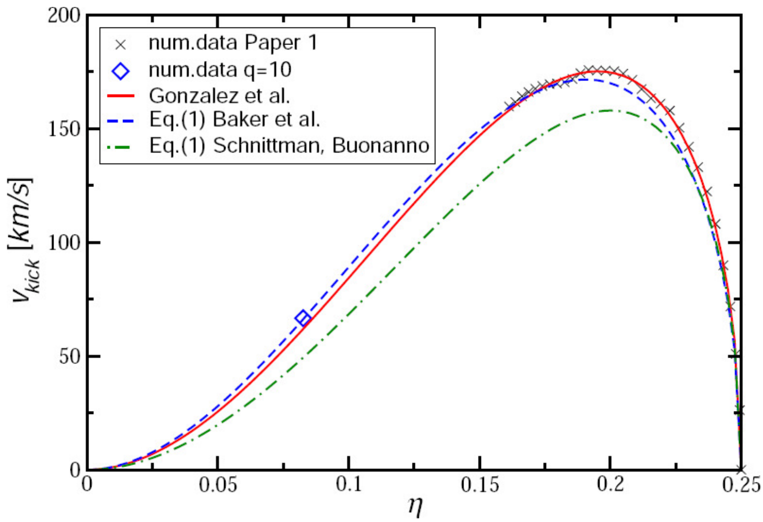

Fig. 9. Kick velocity generated in the inspiral and merger of non-spinning BH binaries with mass ratio $\eta \equiv M_1 M_2/(M_1 + M_2)^2$. Numerical data from Refs. [231, 234] are compared with various fits or analytic approximations.

One of the most surprising results of numerical relativity to date has been the discovery of the so-called *superkicks* [235–237] in the inspiral and merger of equal-mass BHs with equal spins in opposite directions in the orbital plane. The simulations resulted in kick velocities up to 2 500 km/s and extrapolation to maximal spin predicts up to 4 000 km/s. A recent investigation of spin configurations dubbed *hang-up kicks* where the spins are partially aligned with the orbital angular momentum resulted in even larger magnitudes up to 5 000 km/s [238]. These superkicks are large enough to eject BHs from even the most massive host galaxies. The ejection of BHs may result in observational signatures (*e.g.* [239–241]) and represents a potential obstacle for BH growth via merger, and thus puts constraints on merger-history models, which must be able to explain the assembly of SMBHs by redshifts $z \gtrsim 6$ [242–244].

Frequent ejection of BHs from their host galaxies would, however, be at odds with the observation that at least massive galaxies appear to ubiquitously harbor BHs [245]. It thus appears that superkicks, while theoretically possible, are not frequently realized in nature. Mechanisms that would result in the suppression of the specific spin orientations that give rise to large kicks have been suggested in the form of partial alignment of spins due to the presence of torques from accretion disks and resonance effects due to spin–orbit coupling in the inspiral [246–250].

6.3. High-energy collisions of black holes

The Standard Model of particle physics provides an exceptionally successful description of subatomic particles and their interactions via the electromagnetic, weak and strong forces. In spite of its success, however, there remain important unanswered questions as, for example, the unknown nature of dark matter. In the context of this section, the most important open issue is the large discrepancy between the electroweak energy scale 246 GeV and the grand unification scale $\sim 10^{19}$ GeV. This so-called *hierarchy problem* manifests itself in the extraordinary weakness of the gravitational interaction relative to the other fundamental forces; the weak interaction is about 32 orders of magnitude stronger than the gravitational one. At energies comparable to the grand unification energy, on the other hand, gravity is expected to become comparable in strength to the other interactions.

One proposition to explain this enormous discrepancy evokes extra dimensions either in the form of large (relative to the four-dimensional Planck scale M_{Pl}) extra dimensions in the so-called ADD model [13, 251, 252] or by introducing a finite length scale through a warp factor in otherwise infinite extra dimensions in the Randall–Sundrum model [14, 253]. As a consequence of the extra dimensions, gravity becomes a much stronger interaction at microscopic distances than one would expect from the $1/r^2$ fall-off without extra dimensions.

An intriguing consequence of an effective Planck mass much below its four-dimensional value $\sim 10^{19}$ GeV is the possibility of BH formation in parton–parton collisions at the Large Hadron Collider (LHC) [254, 255]; see also the reviews by Cavaglià [256] and Kanti [257]. Once formed, such mini BHs are expected to evaporate in four stages [257]: *(i)* a balding phase during which the BH sheds all multipoles except for mass, spin and charge, *(ii)* a spin-down, and *(iii)* a Schwarzschild phase during which the BH looses first its spin and then its mass via the semi-classical Hawking radiation, and *(iv)* the Planck regime as the BH mass approaches the Planck mass which is described by an as yet unknown theory of quantum gravity.

Of particular interest in the context of NR is the fact that the first three of these phases should be well described by classical and semi-classical calculations provided the BH mass exceeds the Planck scale by at least a factor of a few [257]. BH formation is expected to manifest itself in collision experiments by a special signature in its decay products as, for example, the jet multiplicity or transverse energy [258]. For the identification of these signatures, theoretical predictions from Monte-Carlo event generators such as BlackMax [259] and Charybdis [260, 261] are compared with experimental data. Key input parameters for the event generators are the scattering cross section for BH formation and the initial mass and spin distributions of the formed holes. Providing this information forms the main goal of numerical relativity simulations of high-energy collisions of BHs.

If we assume that most of the energy of the collision process resides in the kinetic energy of the particles, such that their internal structure becomes negligible, the dynamics of the collision should be well modeled by two point particles or BHs in D-dimensional general relativity [255, 262]. This conjecture has been tested by Choptuik and Pretorius [263] for the head-on collision of minimally coupled, massive scalar fields. As expected from Thorne's [264] Hoop conjecture, these boson-field collisions result in the formation of a BH above a threshold value for the Lorentz boost parameter $\gamma_{\rm thr} = 2.9 \pm 10\%$, about a factor three below the upper limit derived from the Hoop conjecture. This study was extended to the case of perfect fluids by East and Pretorius [265] again resulting in the observation that BH formation occurs above a threshold boost.

It thus appears that "matter does not matter" in the collisions provided the total centre-of-mass energy is dominated by the kinetic energy, *i.e.* in the ultra relativistic limit. High-energy collisions of BHs are currently best understood in $D = 4$ dimensions. Even though extension of these results to higher dimensions will be needed, important insight can be gained from the four-dimensional case.

A high-energy collision of non-rotating, electrically neutral BHs is characterized by three parameters, the mass ratio q, the boost $\gamma = 1/\sqrt{1-v^2}$ and the impact parameter $b \equiv L/P$, where L and P denote the orbital angular momentum and the linear momentum of one BH as measured in the centre-of-mass frame. Sperhake *et al.* [126] studied head-on collisions, where $b = 0$, of equal-mass BH binaries and found the energy radiated in GWs to rapidly increase with the collision velocity v and reach $14 \pm 3\%$ of the total centre-of-mass energy as $v \to c$. A follow-up study [174] of grazing collisions identified zoom-whirl behavior when fine-tuning b near a *threshold of immediate merger* [266]. Furthermore, grazing collisions were found to emit enormous amounts of GWs up to 35% of the total energy. The cross section in such collisions was studied by Shibata *et al.* [267] who found a remarkably simple fit to their results giving the scattering threshold as

$$b_{\rm scat} = \frac{2.5 \pm 0.05}{v} M\,. \tag{142}$$

The impact of spins on the collision dynamics was studied in Sperhake *et al.* [128]. Specifically, grazing collisions of non-spinning binaries were compared with configurations where the spins are either aligned or anti-aligned with the orbital angular momentum. These (anti-)hangup configurations are known to have a particularly strong impact on the dynamics of BH binaries [268]. The results for the scattering threshold $b_{\rm scat}$ and the radiated GW energy for five sequences with dimensionless spins $\chi = +0.85$, $+0.6$, 0, -0.6, -0.85 are shown in Fig. 10. Here, positive and negative spin values correspond to the aligned and anti-aligned case, respectively. Clearly the spin orientation has a strong effect on the scattering threshold for low boosts. At velocities above $\sim 90\%$ of the speed of light, however, this impact of the spin is washed out. The radiated GW energy, displayed in the form of the maximum over variations of the impact parameter in the lower panel of the figure, exhibits little dependence on the spin orientation even for velocities as low as $\sim 60\%$ of the speed of light. We see here another manifestation of the principle that structure does not matter for the outcome of the collision dynamics in the ultra relativistic limit. From Fig. 10 we also see that the maximum radiated energy extrapolated to $v \to c$ reaches about 50% of the total energy. In this limit, however, the total energy is identical to the kinetic energy and the question arises what happens to the other half of the kinetic energy that is not radiated to infinity. The answer found in [128] is that the remainder of the kinetic energy is absorbed by the colliding objects either during the merger phase or, in scattering configurations, during the period of close interaction of the non-merging BHs.

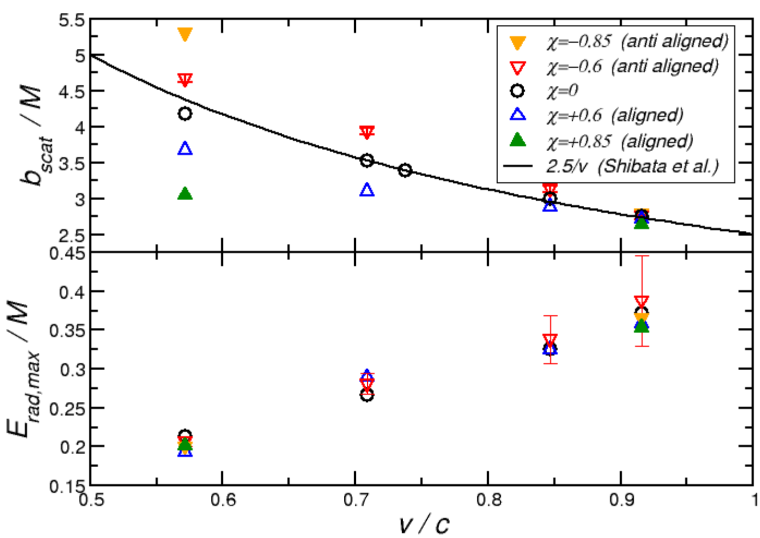

Fig. 10. Upper panel: Scattering threshold of equal-mass BH binaries with aligned, anti-aligned or zero spins as a function of the collision velocity. Lower panel: maximal energy radiated in GWs (maximized over varying the impact parameter b).

BH collisions in $D \geq 5$ have not been studied in the same detail which is largely a consequence of stability problems in the numerical simulations which are the subject of ongoing research. Head-on collisions in $D = 5$ starting from rest have been studied in [80, 186, 269]. These emit about twice as much GW energy as their four-dimensional counterparts, but still orders of magnitude less than the high-energy collisions mentioned above. A first study of grazing collisions in $D = 5$ has been presented by Okawa *et al.* [127]. The scattering threshold has been successfully determined up to speeds of about 0.6 c. For larger boosts stability problems prevent an accurate determination of b_{scat}. Their study furthermore identified super-Planckian regimes in the $D = 5$ scattering collisions and thus the possibility of a quantum regime that is not hidden inside a horizon.

6.4. Gauge–gravity duality

Many applications of the gauge–gravity duality, or AdS/CFT correspondence, are concerned with the equilibration of matter in heavy-ion collisions at the RHIC or LHC and, in particular, its rapid thermalization [270–272]. While the quark-gluon plasma generated in the collisions is far from equilibrium at early stages, its behavior appears to be well described by hydrodynamics after time scales of the order of 1 fm/c. This process is, in principle, governed by QCD but results indicate that many physical aspects can be studied in the framework of $\mathcal{N} = 4$ SYM through the gauge–gravity duality. Small perturbations of a static system in thermal equilibrium are known to decay exponentially fast and correspond to quasi-normal modes on the gravity side [273] and numerical studies in the context of the AdS/CFT correspondence yield a similar picture for far-from-equilibrium configurations.

The use of NR methods to study these processes in AdS/CFT has been pioneered by Chesler and Yaffe [120, 121] who evolve an anisotropic source on the AdS boundary switched on after a short time using a characteristic approach based on ingoing Eddington–Finkelstein coordinates on the Poincaré patch of AdS. Their numerical scheme is reduced to an effective "1+1" scheme by assuming boost invariance as well as rotational and translation symmetry in the transverse plane. Their boundary data generate gravitational waves which propagate into the bulk and lead to formation of a BH. They extract the energy momentum tensor of the CFT dual and follow the time evolution of the energy density as well as the transverse and longitudinal pressure components. Isotropization of the pressure occurs on time scales inversely proportional to the local temperature at the onset of the hydrodynamic regime which translates into an isotropization time of 0.5 fm/c assuming a temperature of 350 MeV. Using the same setup, Chesler and Teaney [274] use different definitions of a "temperature" based on the energy density and on two-point functions. These two versions start agreeing after a time 1 fm/c coincident with the isotropization of transverse and longitudinal pressure. Wu and Romatschke [275] employ a similar approach to collide two superposed shockwaves in a boost invariant approximation and find that the late-time behavior of the energy density is given by a hydrodynamic description involving a scale parameter determined by the initial apparent horizon area.

A comparison of the fully non-linear numerical results with predictions from the linearized close-limit approximation [276] was performed by Heller *et al.* [277, 278]. Instead of sourcing the anisotropy through a boundary term, they prescribe anisotropic data on an initial null hypersurface extending through the bulk. Their results confirm the short isotropization times ~ 1 fm/c and find the linear approach to reproduce these values within 20% even for large initial anisotropies.

A numerical scheme based on the ADM formalism of the Einstein equations was developed by Heller *et al.* [162, 279] who emphasize that thermalization, when defined as the onset of the hydrodynamical regime[2], may differ from isotropization. By evolving boost-invariant, transversely homogeneous plasmas with various different initial conditions, they find that a hydrodynamic description may well be applicable when the pressure is still anisotropic.

In Ref. [122], Chesler and Yaffe relax their symmetry assumptions to translation invariance in the transverse direction which effectively constitutes a 2+1 numerical scheme. Their characteristic formulation works well in this scenario without showing any signs of formation of caustics and enables them to model heavy-ion collisions by colliding two shock waves. Specifically, they consider a single shock-wave solution in Fefferman–Graham coordinates, superpose two of those and transform the result to ingoing Eddington–Finkelstein coordinates. For stability purposes, they introduce a small energy offset on the CFT side which generates an apparent horizon in the gravity dual above the Poincaré boundary to absorb steep gradients encountered in the metric functions deep in the bulk. By comparing the numerically determined pressure components with hydrodynamical predictions, they confirm the picture of rapid isotropization obtained in scenarios of higher symmetry. Translated into values for gold ion collisions at the RHIC, they observe isotropization about 0.35 fm/c after their shock waves start overlapping. Most recently, they presented a detailed description of their computational methods which also includes a study of two-dimensional turbulent fluid flow modeled through the gravity dual in 3+1 dimensions [280]; see also Adams *et al.* [281] and [282] for a recent review.

[2] See Eq. (5) in Ref. [162] for their precise definition.

A numerical code based on Cauchy type evolutions of asymptotically global AdS spacetimes using the GHG scheme has been developed by Bantilan *et al.* [152]. By assuming an SO(3) symmetry, they reduce their computational domain to 2+1 dimensions. Initial data is specified in the form of a localized scalar field which promptly collapses to a BH with a highly distorted horizon and settles down into a stationary configuration through quasi-normal ringdown. Whereas the lowest ringdown modes agree with linearized predictions, higher angular modes exhibit significant coupling due to non-linear effects. The dual stress-energy tensor of the CFT is mapped from the global $\mathbb{R} \times S^3$ AdS boundary to a Minkowski background and found to evolve in agreement with that of a thermalized SYM fluid from the start of the simulations. Their work furthermore discusses in detail a number of regularization procedures required to obtain a numerically stable framework.

6.5. Fundamental properties of black-hole spacetimes

One of the first and most influential NR results has been obtained in Choptuik's [135] seminal study of the collapse of spherically symmetric massless scalar fields minimally coupled to the Einstein gravity in four-dimensional, asymptotically flat spacetimes. By evolving various one-parameter families of scalar pulses, he identified critical behavior as the parameter p which characterizes the gravitational interaction strength of the field approaches a critical value p^*. For $p > p^*$, the field collapses to a BH and for $p < p^*$ it disperses to infinity. Furthermore, near-critical field configurations exhibit *universal* behavior in the strong field limit: *(i)* BHs which form have a mass $M \sim |p - p^*|^\gamma$ with a universal constant $\gamma \approx 0.37$. *(ii)* Advancing the evolution from a time t to $t + \Delta$, the field profile is recovered up to a "zoom-in" by a factor e^Δ. The numerical study reveals Δ to be a universal constant of about 3.4. For subcritical configurations, Garfinkle and Comer Duncan [283] found a similar scaling of the maximal scalar curvature in the spacetime $R_{\max} \sim |p - p^*|^{2\gamma}$. Continuously self-similar solutions were found by Pretorius and Choptuik [284] for scalar fields in 2+1 dimensional asymptotically AdS spacetimes with a mass scaling characterized by $\gamma/2 = 1.2$. Sorkin and Oren [285] generalized Choptuik's result to higher dimensions by evolving scalar fields up to $d = 11$ dimensions. Their results indicate that γ reaches a maximum and Δ a minimum around $d \approx 11 \ldots 13$. An extended review of critical collapse phenomena is given by Gundlach and Martín-García [286].

More recently, critical-collapse studies have been extended to asymptotically AdS spacetimes in 3+1 and higher dimensions. In a remarkable study, Bizoń and Rostworowski found evidence suggesting that 3+1 AdS is unstable to BH formation under arbitrarily small perturbations. By evolving spherically symmetric scalar fields they recover Choptuik's results for large initial field amplitudes. For configurations below this critical value, however, the AdS boundary substantially modifies the outcome. In contrast to asymptotically flat spacetimes, spatial infinity in AdS is reached in finite time by massless fields and reflected back onto the origin. As the initial amplitude is reduced below a critical value ϵ_0, the scalar pulse forms a BH upon its second implosion on the origin. Further reduction of the amplitude leads to a second critical amplitude ϵ_1 and this pattern repeats itself with no indication of a threshold amplitude for BH formation; *cf.* their Fig. 1. For each critical amplitude, they furthermore recover Choptuik's scaling law with $\gamma = 0.37$. They interpret this behavior as a resonant mixing of modes which transfers energy from low to high frequencies. This study has been generalized to higher-dimensional AdS spacetimes by Jałmużna *et al.* [287] suggesting that AdS is unstable to BH formation for generic spacetime dimensions. Presumably, this result has eluded a similar study by Garfinkle and Pando Zayas [288], because of insufficient length of their numerical simulations for smaller field amplitudes. In a similar investigation using complex scalar fields, Buchel *et al.* [289] reproduce the instability of AdS and the transfer of energy from low to high frequencies. In consequence, the width of initially weak pulses narrows in each reflection cycle and eventually collapses to a BH; *cf.* their Fig. 5. Garfinkle *et al.* [290] have monitored the time of BH formation and the horizon radius, and found the amplitude of the scalar field to have a stronger influence on the outcome compared with the width of the pulse. The same type of instability to BH formation has been found by Maliborski [291] for a Minkowski spacetime enclosed inside a reflecting wall, indicating that the global structure plays a major role for the effect. Nevertheless, there are strong indications that there also exist classes of stable asymptotically AdS spacetimes containing, for example, boson stars, geons or time-periodic scalar field configurations [292–295]. In 2+1 dimensions, where BH solutions only exist for mass parameters above a threshold value, Bizoń and Jałmużna [296] have studied the collapse of scalar field configurations with a total mass below the mass threshold. They observe that the fields evolve towards ever finer structure but remain smooth and exhibit no sign of formation of naked singularities.

The instability of black strings has been studied numerically in a sequence of papers by Lehner and Pretorius and collaborators [297–299], see also [300]. It had been known since the 1990s that black strings are subject to the Gregory–Laflamme instability, but the eventual fate of the string remained unclear. In Ref. [299], Lehner and Pretorius found evidence supporting indications by earlier work that the string evolves to a sequence of spherical BHs connected by thin string segments which themselves are subject to the Gregory–Laflamme instability, resulting in a self-similar cascade reaching zero string width in finite asymptotic time. This behavior shows striking similarity with satellite formation in the flow of low-viscosity fluids. The eventual bifurcation of the horizon resulting from the cascade implies formation of a naked singularity [2]. Because no fine-tuning is required to trigger the instability, the result constitutes a violation of the cosmic censorship conjecture without "unnatural" assumptions about the initial data. In contrast to the higher-dimensional case, NR has as yet not observed any such violation of cosmic censorship in 3+1 dimensions. In a recent study [160], BH collisions in asymptotically de Sitter spacetimes have been found to comply with censorship; BH binaries with a combined mass exceeding the inverse of the Hubble constant do not merge for any initial separation provided the initial data do not contain a naked singularity.

7. Concluding remarks

The study of BH spacetimes through numerical integration of the Einstein equations has been an extremely active field of research, especially following the numerical relativity breakthroughs of the year 2005. Probably one of the most amazing developments is the wide variety of applications of BH studies using numerical relativity which has extended beyond the more traditional applications to GW physics and astrophysics to high-energy collisions of partons, quark-gluon plasma, condensed matter and conductivity. Furthermore, the modeling of BHs and their formation still presents us with surprising outcomes about a century after the publication of the theory of general relativity.

In spite of the great success of the computational tools employed for the 2005 breakthrough simulations of BH binaries, the numerical relativity community still explores new developments in numerical methods, the formulation of the Einstein equations and the diagnostic tools used for the extraction of physical information from the spacetimes. As we have seen, time evolutions of BHs in higher dimensions, in particular, still encounter stability issues which need to be overcome to facilitate a comprehensive understanding of the BH dynamics. The field of numerical relativity is thus a highly dynamic field and it is quite possible that some chapter or other of these notes may become outdated in the not-too-distant future. The Reader is encouraged to stay tuned and remain on the lookout for new developments.

This work was supported by the FP7-PEOPLE-2011-CIG Grant CBHEO-293412, the FP7-PEOPLE-2011-IRSES Grant NRHEP-295189, the ERC Starting Grant DyBHo-236667, the NSF Grant No. PHY-090003 through XSEDE, the STFC GR Roller grant ST/I002006/1, the Grant ICTS-234 through CESGA. Part of this work was performed with the support of the Cosmos System, part of the DiRAC HPC Facility funded by STFC and BIS, and the Baltasar System of IST-CENTRA.

REFERENCES

[1] R.P. Kerr, *Phys. Rev. Lett.* **11**, 237 (1963).

[2] S.W. Hawking, G.F.R. Ellis, *The Large Scale Structure of Space-Time*, Cambridge University Press, 1973.

[3] J. van Paradijs, *Bull. Am. Astron. Soc.* **30**, 1291 (1998) [arXiv:astro-ph/9802177].

[4] M.J. Rees, *Phys. Scr.* **17**, 193 (1978).

[5] B.S. Sathyaprakash, B.F. Schutz, *Living Rev. Relativity* **12**, 2 (2009) [http://www.livingreviews.org/lrr-2009-2].

[6] LIGO website: http://www.ligo.org

[7] Advanced Virgo website: http://wwwcascina.virgo.infn.it/advirgo/

[8] GEO600 website: http://www.geo600.org/

[9] KAGRA website: http://gwcenter.icrr.u-tokyo.ac.jp/en/

[10] eLISA website: https://www.elisascience.org/

[11] J.M. Maldacena, *Adv. Theor. Math. Phys.* **2**, 231 (1997) [arXiv:hep-th/9711200].

[12] E. Witten, *Adv. Theor. Math. Phys.* **2**, 253 (1998) [arXiv:hep-th/9802150].

[13] N. Arkani-Hamed, S. Dimopoulos, G.R. Dvali, *Phys. Lett.* **B429**, 263 (1998) [arXiv:hep-ph/9803315].

[14] L. Randall, R. Sundrum, *Phys. Rev. Lett.* **83**, 3370 (1999) [arXiv:hep-ph/9905221].

[15] M. Sasaki, H. Tagoshi, *Living Rev. Relativity* **6**, 6 (2003) [http://www.livingreviews.org/lrr-2003-6].

[16] L. Blanchet, *Living Rev. Relativity* **9**, 4 (2006) [http://www.livingreviews.org/lrr-2006-4].

[17] S. Almeida, *Int. J. Mod. Phys.* **A28**, 1340021 (2013).

[18] R. Arnowitt, S. Deser, C.W. Misner, *The Dynamics of General Relativity* in L. Witten, ed. *Gravitation: an Introduction to Current Research*, John Wiley, New York 1962, pp. 227–265 [arXiv:gr-qc/0405109] doi:10.1007/s10714-008-0661-1.

[19] J.W. York, Jr., *Kinematics, Dynamics of General Relativity* in: L. Smarr, ed., *Sources of Gravitational Radiation*, Cambridge University Press, Cambridge 1979, pp. 83–126.

[20] E. Gourgoulhon, arXiv:gr-qc/0703035.

[21] O.A. Reula, *Living Rev. Relativity* **1**, 3 (1998).

[22] O. Sarbach, M. Tiglio, *Living Rev. Relativity* **15**, 9 (2012) [arXiv:1203.6443 [gr-qc]].

[23] D. Hilditch, *Int. J. Mod. Phys.* **A28**, 1340015 (2013) [arXiv:1309.2012 [gr-qc]].

[24] G. Nagy, O.E. Ortiz, O.A. Reula, *Phys. Rev.* **D70**, 044012 (2004) [arXiv:gr-qc/0402123].

[25] O.A. Reula, arXiv:gr-qc/0403007.

[26] M.E. Taylor, *Pseudodifferential Operators*, Princetone University Press, Princeton 1981.

[27] M.E. Taylor, *Pseudodifferential Operators, Nonlinear PDE (Progress in Mathematics 100)*, Birkhäuser, Boston–Basel–Berlin 1991.

[28] L.E. Kidder, M.A. Scheel, S.A. Teukolsky, *Phys. Rev.* **D64**, 064017 (2001) [arXiv:gr-qc/0105031].

[29] T.W. Baumgarte, S.L. Shapiro, *Phys. Rev.* **D59**, 024007 (1998) [arXiv:gr-qc/9810065].

[30] M. Shibata, T. Nakamura, *Phys. Rev.* **D52**, 5428 (1995).

[31] H.-J. Yo, T.W. Baumgarte, S.L. Shapiro, *Phys. Rev.* **D66**, 084026 (2002) [arXiv:gr-qc/0209066].

[32] M. Alcubierre, B. Brügmann, *Phys. Rev.* **D63**, 104006 (2001) [arXiv:gr-qc/0008067].

[33] F. Pretorius, *Phys. Rev. Lett.* **95**, 121101 (2005) [arXiv:gr-qc/0507014].

[34] H. Ringström, *Acta Phys. Pol. B* **44**, 2621 (2013), this issue.

[35] Y. Fourés-Bruhat, *Acta Math.* **88**, 141 (1952).

[36] Y. Bruhat, *The Cauchy Problem* in: L. Witten, ed., *Gravitation: An Introduction to Current Research*, Wiley, New York 1962.

[37] A.E. Fischer, J.E. Marsden, *Commun. Math. Phys.* **28**, 1 (1972).

[38] H. Friedrich, *Commun. Math. Phys.* **100**, 525 (1985).

[39] D. Garfinkle, *Phys. Rev.* **D65**, 044029 (2002) [arXiv:gr-qc/0110013].

[40] F. Pretorius, *Class. Quantum Grav.* **22**, 425 (2005) [arXiv:gr-qc/0407110].

[41] L. Lindblom *et al.*, *Class. Quantum Grav.* **23**, S447 (2006) [arXiv:gr-qc/0512093].

[42] C. Gundlach, G. Calabrese, I. Hinder, J.M. Martín-García, *Class. Quantum Grav.* **22**, 3767 (2005).

[43] H.R. Beyer, O. Sarbach, *Phys. Rev.* **D70**, 104004 (2004) [arXiv:gr-qc/0406003].

[44] C. Gundlach, J.M. Martín-García, *Phys. Rev.* **D70**, 044032 (2004) [arXiv:gr-qc/0403019].

[45] C. Gundlach, J.M. Martín-García, *Phys. Rev.* **D70**, 044031 (2004) [arXiv:gr-qc/0403019].

[46] O. Rinne, *Axisymmetric Numerical Relativity*, Ph.D. Thesis, Cambridge University, 2005.

[47] H.-O. Kreiss, J. Winicour, *Class. Quantum Grav.* **23**, S405 (2006) [arXiv:gr-qc/0602051].

[48] M. Ruiz, O. Rinne, O. Sarbach, *Class. Quantum Grav.* **24**, 6349 (2007) [arXiv:0707.2797 [gr-qc]].

[49] C. Bona, T. Ledvinka, C. Palenzuela, M. Žáček, *Phys. Rev.* **D67**, 104005 (2003) [arXiv:gr-qc/0302083].

[50] C. Bona, T. Ledvinka, C. Palenzuela, M. Žáček, *Phys. Rev.* **D69**, 064036 (2004) [arXiv:gr-qc/0307067].

[51] C. Bona, T. Ledvinka, C. Palenzuela-Luque, M. Žáček, *Class. Quantum Grav.* **22**, 2615 (2005) [arXiv:gr-qc/0411110].

[52] D. Alic *et al.*, *Phys. Rev.* **D85**, 064040 (2012) [arXiv:1106.2254 [gr-qc]].

[53] Z. Cao, D. Hilditch, *Phys. Rev.* **D85**, 124032 (2012) [arXiv:1111.2177 [gr-qc]].

[54] A. Weyhausen, S. Bernuzzi, D. Hilditch, *Phys. Rev.* **D85**, 024038 (2012) [arXiv:1107.5539 [gr-qc]].

[55] D. Hilditch *et al.*, arXiv:1212.2901 [gr-qc].

[56] M. Ruiz, D. Hilditch, S. Bernuzzi, *Phys. Rev.* **D83**, 024025 (2011) [arXiv:1010.0523 [gr-qc]].

[57] P. Laguna, D. Shoemaker, *Class. Quantum Grav.* **19**, 3679 (2002).

[58] H. Witek, D. Hilditch, U. Sperhake, *Phys. Rev.* **D83**, 104041 (2011) [arXiv:1011.4407 [gr-qc]].

[59] H. Witek, *Black Hole Dynamics in Generic Specatimes*, Ph.D. Thesis, IST/CENTRA Lisbon, 2012 [arXiv:1307.1145 [gr-qc]].

[60] H. Bondi, M.G.J. van der Burg, A.W.K. Metzner, *Proc. R. Lond. Soc.* **A269**, 21 (1962).

[61] R.K. Sachs, *Proc. R. Soc. Lond.* **A270**, 103 (1962).

[62] J. Winicour, *Living Rev. Relativity* **15**, 2 (2012) [http://www.livingreviews.org/lrr-2012-2].

[63] M.C. Babiuc, H.-O. Kreiss, J. Winicour, arXiv:1305.7179 [gr-qc].

[64] C. Reisswig, N.T. Bishop, D. Pollney, B. Szilagyi, *Phys. Rev. Lett.* **103**, 221101 (2009) [arXiv:0907.2637 [gr-qc]].

[65] M.C. Babiuc, B. Szilagyi, J. Winicour, Y. Zlochower, *Phys. Rev.* **D84**, 044057 (2011) [arXiv:1011.4223 [gr-qc]].

[66] M.M. May, R.H. White, *Phys. Rev.* **141**, 1232 (1966).

[67] M.M. May, R.H. White, *Methods Comput. Phys.* **7**, 219 (1967).

[68] V. Cardoso *et al.*, *Class. Quantum Grav.* **29**, 244001 (2012) [arXiv:1201.5118 [hep-th]].

[69] U. Sperhake, *Int. J. Mod. Phys.* **D22**, 1330005 (2013) [arXiv:1301.3772 [gr-qc]].

[70] H. Yoshino, M. Shibata, *Prog. Theor. Phys. Suppl.* **189**, 269 (2011).

[71] H. Yoshino, M. Shibata, *Prog. Theor. Phys. Suppl.* **190**, 282 (2011).

[72] H. Witek, *Int. J. Mod. Phys.* **A28**, 1340017 (2013) [arXiv:1308.1686 [gr-qc]].

[73] R. Geroch, *J. Math. Phys.* **12**, 918 (1970).

[74] K.R.P. Sjödin, U. Sperhake, J.A. Vickers, *Phys. Rev.* **D63**, 024011 (2000) [arXiv:gr-qc/0002096].

[75] U. Sperhake, K.R.P. Sjödin, J.A. Vickers, *Phys. Rev.* **D63**, 024012 (2000) [arXiv:gr-qc/0003114].

[76] M.W. Choptuik, E.W. Hirschmann, S.L. Liebling, F. Pretorius, *Class. Quantum Grav.* **20**, 1857 (2003) [arXiv:gr-qc/0301006].

[77] Y.M. Cho, *Phys. Lett.* **B186**, 38 (1987).

[78] Y.M. Cho, D.S. Kim, *J. Math. Phys.* **30**, 1570 (1989).

[79] M. Zilhão, *New Frontiers in Numerical Relativity*, Ph.D. Thesis, University of Porto, 2012 [arXiv:1301.1509 [gr-qc]].

[80] M. Zilhão *et al.*, *Phys. Rev.* **D81**, 084052 (2010) [arXiv:1001.2302 [gr-qc]].

[81] M. Alcubierre *et al.*, *Int. J. Mod. Phys.* **D10**, 273 (2001) [arXiv:gr-qc/9908012].

[82] H. Yoshino, M. Shibata, *Phys. Rev.* **D80**, 084025 (2009) [arXiv:0907.2760 [gr-qc]].

[83] M. Shibata, H. Yoshino, *Phys. Rev.* **D81**, 104035 (2010) [arXiv:1004.4970 [gr-qc]].

[84] G.B. Cook, *Living Rev. Relativity* **3**, 5 (2000) [http://www.livingreviews.org/lrr-2000-5].

[85] H. Okawa, *Int. J. Mod. Phys.* **A28**, 1340016 (2013).

[86] C.W. Misner, *Phys. Rev.* **118**, 1110 (1960).

[87] D.R. Brill, R.W. Lindquist, *Phys. Rev.* **131**, 471 (1963).

[88] A. Lichnerowicz, *Journal de Mathématiques Pures et Appliquées* **23**, 37 (1944).

[89] J.W. York, Jr., *Phys. Rev. Lett.* **26**, 1656 (1971).

[90] J.W. York, Jr., *Phys. Rev. Lett.* **28**, 1082 (1972).

[91] J.W. York, Jr., *Phys. Rev. Lett.* **82**, 1350 (1999).

[92] G.B. Cook, H. Pfeiffer, *Phys. Rev.* **D70**, 104016 (2004) [arXiv:gr-qc/0407078].

[93] M. Caudill, G.B. Cook, J.D. Grigsby, H.P. Pfeiffer, *Phys. Rev.* **D74**, 064011 (2006) [arXiv:gr-qc/0605053].

[94] J.M. Bowen, J.W. York, Jr., *Phys. Rev.* **D21**, 2047 (1980).

[95] J.W. York, Jr., *Energy, Momentum of the Gravitational Field* in: F.J. Tipler, ed., *Essays in General Relativity*, Academic, New York 1980, pp. 39–58.

[96] S. Brandt, B. Brügmann, *Phys. Rev. Lett.* **78**, 3606 (1997) [arXiv:gr-qc/9703066].

[97] A. Garat, R.H. Price, *Phys. Rev.* **D61**, 124011 (2000) [arXiv:gr-qc/0002013].

[98] G.B. Cook, J.W. York, Jr., *Phys. Rev.* **D41**, 1077 (1990).

[99] S. Dain, C.O. Lousto, R. Takahashi, *Phys. Rev.* **D65**, 104038 (2002) [arXiv:gr-qc/0201062].

[100] S. Dain, C.O. Lousto, Y. Zlochower, *Phys. Rev.* **D78**, 024039 (2008) [arXiv:0803.0351 [gr-qc]].

[101] G. Lovelace, R. Owen, H. Pfeiffer, T. Chu, *Phys. Rev.* **D78**, 084017 (2008) [arXiv:0805.4192 [gr-qc]].

[102] G. Lovelace, M.A. Scheel, B. Szilagyi, *Phys. Rev.* **D83**, 024010 (2011) [arXiv:1010.2777 [gr-qc]].

[103] R.P. Kerr, A. Schild, *Some Algebraically Degenerate Solutions of Einstein's Gravitational Field Equations* in: Proceedings of Symposia in Applied Mathematics Vol. XVII, 1965, pp. 199–209.

[104] L. Smarr, J.W. York, Jr., *Phys. Rev.* **D17**, 2529 (1978).

[105] C. Bona, J. Massó, E. Seidel, J. Stela, *Phys. Rev. Lett.* **75**, 600 (1995) [arXiv:gr-qc/9412071].

[106] M. Alcubierre, *Class. Quantum Grav.* **20**, 607 (2003) [arXiv:gr-qc/0210050].

[107] M. Alcubierre *et al.*, *Phys. Rev.* **D67**, 084023 (2003) [arXiv:gr-qc/0206072].

[108] M. Campanelli, C.O. Lousto, P. Marronetti, Y. Zlochower, *Phys. Rev. Lett.* **96**, 111101 (2006) [arXiv:gr-qc/0511048].

[109] J.G. Baker *et al.*, *Phys. Rev. Lett.* **96**, 111102 (2006) [arXiv:gr-qc/0511103].

[110] E. Schnetter, *Class. Quantum Grav.* **27**, 167001 (2010) [arXiv:arXiv:1003.0859 [gr-qc]].

[111] D. Müller, B. Brügmann, *Class. Quantum Grav.* **27**, 114008 (2010) [arXiv:0912.3125 [gr-qc]].

[112] D. Müller, J. Grigsby, B. Brügmann, *Phys. Rev.* **D82**, 064004 (2010) [arXiv:1003.4681 [gr-qc]].

[113] D. Alic, L. Rezzolla, I. Hinder, P. Mösta, *Class. Quantum Grav.* **27**, 245023 (2010) [arXiv:1008.2212 [gr-qc]].

[114] L. Lindblom, B. Szilágyi, *Phys. Rev.* **D80**, 084019 (2009) [arXiv:0904.4873 [gr-qc]].

[115] B. Szilágyi, L. Lindblom, M.A. Scheel, *Phys. Rev.* **D80**, 124010 (2009) [arXiv:0909.3557 [gr-qc]].

[116] M. Boyle *et al.*, *Phys. Rev.* **D76**, 124038 (2007) [arXiv:0710.0158 [gr-qc]].

[117] M. Boyle *et al.*, *Phys. Rev.* **D78**, 104020 (2008) [arXiv:0804.4184 [gr-qc]].

[118] T. Chu, H.P. Pfeiffer, M.A. Scheel, *Phys. Rev.* **D80**, 124051 (2009) [arXiv:0909.1313 [gr-qc]].

[119] G. Lovelace, M. Boyle, M.A. Scheel, B. Szilágyi, *Class. Quantum Grav.* **29**, 045003 (2012) [arXiv:1110.2229 [gr-qc]].

[120] P.M. Chesler, L.G. Yaffe, *Phys. Rev. Lett.* **102**, 211601 (2009) [arXiv:0812.2053 [hep-th]].

[121] P.M. Chesler, L.G. Yaffe, *Phys. Rev.* **D82**, 026006 (2010) [arXiv:0906.4426 [hep-th]].

[122] P.M. Chesler, L.G. Yaffe, *Phys. Rev. Lett.* **106**, 021601 (2011) [arXiv:1011.3562 [hep-th]].

[123] M. Ansorg, B. Brügmann, W. Tichy, *Phys. Rev.* **D70**, 064011 (2004) [arXiv:gr-qc/0404056].

[124] M. Ansorg, *Class. Quantum Grav.* **24**, S1 (2007) [arXiv:gr-qc/0612081].

[125] M. Zilhão *et al.*, *Phys. Rev.* **D84**, 084039 (2011) [arXiv:1109.2149 [gr-qc]].

[126] U. Sperhake *et al.*, *Phys. Rev. Lett.* **101**, 161101 (2008) [arXiv:0806.1738 [gr-qc]].

[127] H. Okawa, K.-i. Nakao, M. Shibata, *Phys. Rev.* **D83**, 121501 (2011) [arXiv:1105.3331 [gr-qc]].

[128] U. Sperhake, E. Berti, V. Cardoso, F. Pretorius, *Phys. Rev. Lett.* **111**, 041101 (2012) [arXiv:1211.6114 [gr-qc]].

[129] C.O. Lousto, Y. Zlochower, *Phys. Rev. Lett.* **106**, 041101 (2011) [arXiv:1009.0292 [gr-qc]].

[130] C.O. Lousto, H. Nakano, Y. Zlochower, M. Campanelli, *Phys. Rev.* **D82**, 104057 (2010) [arXiv:1008.4360 [gr-qc]].

[131] U. Sperhake *et al.*, *Phys. Rev.* **D84**, 084038 (2011) [arXiv:1105.5391 [gr-qc]].

[132] P. Grandclément, J. Novak, *Living Rev. Relativity* **12**, 1 (2009) [http://www.livingreviews.org/lrr-2009-1].

[133] J. Crank, P. Nicolson, *Proc. Camb. Phil. Soc.* **43**, 50 (1947).

[134] W.H. Press, B.P. Flannery, S.A. Teukolsky, W.T. Vetterling, *Numerical Recipes*, Cambridge University Press, Cambridge 1989.

[135] M.W. Choptuik, *Phys. Rev. Lett.* **70**, 9 (1993).

[136] B. Brügmann, *Phys. Rev.* **D54**, 7361 (1996) [arXiv:gr-qc/9608050].

[137] P. MacNeice *et al.*, *Comput. Phys. Commun.* **126**, 330 (2000).

[138] Samrai homepage: http://computation.llnl.gov/casc/SAMRAI/

[139] E. Schnetter, S.H. Hawley, I. Hawke, *Class. Quantum Grav.* **21**, 1465 (2004) [arXiv:gr-qc/0310042].

[140] Carpet Code homepage: http://www.carpetcode.org/

[141] Cactus Computational Toolkit homepage: http://www.cactuscode.org/

[142] Einstein Toolkit webpage: http://einsteintoolkit.org/

[143] M. Zilhão, F. Löffler, *Int. J. Mod. Phys.* **A28**, 1340014 (2013) arXiv:1305.5299 [gr-qc].

[144] M.J. Berger, J. Oliger, *J. Comput. Phys.* **53**, 484 (1984).

[145] I. Hinder *et al.*, arXiv:1307.5307 [gr-qc].

[146] S.M. Carroll, arXiv:gr-qc/9712019.

[147] J. Thornburg, *Class. Quantum Grav.* **4**, 1119 (1987).

[148] D. Shoemaker *et al.*, *Class. Quantum Grav.* **20**, 3729 (2003) [arXiv:gr-qc/0301111].

[149] U. Sperhake *et al.*, *Phys. Rev.* **D69**, 024012 (2004) [arXiv:gr-qc/0307015].

[150] U. Sperhake *et al.*, *Phys. Rev.* **D71**, 124042 (2005) [arXiv:gr-qc/0503071].

[151] M.A. Scheel *et al.*, *Phys. Rev.* **D74**, 104006 (2006) [arXiv:gr-qc/0607056].

[152] H. Bantilan, F. Pretorius, S.S. Gubser, *Phys. Rev.* **D85**, 084038 (2012) [arXiv:1201.2132 [hep-th]].

[153] D.A. Hemberger *et al.*, *Class. Quantum Grav.* **30**, 115001 (2013) [arXiv:1211.6079 [gr-qc]].

[154] M.D. Hannam *et al.*, *Phys. Rev. Lett.* **99**, 241102 (2007) [arXiv:gr-qc/0606099].

[155] J.D. Brown, *Class. Quantum Grav.* **25**, 205004 (2008) [arXiv:0705.3845 [gr-qc]].

[156] J.D. Brown, *Phys. Rev.* **D77**, 044018 (2008) [arXiv:0705.1359 [gr-qc]].

[157] M. Hannam *et al.*, *Phys. Rev.* **D78**, 064020 (2008) [arXiv:0804.0628 [gr-qc]].

[158] J.D. Brown, *Phys. Rev.* **D80**, 084042 (2009) [arXiv:0908.3814 [gr-qc]].

[159] K.A. Dennison, J.P. Wendell, T.W. Baumgarte, J.D. Brown, *Phys. Rev.* **D82**, 124057 (2010) [arXiv:1010.5723 [gr-qc]].

[160] M. Zilhao *et al.*, *Phys. Rev.* **D85**, 104039 (2012) [arXiv:1204.2019 [gr-qc]].

[161] C.A. Bayona, N.R.F. Braga, *Gen. Relativ. Gravitation* **39**, 1367 (2007) [arXiv:hep-th/0512182].

[162] M.P. Heller, R.A. Janik, P. Witaszczyk, *Phys. Rev. Lett.* **108**, 201602 (2012) [arXiv:1103.3452 [hep-th]].

[163] P. Bizoń, A. Rostworowski, *Phys. Rev. Lett.* **107**, 031102 (2011) [arXiv:1104.3702 [gr-qc]].

[164] R. Emparan, H.S. Reall, *Living Rev. Relativity* **11**, 6 (2008) [http://www.livingreviews.org/lrr-2008-6].

[165] P. Diener, *Class. Quantum Grav.* **20**, 4901 (2003) [arXiv:gr-qc/0305039].

[166] M.I. Cohen, H.P. Pfeiffer, M.A. Scheel, *Class. Quantum Grav.* **26**, 035005 (2009).

[167] J. Thornburg, *Living Rev. Relativity* **10**, 3 (2007) [http://www.livingreviews.org/lrr-2007-3].

[168] C. Gundlach, *Phys. Rev.* **D57**, 863 (1998) [arXiv:gr-qc/9707050].

[169] M. Alcubierre *et al.*, *Class. Quantum Grav.* **17**, 2159 (2000) [arXiv:gr-qc/9809004].

[170] J. Thornburg, *Phys. Rev.* **D54**, 4899 (1996) [arXiv:gr-qc/9508014].
[171] E. Schnetter, *Class. Quantum Grav.* **20**, 4719 (2003) [arXiv:gr-qc/0306006].
[172] J. Thornburg, *Class. Quantum Grav.* **21**, 743 (2004) [arXiv:gr-qc/0306056].
[173] D. Christodoulou, *Phys. Rev. Lett.* **25**, 1596 (1970).
[174] U. Sperhake *et al.*, *Phys. Rev. Lett.* **103**, 131102 (2009) [arXiv:0907.1252 [gr-qc]].
[175] M. Ortaggio, V. Pravda, A. Pravdova, H.S. Reall, *Class. Quantum Grav.* **29**, 205002 (2012) [arXiv:1205.1119 [gr-qc]].
[176] E.T. Newman, R. Penrose, *J. Math. Phys.* **3**, 566 (1962).
[177] A. Nerozzi, arXiv:1109.4400 [gr-qc].
[178] H. Friedrich, *Class. Quantum Grav.* **13**, 1451 (1996).
[179] M. Ruiz, R. Takahashi, M. Alcubierre, D. Nuñez, *Gen. Relativ. Gravitation* **40**, 2467 (2008) [arXiv:0707.4654 [gr-qc]].
[180] C. Reisswig, D. Pollney, *Class. Quantum Grav.* **28**, 195015 (2011) [arXiv:1006.1632 [gr-qc]].
[181] T. Regge, J.A. Wheeler, *Phys. Rev.* **108**, 1063 (1957).
[182] V. Moncrief, *Ann. Phys.* **88**, 323 (1974).
[183] A. Nagar, L. Rezzolla, *Class. Quantum Grav.* **22**, R167 (2005) [arXiv:gr-qc/0502064].
[184] C. Reisswig, C.D. Ott, U. Sperhake, E. Schnetter, *Phys. Rev.* **D83**, 064008 (2011) [arXiv:1012.0595 [gr-qc]].
[185] H. Kodama, A. Ishibashi, *Prog. Theor. Phys.* **110**, 701 (2003) [arXiv:hep-th/0305147].
[186] H. Witek *et al.*, *Phys. Rev.* **D82**, 104014 (2010) [arXiv:1006.3081 [gr-qc]].
[187] F.R. Tangherlini, *Nuovo Cim.* **27**, 636 (1963).
[188] S. de Haro, N. Solodukhin, S.K. Skenderis, *Commun. Math. Phys.* **217**, 595 (2001) [arXiv:hep-th/0002230].
[189] V. Balasubramanian, P. Kraus, *Commun. Math. Phys.* **208**, 413 (1999) [arXiv:hep-th/9902121].
[190] K. Skenderis, *Class. Quantum Grav.* **19**, 5849 (2002) [arXiv:hep-th/0209067].
[191] J.D. Brown, J.W. York, Jr., *Phys. Rev.* **D47**, 1407 (1993) [arXiv:gr-qc/9209012].
[192] C. Fefferman, R. Graham, *Conformal Invariants* in: *Elie Cartan et les Mathématiques d'Aujourd'hui*, Astérisque, 1985, p. 95.
[193] F. Pretorius, *Binary Black Hole Coalescence*, in: M. Colpi *et al.*, eds. *Physics of Relativistic Objects in Compact Binaries: From Birth to Coalescence*, Springer, New York 2009 [arXiv:0710.1338 [gr-qc]].

[194] M. Hannam, *Class. Quantum Grav.* **26**, 114001 (2009) [0901.2931 [gr-qc]].

[195] J.M. Centrella, J.G. Baker, B.J. Kelly, J.R. van Meter, *Rev. Mod. Phys.* **82**, 3069 (2010) [arXiv:1010.5260 [gr-qc]].

[196] I. Hinder, *Class. Quantum Grav.* **27**, 114004 (2010) [arXiv:1001.5161 [gr-qc]].

[197] U. Sperhake, E. Berti, V. Cardoso, *Comptes Rendus Physique* **14**, 306 (2013) [arXiv:1107.2819 [gr-qc]].

[198] H.P. Pfeiffer, *Class. Quantum Grav.* **29**, 124004 (2012) [arXiv:1203.5166 [gr-qc]].

[199] L.S. Finn, *Phys. Rev.* **D46**, 5236 (1992) [arXiv:gr-qc/9209010].

[200] P.C. Peters, J. Mathews, *Phys. Rev.* **131**, 435 (1963).

[201] U. Sperhake, B. Brügmann, D. Müller, C.F. Sopuerta, *Class. Quantum Grav.* **28**, 134004 (2011) [arXiv:1012.3173 [gr-qc]].

[202] M.D. Hannam *et al.*, *Phys. Rev.* **D77**, 044020 (2008) [arXiv:0706.1305 [gr-qc]].

[203] P. Ajith *et al.*, *Class. Quantum Grav.* **24**, S689 (2007) [arXiv:0704.3764 [gr-qc]].

[204] P. Ajith *et al.*, *Phys. Rev.* **D77**, 104017 (2008) [arXiv:0710.2335 [gr-qc]].

[205] P. Ajith, *Class. Quantum Grav.* **25**, 114033 (2008) [arXiv:0712.0343 [gr-qc]].

[206] P. Ajith *et al.*, *Phys. Rev. Lett.* **106**, 241101 (2011) [arXiv:0909.2867 [gr-qc]].

[207] L. Santamaria *et al.*, *Phys. Rev.* **D82**, 064016 (2010) [arXiv:1005.3306 [gr-qc]].

[208] T.A. Apostolatos, C. Cutler, G.J. Sussman, K.S. Thorne, *Phys. Rev.* **D49**, 6274 (1994).

[209] D.A. Brown, A. Lundgren, R. O'Shaughnessy, *Phys. Rev.* **D86**, 064020 (2012) [arXiv:1203.6060 [gr-qc]].

[210] M. Pürrer, M. Hannam, P. Ajith, S. Husa, *Phys. Rev.* **D88**, 064007 (2013) [arXiv:1306.2320 [gr-qc]].

[211] A. Buonanno, T. Damour, *Phys. Rev.* **D59**, 084006 (1999).

[212] A. Buonanno, T. Damour, *Phys. Rev.* **D62**, 064015 (2000) [arXiv:gr-qc/0001013].

[213] T. Damour, A. Nagar, *Phys. Rev.* **D77**, 024043 (2008) [arXiv:0711.2628 [gr-qc]].

[214] T. Damour *et al.*, *Phys. Rev.* **D78**, 044039 (2008) [arXiv:0803.3162 [gr-qc]].

[215] A. Buonanno *et al.*, *Phys. Rev.* **D79**, 124028 (2009) [arXiv:0902.0790 [gr-qc]].

[216] Y. Pan *et al.*, *Phys. Rev.* **D81**, 084041 (2010) [arXiv:0912.3466 [gr-qc]].

[217] T. Damour, M. Trias, A. Nagar, *Phys. Rev.* **D83**, 024006 (2011) [arXiv:1009.5998 [gr-qc]].

[218] A. Pan *et al.*, *Phys. Rev.* **D84**, 124052 (2011) [arXiv:1106.1021 [gr-qc]].

[219] NRAR homepage: https://www.ninja-project.org/doku.php?id=nrar:home

[220] A.H. Mroué *et al.*, arXiv:1304.6077 [gr-qc].

[221] Ninja homepage: https://www.ninja-project.org/doku.php

[222] B. Aylott *et al.*, *Class. Quantum Grav.* **26**, 165008 (2009) arXiv:0901.4399 [gr-qc].

[223] B. Aylott *et al.*, *Class. Quantum Grav.* **26**, 114008 (2009) [arXiv:0905.4227 [gr-qc]].

[224] P. Ajith *et al.*, *Class. Quantum Grav.* **29**, 124001 (2012) [arXiv:1201.5319 [gr-qc]].

[225] J. Healy *et al.*, arXiv:1112.3928 [gr-qc].

[226] E. Berti *et al.*, *Phys. Rev.* **D87**, 124020 (2013) [arXiv:1304.2836 [gr-qc]].

[227] W.B. Bonnor, M.A. Rotenberg, *Proc. R. Soc. Lond.* **A265**, 109 (1961).

[228] A. Peres, *Phys. Rev.* **128**, 2471 (1962).

[229] J.D. Bekenstein, *Astrophys. J.* **183**, 657 (1973).

[230] D. Merritt *et al.*, *Astrophys. J.* **607**, L9 (2004) [arXiv:astro-ph/0402057].

[231] J.A. González *et al.*, *Phys. Rev. Lett.* **98**, 091101 (2007) [arXiv:gr-qc/0610154].

[232] J.G. Baker *et al.*, *Astrophys. J.* **653**, 93 (2006) [arXiv:gr-qc/0603204].

[233] F. Herrmann, I. Hinder, D. Shoemaker, P. Laguna, *Class. Quantum Grav.* **24**, S33 (2007) [arXiv:gr-qc/0601026].

[234] J.A. Gonzalez, U. Sperhake, B. Brügmann, *Phys. Rev.* **D79**, 124006 (2009) [arXiv:0811.3952 [gr-qc]].

[235] J.A. González *et al.*, *Phys. Rev. Lett.* **98**, 231101 (2007) [arXiv:gr-qc/0702052].

[236] M. Campanelli, C.O. Lousto, Y. Zlochower, D. Merritt, *Astrophys. J.* **659**, L5 (2007) [arXiv:gr-qc/0701164].

[237] M. Campanelli, C.O. Lousto, Y. Zlochower, D. Merritt, *Phys. Rev. Lett.* **98**, 231102 (2007) [gr-qc/0702133].

[238] C.O. Lousto, Y. Zlochower, *Phys. Rev. Lett.* **107**, 231102 (2011) [arXiv:1108.2009 [gr-qc]].

[239] S. Komossa, H. Zhou, H. Lu, *Astrophys. J.* **678**, L81 (2008) [arXiv:0804.4585 [astro-ph]].

[240] P. Chang, L.E. Strubbe, K. Menou, E. Quataert, *Mon. Not. R. Astron. Soc.* **407**, 2007 (2010) [arXiv:0906.0825 [astro-ph]].

[241] J. Guedes, P. Madau, L. Mayer, S. Callegari, *Astrophys. J.* **729**, 125 (2011) [arXiv:1008.2032 [astro-ph]].

[242] Z. Haiman, A. Loeb, *Astrophys. J.* **552**, 459 (2001).

[243] Y. Li *et al.*, *Astrophys. J.* **665**, 187 (2007) [arXiv:astro-ph/0608190].

[244] M. Volonteri, K. Gültekin, M. Dotti, *Mon. Not. R. Astron. Soc.* **404**, 2143 (2010) [arXiv:1001.1743 [astro-ph]].

[245] J. Magorrian *et al.*, *Astron. J.* **115**, 2285 (1998) [arXiv:astro-ph/9708072].

[246] T. Bogdanović, C.S. Reynolds, M.C. Miller, *Astrophys. J.* **661**, L147 (2007) [arXiv:astro-ph/0703054].

[247] J.D. Schnittman, *Phys. Rev.* **D70**, 124020 (2004) [arXiv:astro-ph/0409174].

[248] M. Kesden, U. Sperhake, E. Berti, *Phys. Rev.* **D81**, 084054 (2010) [arXiv:1002.2643 [astro-ph]].

[249] M. Kesden, U. Sperhake, E. Berti, *Astrophys. J.* **715**, 1006 (2010) [arXiv:1003.4993 [astro-ph]].

[250] E. Berti, M. Kesden, U. Sperhake, *Phys. Rev.* **D85**, 124049 (2012) [arXiv:1203.2920 [astro-ph]].

[251] I. Antoniadis, *Phys. Lett.* **B246**, 377 (1990).

[252] I. Antoniadis, N. Arkani-Hamed, S. Dimopoulos, G.R. Dvali, *Phys. Lett.* **B436**, 257 (1998) [arXiv:hep-ph/9804398].

[253] L. Randall, R. Sundrum, *Phys. Rev. Lett.* **83**, 4690 (1999) [arXiv:hep-th/9906064].

[254] S. Dimopoulos, G. Landsberg, *Phys. Rev. Lett.* **87**, 161602 (2001) [arXiv:hep-th/0106295].

[255] S.B. Giddings, S. Thomas, *Phys. Rev.* **D65**, 056010 (2002) [arXiv:hep-ph/0106219].

[256] M. Cavaglià, *Int. J. Mod. Phys.* **A18**, 1843 (2003) [arXiv:hep-ph/0210296].

[257] P. Kanti, *Lect. Notes Phys.* **769**, 387 (2009) [arXiv:0802.2218 [hep-th]].

[258] S. Chatrchyan *et al.*, *J. High Energy Phys.* **1204**, 061 (2012) [arXiv:1202.6396 [hep-ex]].

[259] D.-C. Dai *et al.*, *Phys. Rev.* **D77**, 076007 (2008) [arXiv:0711.3012 [hep-ph]].

[260] C.M. Harris, P. Richardson, B.R. Webber, *J. High Energy Phys.* **0308**, 033 (2003) [arXiv:hep-ph/0307305].

[261] J.A. Frost *et al.*, *J. High Energy Phys.* **10**, 014 (2009) [arXiv:0904.0979 [hep-th]].

[262] T. Banks, W. Fischler, arXiv:hep-th/9906038.

[263] M.W. Choptuik, F. Pretorius, *Phys. Rev. Lett.* **104**, 111101 (2010) [arXiv:0908.1780 [gr-qc]].

[264] K.S. Thorne, *Nonspherical Gravitational Collapse: A Short Review*, in: J. Klauder, ed., *Magic Without Magic*, Freeman, San Francisco 1972, p. 231.

[265] W.E. East, F. Pretorius, *Phys. Rev. Lett.* **110**, 101101 (2013) [arXiv:1210.0443 [gr-qc]].
[266] F. Pretorius, D. Khurana, *Class. Quantum Grav.* **24**, S83 (2007) [arXiv:gr-qc/0702084].
[267] M. Shibata, H. Okawa, T. Yamamoto, *Phys. Rev.* **D78**, 101501(R) (2008) [arXiv:0810.4735 [gr-qc]].
[268] M. Campanelli, C.O. Lousto, Y. Zlochower, *Phys. Rev.* **D74**, 041501 (2006) [arXiv:gr-qc/0604012].
[269] H. Witek *et al.*, *Phys. Rev.* **D83**, 044017 (2011) [arXiv:1011.0742 [gr-qc]].
[270] E.V. Shuryak, *Prog. Part. Nucl. Phys.* **53**, 273 (2004) [arXiv:hep-ph/0312227].
[271] E.V. Shuryak, *Nucl. Phys.* **A750**, 64 (2005) [arXiv:hep-ph/0405066].
[272] B. Müller, *Prog. Theor. Phys. Suppl.* **174**, 103 (2008).
[273] G.T. Horowitz, V.E. Hubeny, *Phys. Rev.* **D62**, 024027 (2000) [arXiv:hep-th/9909056].
[274] P.M. Chesler, D. Teaney, arXiv:1112.6196 [hep-th].
[275] B. Wu, P. Romatschke, *Int. J. Mod. Phys.* **C22**, 1317 (2011) [arXiv:1108.3715 [hep-th]].
[276] R.H. Price, J. Pullin, *Phys. Rev. Lett.* **72**, 3297 (1994) [arXiv:gr-qc/9402039].
[277] M.P. Heller, D. Mateos, W. van der Schee, D. Trancanelli, *Phys. Rev. Lett.* **108**, 191601 (2012) [arXiv:1202.0981 [hep-th]].
[278] M.P. Heller, D. Mateos, W. van der Schee, M. Triana, *J. High Energy Phys.* **1309**, 026 (2013) [arXiv:1304.5172 [hep-th]].
[279] M.P. Heller, R.A. Janik, P. Witaszczyk, *Phys. Rev.* **D85**, 126002 (2012) [arXiv:1203.0755 [hep-th]].
[280] P.M. Chesler, L.G. Yaffe, arXiv:1309.1439 [hep-th].
[281] A. Adams, P.M. Chesler, H. Liu, arXiv:1212.0281 [hep-th].
[282] M. Maliborski, A. Rostworowski, *Int. J. Mod. Phys.* **A28**, 1340020 (2013) [arXiv:1308.1235 [gr-qc]].
[283] D. Garfinkle, G.C. Duncan, *Phys. Rev.* **D58**, 064024 (1998) [arXiv:gr-qc/9802061].
[284] F. Pretorius, M.W. Choptuik, *Phys. Rev.* **D62**, 124012 (2000) [arXiv:gr-qc/0007008].
[285] E. Sorkin, Y. Oren, *Phys. Rev.* **D71**, 124005 (2005) [arXiv:hep-th/0502034].
[286] C. Gundlach, J.M. Martín-García, *Living Rev. Relativity* **10**, 5 (2007) [http://www.livingreviews.org/lrr-2007-5].
[287] J. Jałmużna, A. Rostworowski, P. Bizoń, *Phys. Rev.* **D84**, 085021 (2011) [arXiv:1108.4539 [gr-qc]].

[288] D. Garfinkle, L.A. Pando Zayas, *Phys. Rev.* **D84**, 066006 (2011) [arXiv:1106.2339 [hep-th]].

[289] A. Buchel, L. Lehner, S.L. Liebling, *Phys. Rev.* **D86**, 123011 (2012) [arXiv:1210.0890 [gr-qc]].

[290] D. Garfinkle, L.A. Pando Zayas, D. Reichmann, *J. High Energy Phys.* **1202**, 119 (2012) [arXiv:1110.5823 [hep-th]].

[291] M. Maliborski, arXiv:1208.2934 [gr-qc].

[292] O.J.C. Dias, G.T. Horowitz, D. Marolf, J.E. Santos, *Class. Quantum Grav.* **29**, 235019 (2012) [arXiv:1208.5772 [gr-qc]].

[293] A. Buchel, S.L. Liebling, L. Lehner, *Phys. Rev.* **D87**, 123006 (2013) [arXiv:1304.4166 [gr-qc]].

[294] M. Maliborski, A. Rostworowski, *Phys. Rev. Lett.* **111**, 051102 (2013) [arXiv:1303.3186 [gr-qc]].

[295] M. Maliborski, A. Rostworowski, arXiv:1307.2875 [gr-qc].

[296] P. Bizoń, J. Jałmużna, *Phys. Rev. Lett.* **111**, 041102 (2013) [arXiv:1306.0317 [gr-qc]].

[297] M.W. Choptuik *et al.*, *Phys. Rev.* **D68**, 044001 (2003) [arXiv:gr-qc/0304085].

[298] D. Garfinkle, L. Lehner, F. Pretorius, *Phys. Rev.* **D71**, 064009 (2005) [arXiv:gr-qc/0412014].

[299] L. Lehner, F. Pretorius, *Phys. Rev. Lett.* **105**, 101102 (2010) [arXiv:1006.5960 [hep-th]].

[300] L. Lehner, F. Pretorius, arXiv:1106.5184 [gr-qc].